Geometrical Model of Hadron-nucleus and Nucleus-nucleus Scattering

(強子-核子及核子-核子散射幾何模型之研究)

by

Chan Yuk-ping

A Thesis Submitted In Partial Fulfillment
of the Requirements for the Degree of
Master of Philosophy in Physics

The Chinese University of Hong Kong

June 1990

TABLE OF CONTENTS

LIST OF FIGURES

Acknowledgement

I would like to express my gratitude towards my supervisor, Prof. K. Young, for his patient and brilliant guidance. I also wish to thank Prof. D. Kiang and Mr. T. Ochiai, for their useful suggestions. Lastly I would like to thank all the staffs and postgraduate students of the Physics Department for their kind help in the past two years.

Abstract

Experimental results and our earlier works for hadron-hadron and hadron-nucleus scattering are reviewed. Based on our earlier model and with certain new ideas, the multiplicity distributions for hadron-nucleus scattering in limited rapidity windows are investigated. For nucleus-nucleus scattering, the experimental features of the multiplicity distribution in full rapidity window are explained. All our calculated results are compared with the experimental data published recently with satisfactory agreement.

CHAPTER 1

Introduction

Since the invention of accelerators in the early 20th century, collision of high energy particles has become the most important method to examine the internal structure of the microscopical world in the elementary particle. So far, a large amount of experimental data have been obtained and certain experimental facts are known. However, in the theoretical aspect, for the hadronic multiparticle production, which is going to be discussed in this thesis, the progress is rather slow. Even though a large number of models have been proposed, among these models, none can capture all the experimental features and hence none is universally well accepted. Fig. 1.1 shows the various theoretical approaches and the complicated relation among them as summarized by R. C. Hwa (1987). From the figure we can see how confusing the situation is. Moreover, most of these model are so complicated that they can hardly be understood by the outsider.

In the past two years, we have tried to explain the process of the hadronic multiparticle production in hadron-nucleus

and nucleus-nucleus scattering with a model which is constructed from simple physics. We hope that our model can capture most of the experimental features with the least theoretical ingredient as input. In this thesis, a brief account of the experimental result of hadron-hadron (hh) and hadron-nucleus (hA) scattering will be presented and discussed in next chapter. In the same chapter, the geometrical picture, which is the basic idea of our model, will be introduced. In chapter 3, Our model for the charged multiplicity distribution of hA scattering in limited rapidity windows will be discussed and our result will be compared with the experimental data published recently. Effort was also made (Kiang *et al.*, 1990) to modify the geometric model to explain the experimental data of the heavy ion collisions (nucleus-nucleus scattering) obtained recently and all of these will be presented in chapter 4. Our work in the past two years will be summarized in the last chapter.

(a)

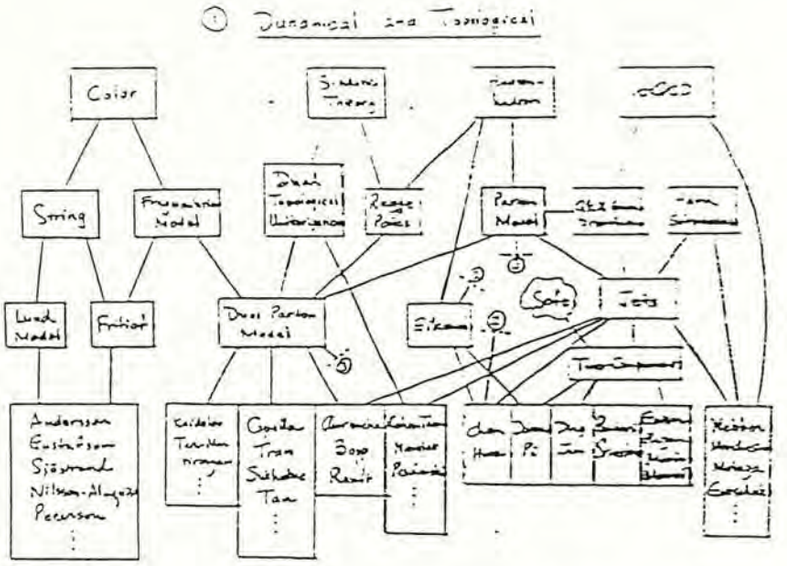

(b)

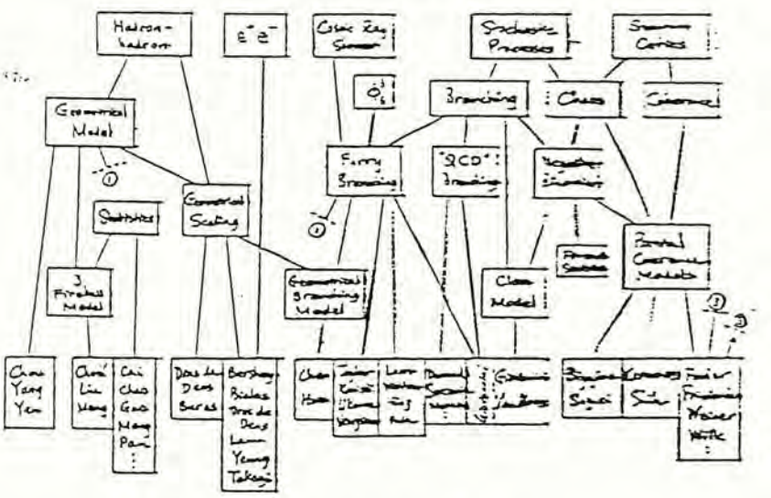

(c)

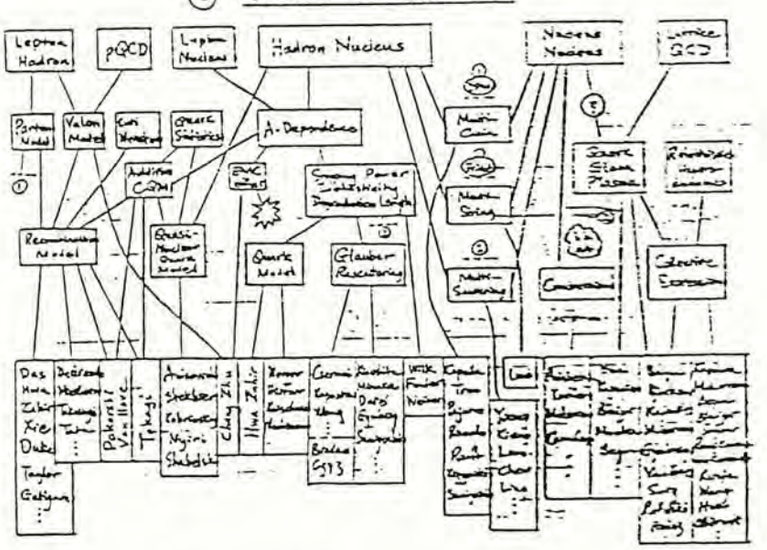

Fig. 1.1 a-c Varios theoretical approaches and their relationship.
(taken from R. C. Hwa and Q. B. Xie, 1987)

CHAPTER 2

Overview

2.1 Hadron-hadron Scattering

2.1.1 Introduction

In high energy collisions, there are two kinds of collision, elastic and inelastic. In elastic collisions the final state particle is identical to that before the collision (Fig. 2.1a), while for the inelastic collision at least one of the final state particle is different from one of the initial state particle. Moreover inelastic collisions can be further divided into three different processes:

a. Single diffraction - in this process the produced particles is concentrated in one side (forward or backward) and only a few are produced in the other side (Fig. 2.1b);

b. Double diffraction - during the collision both of the colliding particles are excited and decay later into the fast hadrons (Fig. 2.1c);

c. Non-diffractive process - the two incident particles collide violently at relatively small impact parameter b. The overlapping region is highly excited and contribute to the produced hadrons. For the non-overlapping part of the incident hadron, they retain their velocity and form the leading particle (Fig. 2.1d).

2.1.2 Geometrical Picture

Before the mid-sixties the following experimental facts about the elastic hadron-hadron scattering are known:

a. The total cross section σ_{tot} varies extremely slowly with the energy (Fig. 2.2);

b. The differential cross section $d\sigma/dt$ at small scattering angles (i.e. small $|t|$) can be well fitted by (Fig. 2.3)

$$\frac{d\sigma}{dt} = Ae^{-b|t|}. \qquad (2.1)$$

Noticing the similarity between the experimental result of $p\bar{p}$ elastic scattering and that of the optical diffraction, and generalizing the work of Glauber (1959) in nuclear scattering, Wu and Yang (1965) proposed the geometrical model to explain the process. In their model, they treat the process as two spatially extended objects going through each other with attenuation. The essential physics of the geometrical model is the introduction of impact parameter b. (i) The concept of space-time is still valid down to nucleus size ($\sim 10^{-15}$m); (ii) The overall result is the averaging of the uncorrelated outcome at each impact parameter;

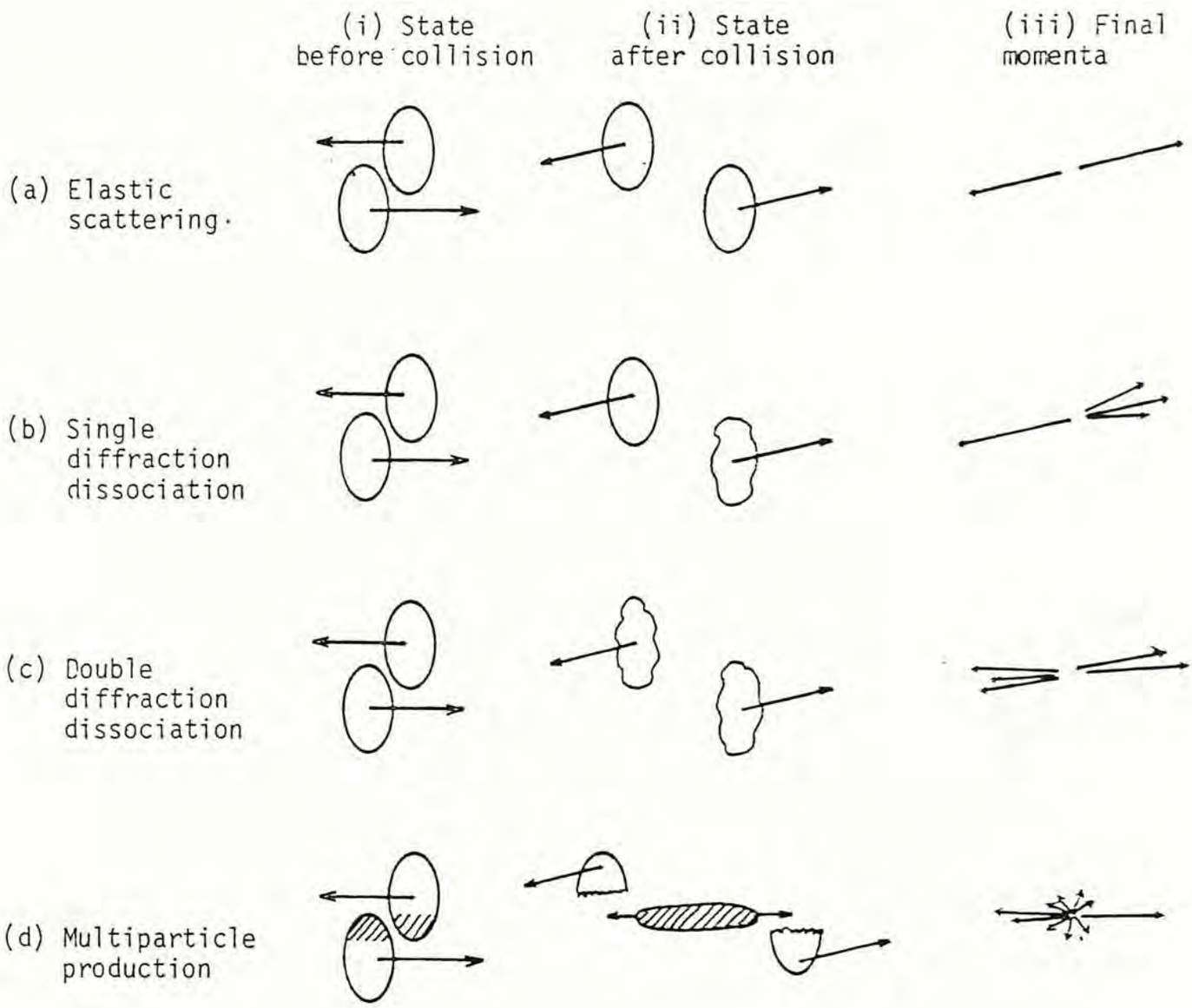

Fig. 2.1 a-d Schematic diagrams depicting (a) elastic scattering; (b) single diffraction dissociation; (b) double diffraction dissociation and (d) multiparticle production processes. (primarily taken from T. T. Chou and C. N. Yang, 1985)

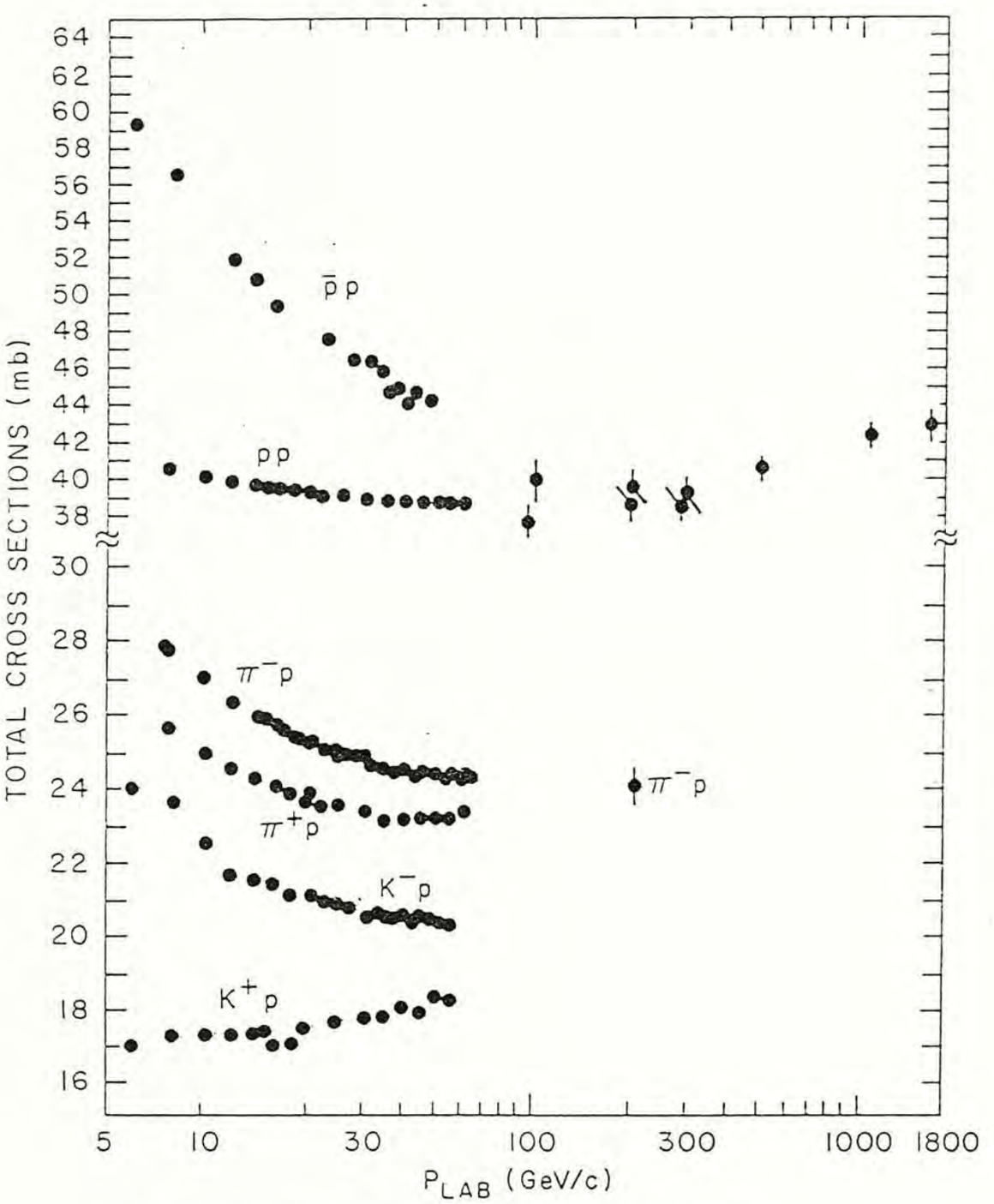

Fig. 2.2 Hadron-hadron total cross-section.
(taken from M. L. Perl, 1974)

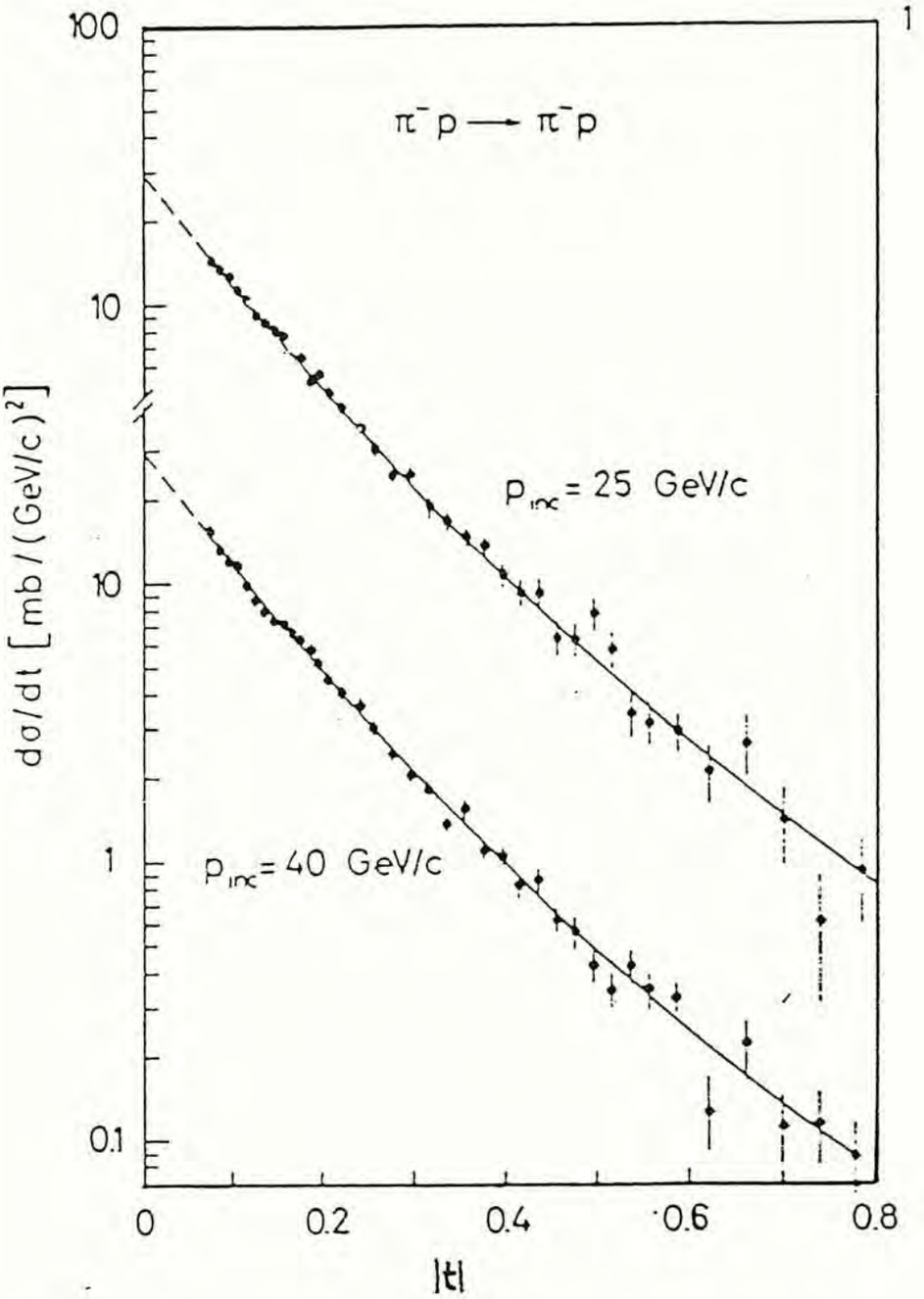

Fig. 2.3 The $d\sigma/dt$ for $\pi^- p$ elastic scattering at small t and high energy.
(taken from M. L. Perl, 1974)

(iii) The constituents of hadron are small enough such that their distribution can be regarded as continuous.

The opaqueness function $\Omega_{AB}(b)$ is defined as

$$\Omega_{AB}(b) \propto \iint \rho_A(\vec{b}-\vec{b}')\rho_B(\vec{b}')d^2b' \qquad (2.2)$$

where ρ_A and ρ_B are the matter density distribution of the colliding hadrons, and describes the overlapping matter distribution of the colliding system at each impact parameter b. Assuming that the absorption coefficient at b is given by $\exp(-\Omega_{AB}(b))$, the scattering coefficient of the incident particle is $1-\exp(-\Omega_{AB}(b))$. Hence by making use of the eikonal approximation, the differential cross-section is

$$\frac{d\sigma}{dt} = |f(t)|^2 \qquad (2.3)$$

with f(t) being the Fourier transform of the scattering coefficient, i.e.

$$f(t) = \int \frac{d^2b}{2\pi} (1-e^{-\Omega(b)})e^{-i\vec{k}\cdot\vec{b}}. \qquad (2.4)$$

The result of the geometrical model fits the experimental data very well. Furthermore, the prediction of existence of dips and peaks, which have not been foreseen by other models, was verified in 1972 and the positions of maximum and minimum are in good agreement with the data (Fig. 2.4).

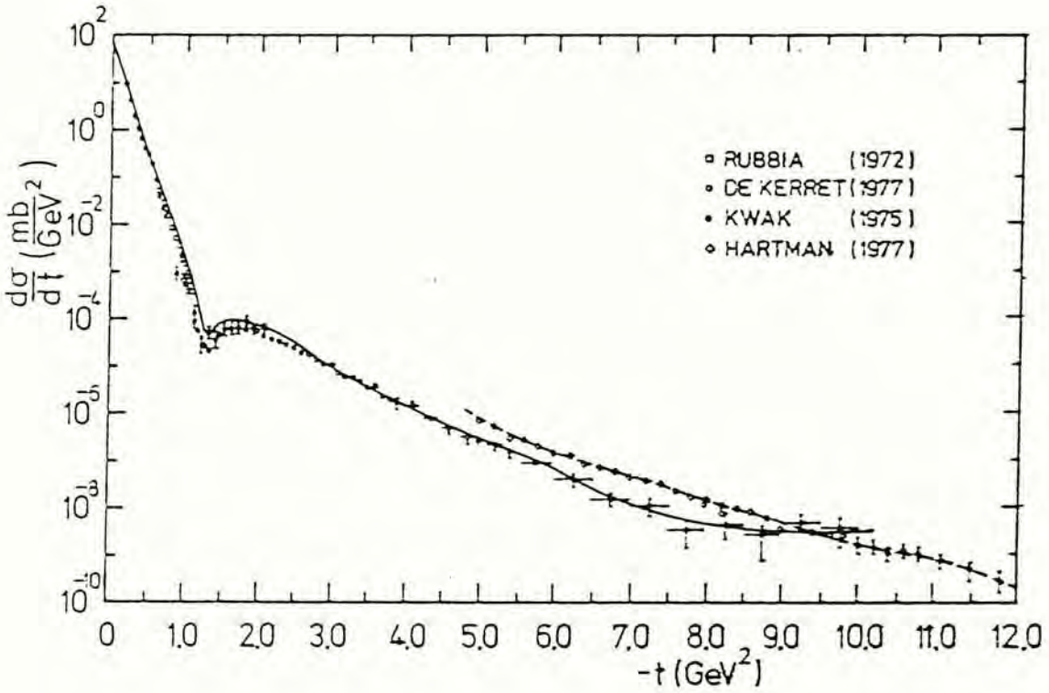

Fig. 2.4 The $d\sigma/dt$ for pp elastic scattering at ISR energies. (taken from D. J. Clarke and S. Y. Lo, 1979)

2.1.3 Inelastic Scattering

At 540 GeV total energy in the centre of mass, over 80% of the total cross section goes into the inelastic scattering. Since the process is rather complicated, experimental data are concentrated on the integrated quantities such as average charged multiplicity, multiplicity distribution, one-particle distribution etc..

A. Charged Multiplicity Distribution In Full Phase Space

As the energy increases, the average charged multiplicity $\langle n \rangle$ increases and it is very interesting that over 80% of the produced particles are pions. In the range 10-900 GeV, the average charged multiplicity is well fitted by the form (UA5, 1986):

$$\langle n \rangle = a + b \cdot \ln(s) + c(\ln(s))^2 \qquad (2.5)$$

with a = 2.7, b = -0.03 and c = 0.167 (Fig. 2.5).

In 1972, Z. Koba, H. B. Niselen and P. Olesen, using the hypothesis of Feymann scaling, predicted that the multiplicity distribution

$$\psi(z=n/\langle n \rangle) = \langle n \rangle P(n) \qquad (2.6)$$

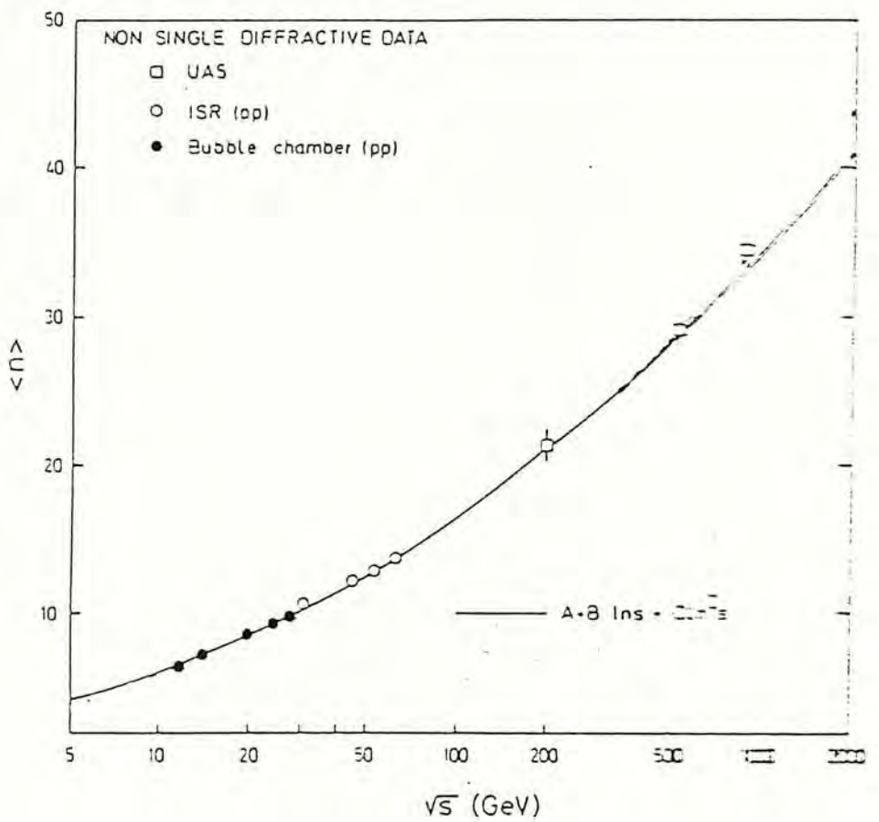

Fig. 2.5 The energy variation of the average charged multiplicity for non single-diffractive events. The solid line is the fitting curve of the experimental data.
(taken from UA5, 1986)

would become energy independent when the energy is sufficiently high and this is known as KNO scaling. The KNO scaling is observed in the ISR energy range (Fig. 2.7) and the invariant KNO curve was parameterized by Slattery (1972) as

$$\psi(z) = \tfrac{1}{2}(3.79z + 33.7z^3 - 6.64z^5 + 0.332z^7)\exp(-3.04z) \qquad (2.7)$$

It should be noted that only if the production of particles is non-stochastic ($\Delta n \sim n$) is KNO scaling possible. In the mid-eighties, Chou and Yang (1985) noticed that at a fixed multiplicity n, the probability distribution of multiplicity in forward hemisphere, n_F (or that in backward hemisphere, n_B) is well fitted by the binomial distribution, i.e.

$$n_F - n_B = 0(\sqrt{n}) \ . \qquad (2.8)$$

Chou and Yang claimed that this prominent feature of hadron-hadron scattering (i.e. along the $n_F + n_B$ direction the distribution is non-stochastic while that along $n_F - n_B$ is stochastic) is the result of superposition of stochastic processes at each impact parameter. Furthermore they argued that the distribution of $e^+ + e^- \longrightarrow$ hadron scattering, in which no impact parameter is involved, and taken to be the elementary process, should be stochastic. However, recent data by TASSO Collaboration (1989) shows that the charged multiplicity distributions of $e^+ + e^- \longrightarrow$ hadron scattering at 43.6 GeV cannot be satisfactorily described by the Poisson distribution (Fig. 2.6).

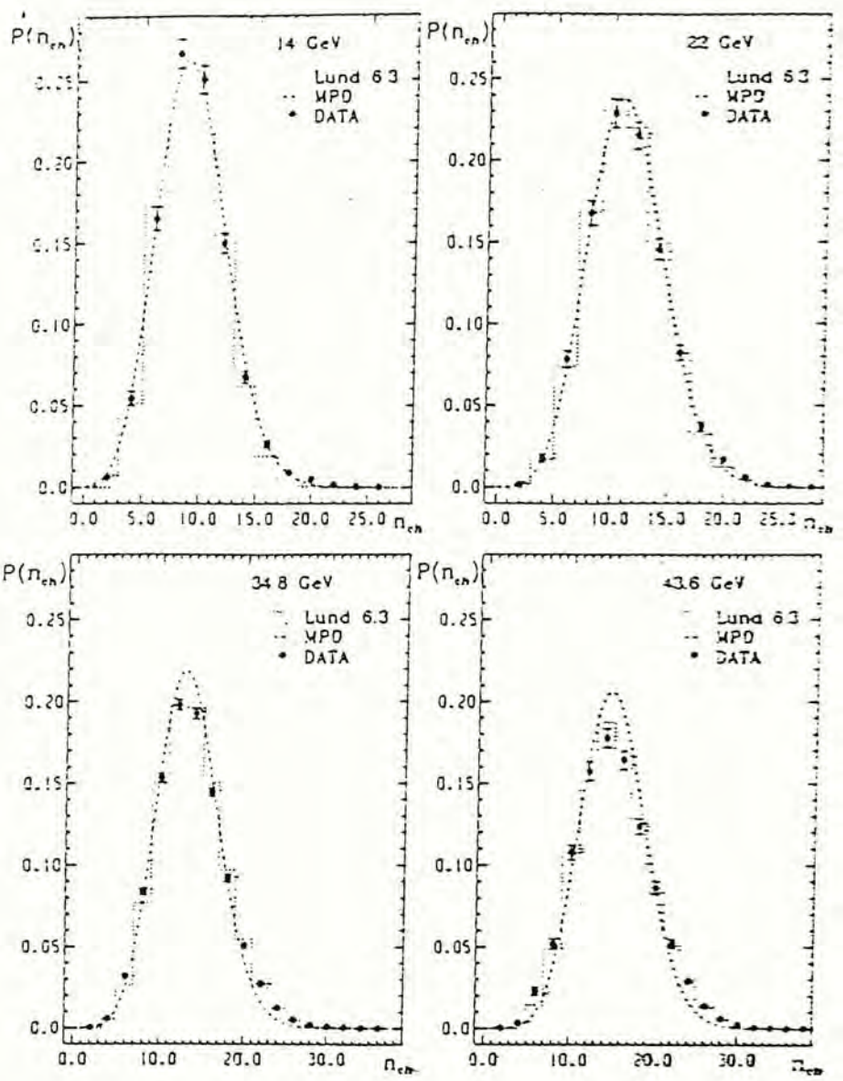

Fig. 2.6 Whole event charged multiplicity distribution compared with the modified Poisson distribution. (taken from TASSO, 1989)

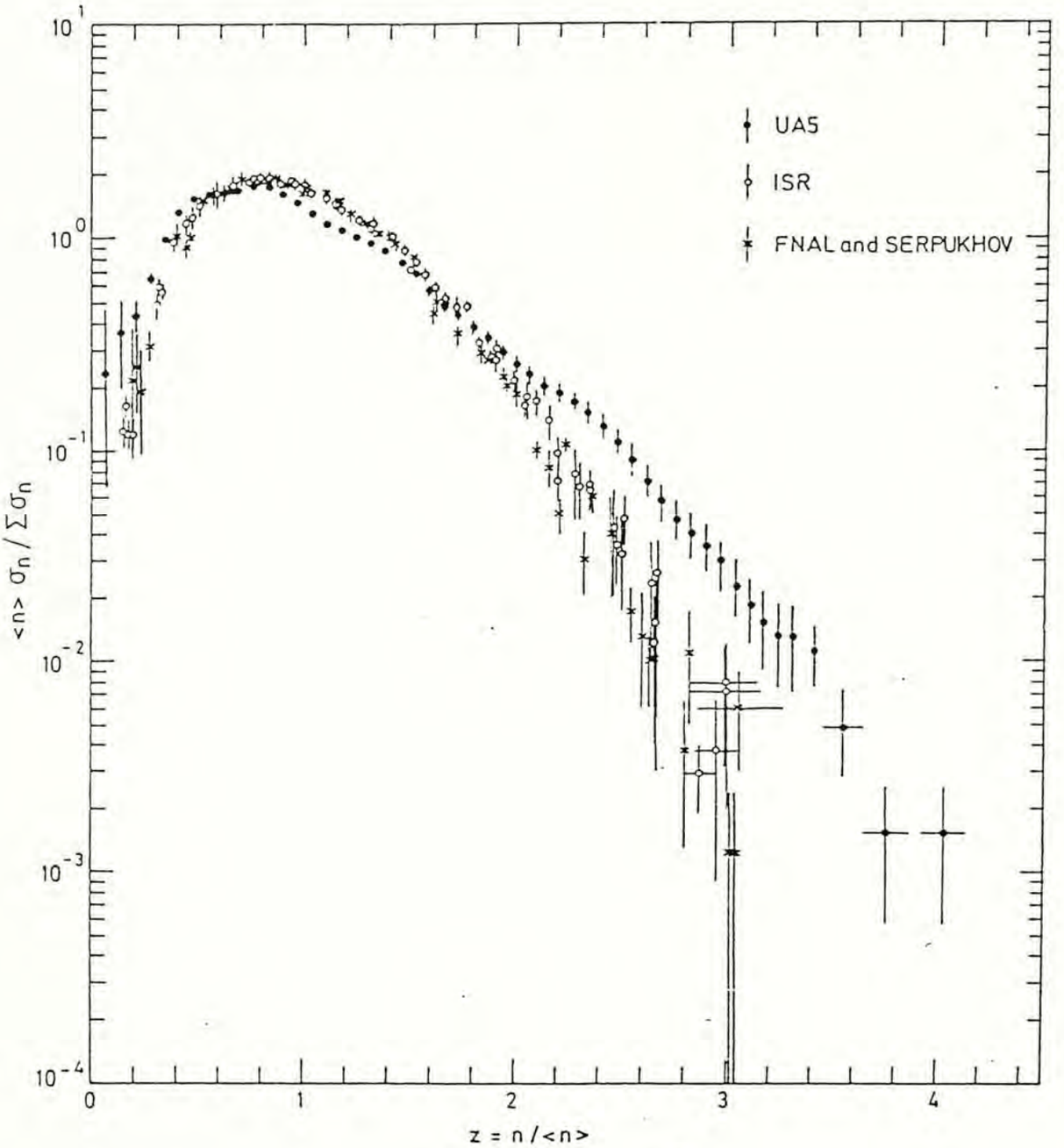

Fig. 2.7 Distibutions in charged multiplicity for non single-diffractive events obtained in the UA5 runs of 1981 and 1982 at 540 GeV CMS energy. Also the distributions from ISR, Serpukhov and FNAL are shown. (taken from UA5, 1984)

KNO scaling describes the multiplicity distribution very well in the ISR energy range. However in 1984, the UA5 collaboration at CERN found that at $\sqrt{s}$ = 540 GeV KNO scaling breaks down (Fig. 2.7). The result of p-$\bar{p}$ scattering at 900 GeV published last year proved this further (Fuglesang, 1988). Ling and Young (1984) have pointed out that there is a mild break at $z = 2.4$ in the multiplicity distribution (Fig. 2.7). They claimed that the breakdown of KNO scaling and the appearance of the break at large z reveal the geometrical nature of the hadron-hadron collision. From the point of view of the geometrical model, the multiplicity distribution $\psi(z)$ for the whole nucleus is just the result of superposition of the elementary distribution ψ_0 at each impact parameter b:

$$\psi(z) \propto \int d^2b\ P(b)\ \psi_0(n/\bar{n}(b))/\bar{n}(b) \qquad (2.9)$$

where P(b) is the interaction probability at b, and $\bar{n}(b)$ is the corresponding average multiplicity. At fixed b, the number of particles emitted, n, fluctuates around $\bar{n}(b)$ according to the elementary distribution ψ_0, which is believed to be stochastic and sharper than the overall distribution (Chou and Yang, 1984). The overall distribution $\psi(z)$ can be divided into two region, $z > z_0$ and $z < z_0$. z_0 is defined as

$$z_0 = \frac{\bar{n}_{max}}{\bar{n}_{tot}} \qquad (2.10)$$

where $\bar{n}_{max}$ is the largest $\bar{n}(b)$ and is equal to $\bar{n}(b = 0)$, while $\bar{n}_{tot}$ is the total average multiplicity. If the elementary distribution is as sharp as a delta function $\delta(n - \bar{n})$, the probability for the multiplicity z greater than z_0 will be equal to zero and there will be a abrupt break at z_0. In the actual situation, the distribution will smear out a little. Hence in the region $z > z_0$, the observed distribution is mainly attributed to the smeared out intrinsic distribution and that in region $z < z_0$ is the result of the superposition of the elementary distribution. Since the two regions are attributed to different physics, a break is expected. Furthermore if the elementary distribution ψ_0 is very sharp, the break will become very prominent. Because the elementary distribution ψ_0 at each impact parameter b is stochastic (i.e. $\Delta n \sim \sqrt{\bar{n}}$), at very high energy, $\Delta n/\bar{n} \sim (\bar{n})^{-1/2} \longrightarrow 0$, the multiplicity will fluctuate very little and the elementary distribution will become very sharp. Hence for high energy, the break should be much more apparent. Moreover due to the fact that $\bar{n}(b = 0)$ increases with energy, Ling and Young also predicted that as the energy increases, the break will shift to higher value of z. In the recent data of $p\text{-}\bar{p}$ scattering at 900 GeV (Fuglesang, 1988), this break is observed apparently (Fig. 2.8a). This idea was generalized by us to the heavy ion collision last year and in chapter 4, the result will be discussed in detail.

In 1985, in place of KNO scaling, a new empirical regularity for the multiplicity distributions was suggested by UA5 (1985b). The charged multiplicity distribution at each energy is found to be well described by the negative binomial distribution

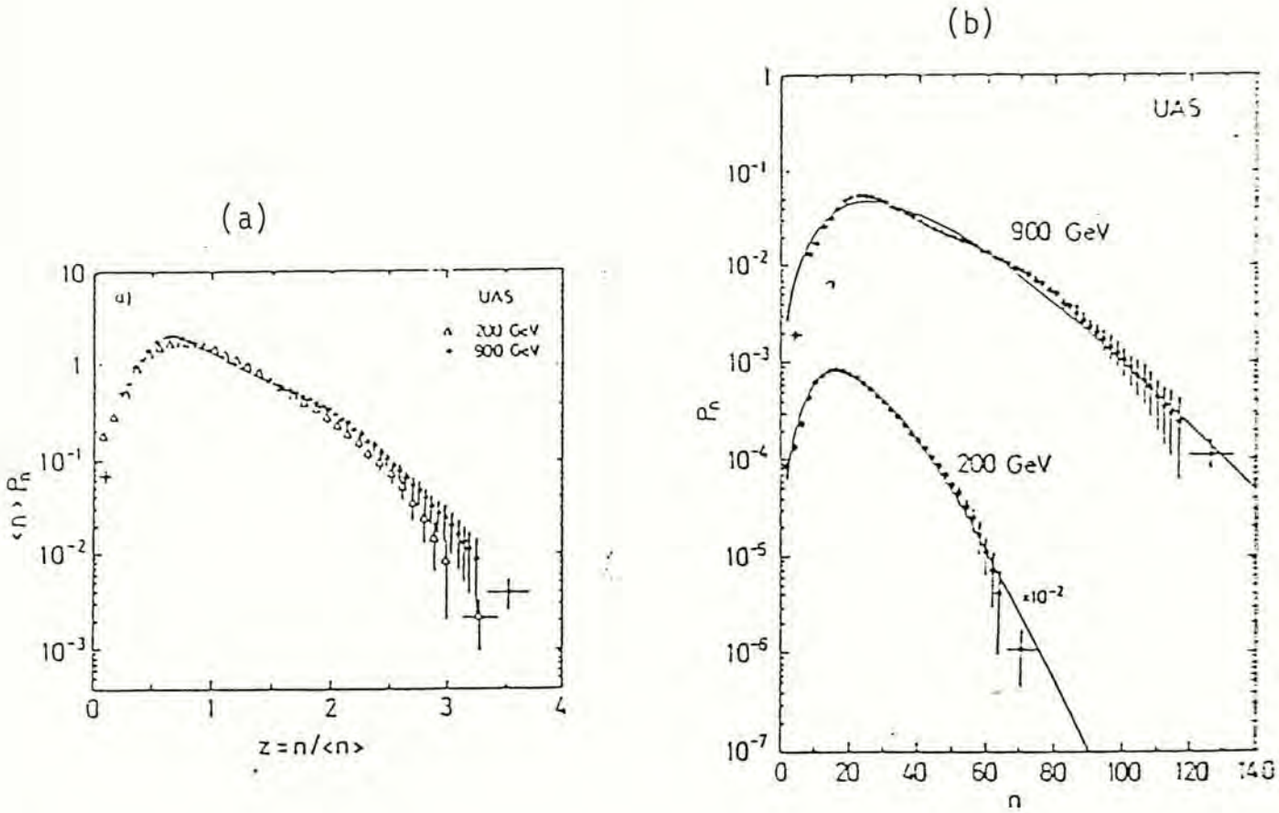

Fig. 2.8 a-b (a) The distributions of charged particles in full phase space for inelastic, non-single diffractive pp events at 200 and 900 GeV, plotted in 'KNO' form. (b) The distributions were compared with the best fits of the negative binomial distribution. (taken from C. Fuglesang, 1988)

$$P(n;\bar{n},k) = \frac{(n+k-1)!}{n!(k-1)!}\left(\frac{\bar{n}/k}{1+\bar{n}/k}\right)^{n}\frac{1}{(1+\bar{n}/k)^{k}} \qquad (2.11)$$

where $\bar{n}$ is the average of the distribution and k is related to the second moment C_2 $(=\langle n^2\rangle/\langle n\rangle^2)$ of the distribution as the following:

$$C_2 - 1 = 1/\bar{n} + 1/k. \qquad (2.12)$$

Even at $\sqrt{s}$ = 540 GeV, at which the KNO scaling is found to be broken down, the distribution is well fitted by the negative binomial distribution. For $k^{-1} = 0$ the negative binomial can be simplified to Poisson distribution and to geometric distribution when k = 1. Furthermore when $\bar{n}$ is sufficiently large ($\bar{n} \gg k$), the negative binomial distribution will be well approximated by the gamma distribution in scaling form,

$$\psi(z;k) = \bar{n}\,P(n/\bar{n})$$

$$= \frac{k^{k}}{\Gamma(k)}\,z^{k-1}\,e^{-kz}. \qquad (2.13)$$

Indeed the fact that the charged multiplicity distribution for hadron-hadron scattering is well fitted by the negative binomial distribution is nothing new. It was first pointed out by Knox in 1974.

The history of negative binomial distribution can be dated back to beginning of the 20th century and the similarity between the origin of the negative binomial and the geometrical

picture is rather interesting (Jeffreys, 1961). In 1920, people found that the distribution of the number of accidents to the worker in a factory is not well described by the Poisson distribution, which was happened to be too sharp. In order to account for this, Greenwood and Yule (1920) assumed that the probability distribution of occurring accidents to each worker in a factory is given by Poisson distribution. However the mean of accidents occurring varied from worker to worker and the distribution was assumed to be given by gamma distribution. Hence the total probability distribution is just the superposition of the Poisson distribution weighted by the gamma distribution. The resulting distribution, which is broader that the Poisson distribution, is known as the negative binomial distribution.

For a wide range of energies (~ 10 - 600 GeV), the multiplicity distribution is well fitted by the negative binomial distribution and the parameter k of the negative binomial distribution varies smoothly with the incident energy (Fig. 2.9). In Fig. 2.9, we also show the variation of $1/\bar{n}$ and the sum of $1/\bar{n} + 1/k = 1/C_2$ with the incident energy. It can be seen that in the ISR energy range, the increase of 1/k is compensated by the decrease of $1/\bar{n}$ and hence $1/C_2$ is nearly constant (~ 0.2). For higher energy, 1/k become dominant and $1/C_2$ increases to ~ 0.3. Hence with the description of negative binomial distribution the KNO scaling observed in ISR energy range is just accidental.

From the experimental result of $p+\bar{p}$ scattering received last year (Fig. 2.8b), the experimental data can no more be well fitted the negative binomial distribution and it seems that this regularity breaks down also.

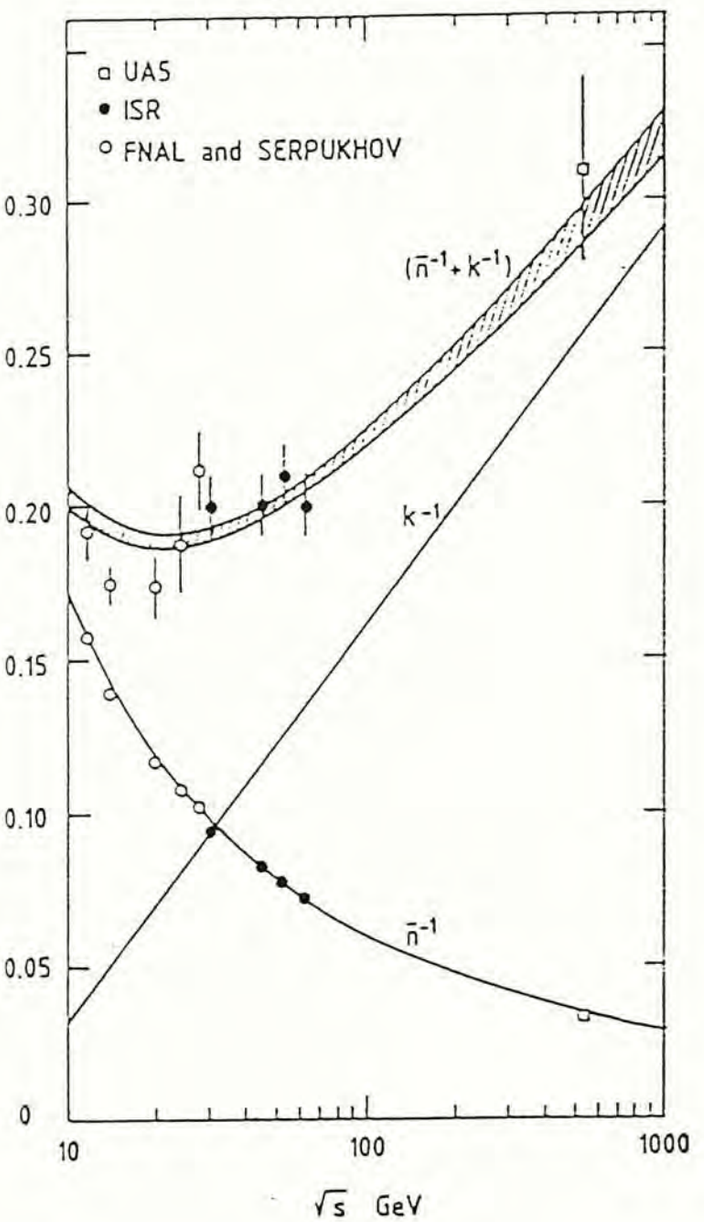

Fig. 2.9 The energy variation of $\bar{n}^{-1}$, k^{-1} and the second moments, $(D/\bar{n})^2 = \bar{n}^{-1} + k^{-1}$.
(taken from UA5, 1985a)

B. Multiplicity Distribution in Limited Rapidity Windows

Instead of the angle of emission θ, in high energy physics the rapidity y and the pseudo-rapidity η are used. They are defined as:

$$\eta = -\ln(\tan(\frac{\theta}{2})) \ , \tag{2.14}$$

$$y = \frac{1}{2} \ln\left(\frac{E + P_l}{E - P_l} \right) \tag{2.15}$$

where P_l is the longitudinal momentum. For small transverse momentum P_t, the rapidity y is approximately equal to the pseudo-rapidity η.

In different rapidity intervals $\Delta\eta$, the multiplicity distribution is again well described by the negative binomial distribution (Fig. 2.10).

C. Correlation

The rapidity distribution of the emitted particles and the multiplicity distribution in various rapidity windows provide much information on the mechanism of the particles production. One of the most important discoveries is the existence of short range correlations among the produced particles (approximately within one unit of pseudo-rapidity η) while the long range

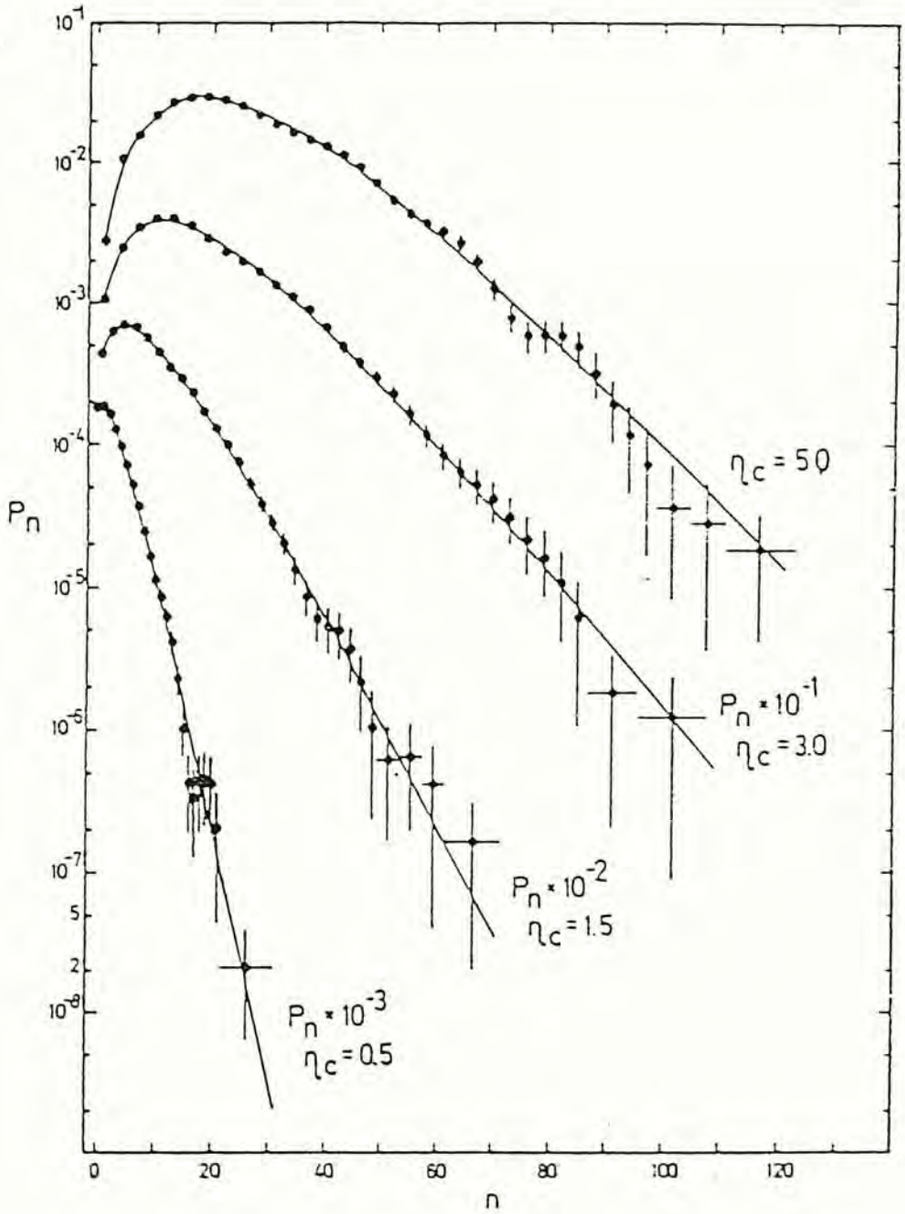

Fig. 2.10 Corrected charged multiplicity distributions in the pseudorapidity intervals $|\eta| < 0.5$, 1.5, 3.0 and 5.0 with the best fitted negative binomial distributions. (taken from UA5, 1985b)

correlation does not exist. It was found that the relation between the average multiplicity in the backward (forward) hemisphere $\langle n_B \rangle$ ($\langle n_F \rangle$) and the forward (backward) multiplicity n_F (n_B) is well described by the linear function (Fig. 2.11):

$$\langle n_B(n_F) \rangle = a + b \cdot n_F \qquad (2.16)$$

where b is the strength of correlation between n_F and n_B. With the phase space divided into two region at $|\eta|=1$, the correlation factor b in region $|\eta|<1$ is greater than that in region $|\eta|>1$. For the region $|\eta|>1$, the forward and backward hemispheres are separated by the gap $|\eta|<1$. Unless long range correlation exists among the particle, the multiplicity n_F and n_B should be independent of each other and the strength of correlation b should be very small. However in the narrow gap at the central region $|\eta|<1$, if short range correlation exists, the highly correlated particle will be emitted into both of the hemisphere. As a result the correlation factor will become very large.

Besides, it was found that the probability distribution of n_F (n_B) at fixed total multiplicity n is well described by the binomial distribution (Fig. 2.12)

$$P(n_F;n) = \frac{n!}{n_F!(n-n_F)!} q^{n_F/k} (1-q)^{(n-n_F)/k} \qquad (2.17)$$

with the probability of a particle being emitted into the forward hemispheres q = 1/2 and k = 2. Now it is well accepted that the particle are emitted in the form of neutral clusters with size k = 2.

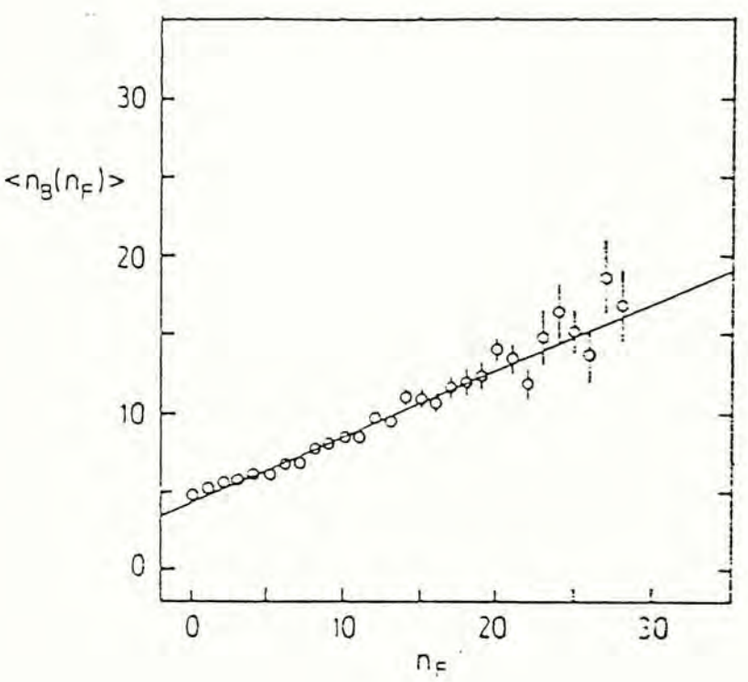

Fig. 2.11 The linear fit of the average value of n_B, taken at fixed n_F, as a function of n_F.
(taken from UA5, 1987)

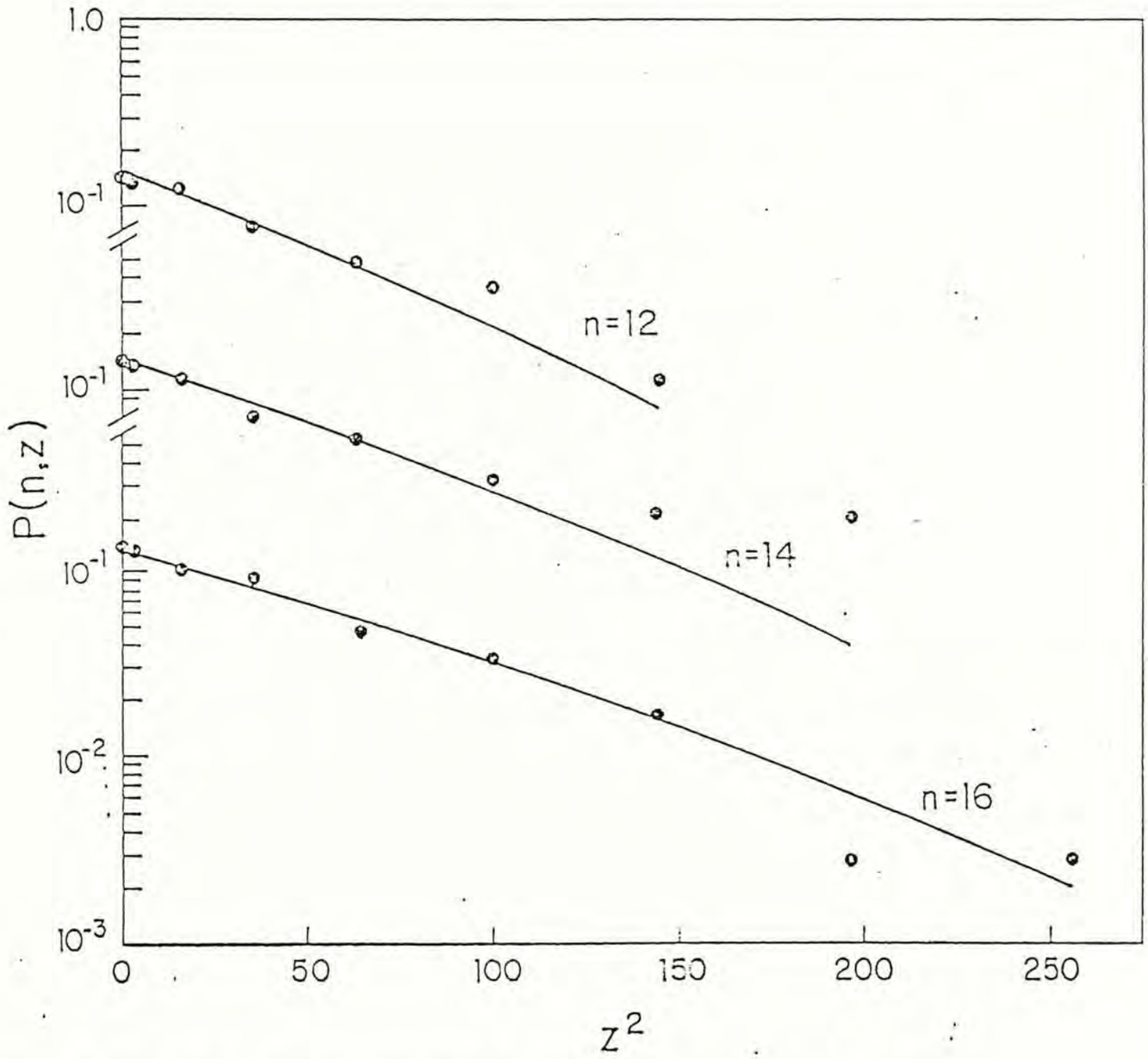

Fig. 2.12 Plot of the calculated z-distribution ($z = n_F - n_B$) with the equation $P(n,z) = (\text{function of } n)\, C^{n/2}_{(n+z)/4}$ and the experimental data points in log scale for n = 12, 14, and 16. Both the theoretical curves and the experimental data points are normalized.
(taken from T. T. Chou and C. N. Yang, 1984)

D. The Partition Temperature Model

To explain the rapidity distribution of the produced hadrons, Chou, Yang and Yen proposed the partition temperature model in 1985. The idea of this model is quite simple. With the condition: (i) conservation of four momentum; (i) the existence of cut-off transverse momentum; (iii) leading particles effect, the collision in the central overlapping region is assumed to be so violent that the distribution can be described by the canonical ensemble,

$$P \propto g(p_\perp) \exp(-E/T)\, d^3p/E \qquad (2.18)$$

where T is the partition temperature of the ensemble, and $g(p_\perp) = \exp(-\alpha p_\perp)$ is the cut-off transverse momentum factor. The cut-off α is chosen to match the experimental observation that the average transverse momentum of the produced particles $\langle p_\perp \rangle \sim 0.4$ GeV/c (UA5, 1987). The existence of this cut-off transverse momentum is quite remarkable; even at very high energy where the average energy of produced particles is 10 GeV, the observation still holds. The well fitted result of the partition temperature for $p\bar{p}$ scattering at $\sqrt{s}$ = 540 GeV is shown in Fig. 2.13.

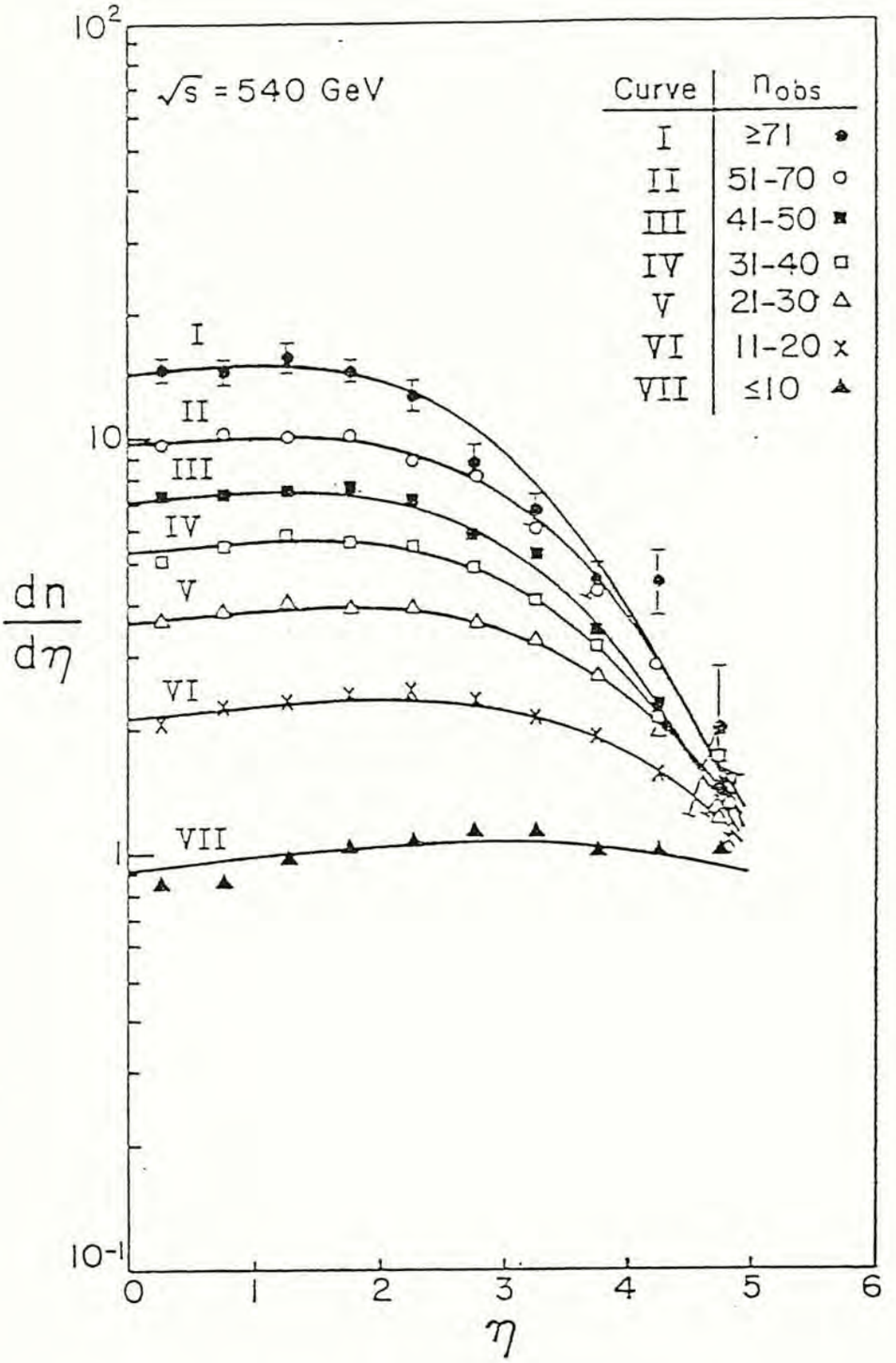

Fig. 2.13 dn/dη versus η at 540 GeV CMS energy by UA5 Collaboration and are compared with the calculated result of the partition temperature model. (taken from T. T. Chou and C. N. Yang)

2.2 Hadron-Nucleus Scattering

In the past ten years much attention has been drawn to hadron-nucleus scattering and experimental data for hA scattering are available. The experimental data are concentrated on multiplicity distribution, average multiplicity, rapidity distribution, etc., which are quite similar to that of hh scattering. The experimental results of hA scattering was summarized by De Marzo *et al.* (1982). Here only several important result is stated:

a. The all charged multiplicity distribution for hadron-nucleus scattering can no longer be fitted by the Slattery distribution. However for the negative charged multiplicity distribution, Slattery described the distribution very well (Fig 2.14).

b. Similar to $p\bar{p}$ scattering, short range correlations is found to be existed in central region and no evident for the existence of long range correlations is found.

c. The width of the multiplicity distribution $D/\langle n\rangle$ for the produced particle at fixed number of collision ν is proportional to $1/\sqrt{\nu}$ (Fig 2.15).

Furthermore, the charged multiplicity distribution in both full and limited rapidity intervals are found to be well described by the negative binomial distribution (Fig.2.16).

For the average multiplicity $\bar{n}$ for different target nuclei, Chao, Hegab and Hufer (1983) parameterized $\bar{n}$ as (Fig. 2.17)

$$\bar{n}(\bar{\nu};E) = n_{pp}(E)\ [1 + \beta(\bar{\nu} - 1)] \qquad (2.19)$$

(a)

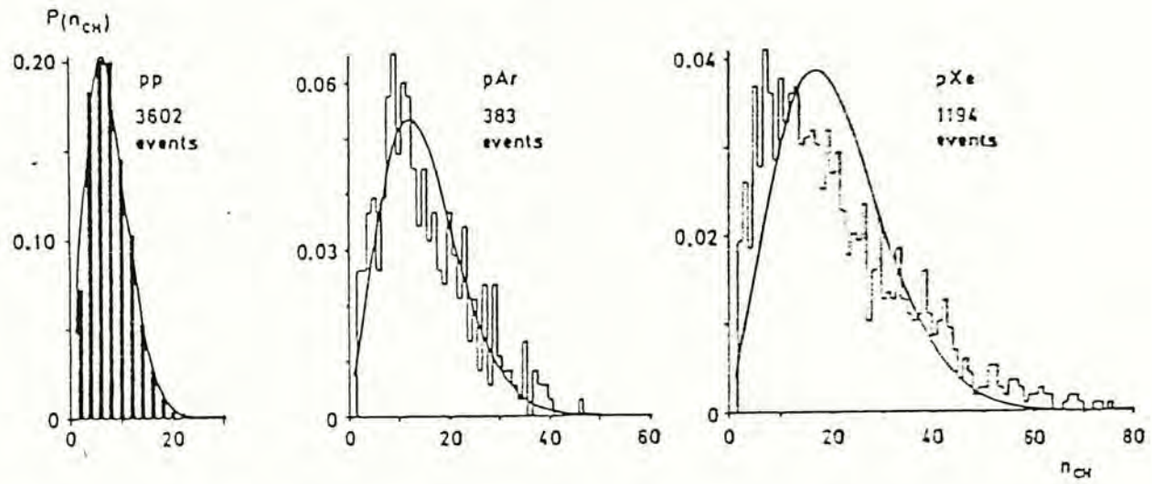

(b)

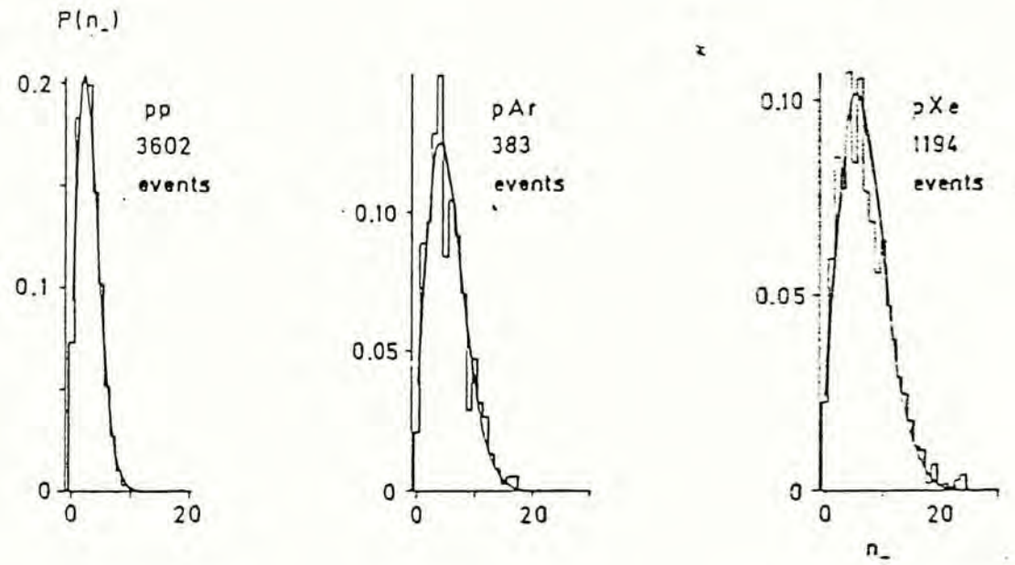

Fig. 2.14 a-b Multiplicitiy distributions for (a) all charged particles and (b) negatives particles. The solid lines represent the KNO distribution in pp interactions.
(taken from C. De Marzo *et al.*, 1982)

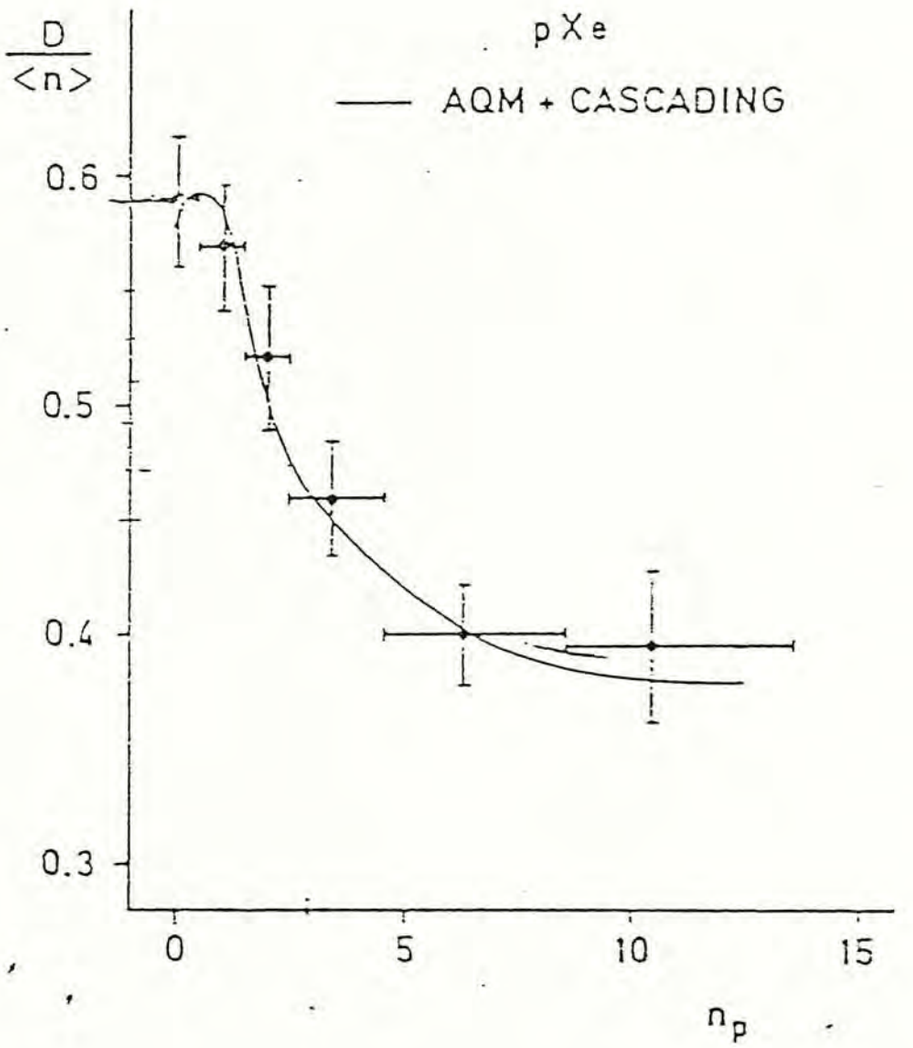

Fig. 2.15 The ratio of the dispersion D to the multiplicity <n> as a function of the number of identified protons n_p. (taken from C. De Marzo *et al.*, 1982)

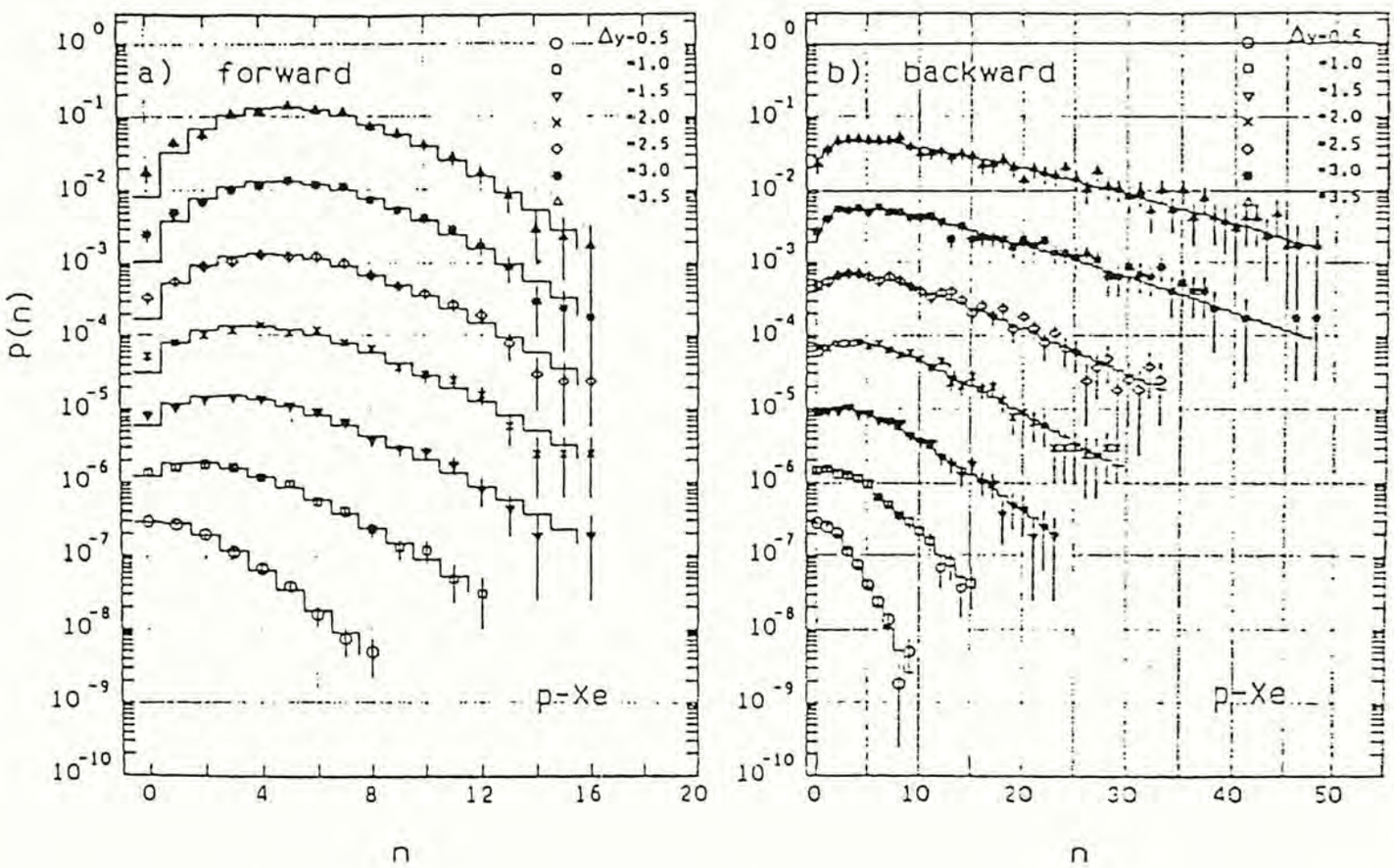

Fig. 2.16 a-b Charged multiplicity distributions of p-Xe interactions for various rapidity spans Δy (a) in the forward, and (b) in the backward hemisphere. The histograms show the negative binomial distributions fitted to the data points. The distribution for the widest span is shown in the ordinary scale, each consecutive one is shifted down by a factor of 10.
(taken from F. Dengler *et al.*, 1986)

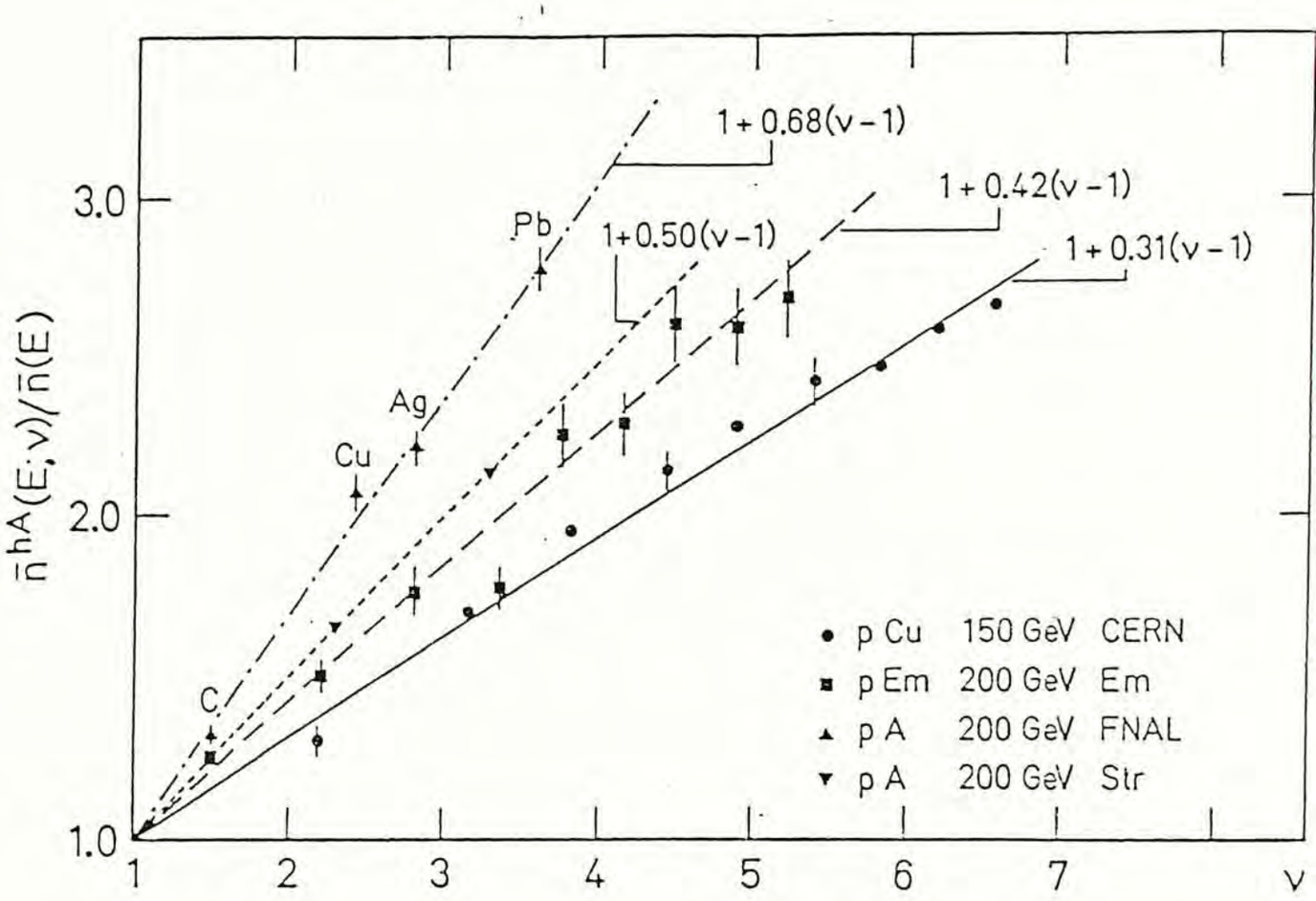

Fig. 2.17 The normalised mean multiplicity $\bar{n}^{hA}(E,\nu)/\bar{n}(E)$ of the produced particles as a function of the number ν of struck nucleons for pA collisions at 150 and 200 GeV. The lines represent the phenomenological fit, $1 + \beta(\nu - 1)$, to the data.
(taken from W. Q. Chao, M. K. Hegab and J. H fner, 1983)

where $n_{pp}(E)$ is the average multiplicity for hadron-hadron scattering at the same incident energy, and $\bar{\nu}$ is the average number of collision for the whole nucleus, defined as

$$\bar{\nu} = A\sigma_{pp}/\sigma_{pA} \tag{2.30}$$

with A = the mass number of the target nucleus;

σ_{pp} = the inelastic cross section for h-h scattering;

σ_{pA} = the inelastic cross section for h-A scattering.

The free parameter β is fixed by the experimental data, and is found approximately equal to 0.5. With β exactly equal to 1/2, Eq.(2.19) can be simplified to

$$\bar{n}(\bar{\nu},E) = n_{pp}(E)\ (1 + \bar{\nu})/2 \tag{2.21}$$

which has the physical meaning that the first term represents the beam particle and the second term, the $\bar{\nu}$ particles in the target undergoing interaction, and each of these particles contributes $n_{pp}/2$ produced particles. (For p+p collision $\bar{\nu}$ = 1, each of the two colliding particles contributes half of the producing particles.)

With the parameterization discussed above and the assumption that the elementary multiplicity distribution ψ_0 at each impact parameter b is given by the universal KNO distribution (universal KNO scaling), Kiang *et al.* (1985) generalized the geometrical picture to hadron-nucleus scattering. The most prominent feature in the result of their model is the shift of the

peak to smaller value of z as the mass of the target nucleus increased. This feature matches the experimental data very well and was verified in several articles published later (e.g. Bailly *et al.*, 1988) (Fig. 2.18). However the assumption of universal KNO scaling has neglected the experimental fact that the width of the distribution is proportional to $1/\sqrt{\nu}$, where ν is the average number of collision and obviously is b dependent (De Marzo *et al.*, 1982).

Besides the geometrical picture, the partition temperature model was also generalized to hadron-nucleus scattering successfully by Li and Young (1986) to account for the rapidity distribution of the produced particles.

In the next chapter, these two models will be discussed in detail and the work of unifying these two models to discuss the experimental result of multiplicity distribution for hadron-nucleus scattering in limited rapidity interval will be presented.

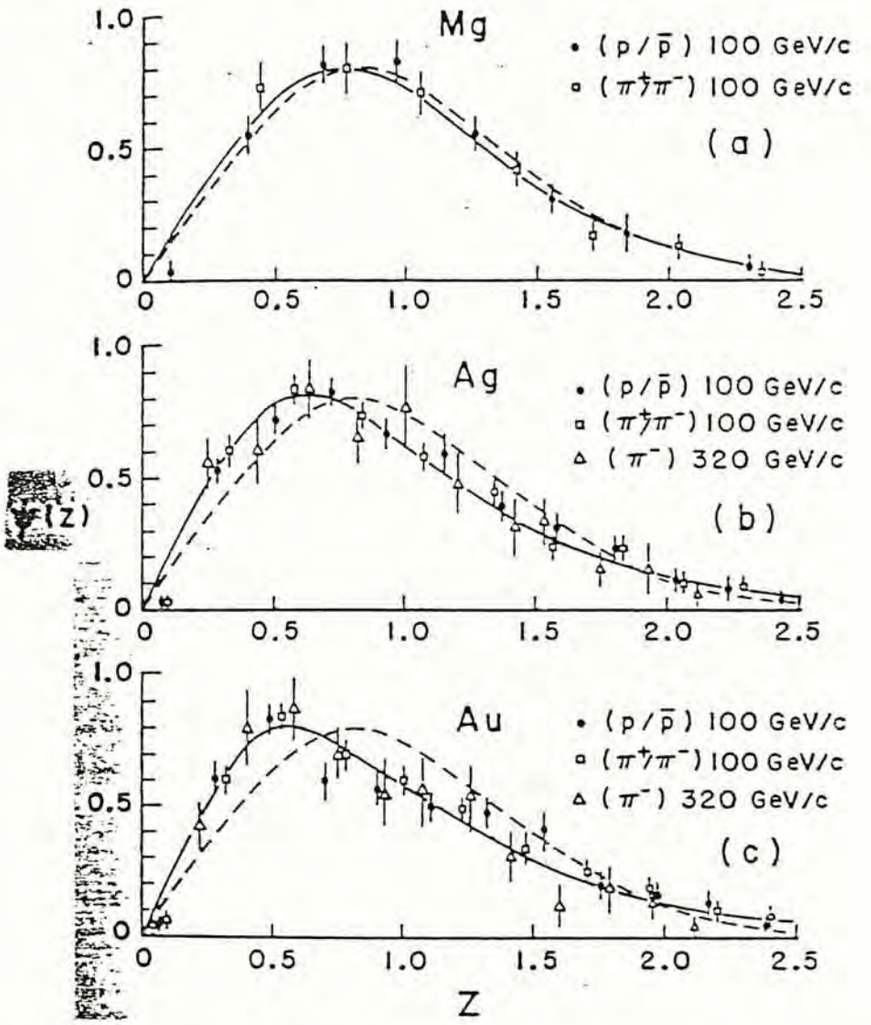

Fig. 2.18 a-b Multiplicity distributions for (a) h-Mg, (b) h-Ag and (c) h-Au interactions. The dashed curve corresponds to the Slattery distribution and the solid curves correspond to the prediction of the model proposed by D. Kaing *et al.* (1985). (taken from N. N. Biswas *et al.*, 1986)

Chapter 3

Charged Particle Multiplicity Distribution in Limited Rapidity Windows in Hadron-Nucleus Scattering

3.1 Introduction

In recent years, a lot of work has been done on the multiplicity distribution of charged particles in hadron-nucleus scattering. Initial interest was concentrated on (a) the number of charged particles n observed in the full rapidity window, with distribution P(n) and average $\bar{n}$, and also on (b) the number of negative charges n_- observed in the full rapidity window, with distribution $P_-(n_-)$ and average $\bar{n}_-$, (De Marzo *et al.*, 1982). The latter may have the advantage of not suffering from contamination due to protons knocked out from the nucleus. To describe how the charged particles are distributed in momentum, more recent interest has focused on (c) the number of charged particles m observed in a limited rapidity window Δy, with distribution $P(m,\Delta y)$ and average $\bar{m}(\Delta y)$ (Bailly *et al.*, 1988) and also on (d) the analogous distribution $P_-(m_-,\Delta y)$ for the number of negative charges m_- (Dengler *et al.*, 1986).

We summarize below the main experiments and the quantities reported.

Reference	Nuclei	Energy/nucleons GeV	Measurements
De Marzo *et al.* (1982)	p+Xe, Ar	200	a, b
Dengler *et al.* (1986)	p+Xe, Ar	200	c, d
Bailly *et al.* (1988)	p+Au, Al	360	c

Table 1: Summary of experimental measurements

It is recognized that these experimental observations involve fairly complicated processes and dynamics, and only relatively simple theoretical models have been advanced. Not many models can give satisfactory description for all the features (a)-(d) of the experimental data. A few years ago Cai, Chao and Meng (1987) extended their statistical model to describe the multiplicity distribution of hadron-nucleus scattering in the full rapidity window. In their paper, they also investigated the dependence of the negative charged multiplicity distributions on various rapidity windows. The multistring model VENUS, constructed by Werner (1989), gave satisfactory agreement with all the feature (a)-(d) of the data. Recently Lam, Kiang and Ochiai (1989) have proposed a model which combines the geometrical picture and the wounded nucleon model, to describe the charged multiplicity distribution in different rapidity windows. Except

for the result in the backward hemisphere for large windows, their model gave good agreement with the data. Besides, other models such as the geometrical branching model (Hwa and Wang, 1989) and the Lund FRITIOF (Bailly *et al.*, 1988) have also been constructed to describe the multiplicity distribution for hadron-nucleus scattering.

In this paper, we build upon three ideas in order to construct a model to account for the experimental data.

The first idea is the geometric model, which thinks of the incident hadron interacting at a specific impact parameter b, and, in fact, with a tube of nuclear matter at b. The observed distribution is the sum over all b's, weighted by the interaction probability. This picture was first successfully applied to hadron-nucleus scattering by Kiang *et al.* (1985) and is found to account very well for the distribution in the full window P(n), see for example Biswas *et al.* (1986).

The second idea is the statistical or thermodynamic model, which has a long history dating back to Fermi (1950) and Landau (1953). It was improved (Feymann, 1969) to take account of some important features of high energy scattering, including the observation of limited transverse momenta, leading particles which do not thermalize, and the need to specify the impact parameter for each event; this version of the statistical model has come to be known as the partition temperature model. Li and Young (1986) further improved the partition temperature model to take account of momentum conservation, so that the mean rapidity of the produced particles depends on the center of mass velocity of the interacting system, which in turn depends on the mass of the

effective target, i.e. the tube. This input successfully accounts for the shift of the rapidity distribution to smaller y with increasing target mass, and will of course be crucial when we wish to discuss the distribution in a given rapidity window.

The third idea is that of independent emission of produced particles, which allows us to go from the average number of observed particles in a window $\bar{m}(\Delta y)$ to the probability for finding m particles in the window, essentially through a binomial distribution. This idea was found to be reasonable in hadron-hadron scattering (UA5, 1983) provided that clusters of two particles are assumed to be emitted independently.

By unifying these three ideas, we can arrive at a model which accounts quite well for all the features (a)-(d) of the data.

3.2 Formalism

According to the geometrical model, the charged multiplicity distribution for the whole nucleus is just the superposition of the uncorrelated distribution at each impact parameter b. For a fixed b, the incident hadron is usually considered to be colliding with a tube-like target with cross-section area d^2b. The relative probability that a collision occurs at b is given by $d\sigma_i(b)/\sigma_i^{hA}$. where $d\sigma_i(b)$ is the inelastic cross section at b:

$$d\sigma_i = d^2b \left(1 - e^{-\sigma t(b)} \right) \qquad (3.1)$$

where σ is the inelastic p-p cross-section fitted by (Amaldi, 1973)

$$\sigma = 26.8 \text{ mb } (E/\text{GeV})^{0.037} \qquad (3.2)$$

for 5 GeV < E < 1500 GeV and t(b) is the thickness of the tube-liked target with matter density $\rho(r)$

$$t(b) = \int dz\, \rho(r), \qquad r = \sqrt{z^2 - b^2}\,.$$

The hA inelastic cross-section is given by

$$\sigma_i^{hA} = \int d\sigma_i(b)\,.$$

For heavy nuclei (A>30) $\rho(r)$ is well described by the Woods-Saxon form

$$\rho(r) \propto [1 + \exp(\frac{r-R}{s})]^{-1}\,, \qquad R = R_o A^{1/3} \qquad (3.3)$$

where s = 0.545 fm, R_o = 1.12 fm and ρ is normalized to A:

$$A = \int \rho(r)\, d^3r\,. \qquad (3.4)$$

Furthermore the average charged multiplicity $\bar{n}$ for the whole nucleus and the average at each impact parameter b, $\bar{n}(b)$, can be described by the well-known phenomenological formula (Chao, Hegab and Hufer, 1983)

$$\bar{n}(E,\bar{\nu}) = \bar{n}^{hN}(E)\ [1+k(\bar{\nu}-1)]; \qquad (3.5a)$$

$$\bar{n}(E,\bar{\nu}(b)) = \bar{n}^{hN}(E)\ [1+k(\nu(b)-1)] \qquad (3.5b)$$

where $\bar{n}^{hN}(E)$ is the average charged multiplicity of p-p scattering and is parameterized as (Thomé *et al.*, 1977):

$$\bar{n}^{hN}(E) = 1.2 + 0.59*\ln(E/GeV) + 0.12*(\ln(E/GeV))^2 \qquad (3.6)$$

and $\bar{\nu}$, $\nu(b)$ are the average numbers of collisions for the whole nucleus and at fixed b respectively, defined as

$$\nu(b) = \frac{\sigma t(b)}{1 - e^{-\sigma t(b)}}, \qquad (3.7)$$

$$\bar{\nu} = \frac{\int d^2b\ (1-e^{-\sigma t})\ \nu(b)}{\int d^2b\ (1-e^{-\sigma t})} = A\sigma/\sigma_i^{pA}. \qquad (3.8)$$

The parameter k is found to be around 0.5 (Chao, Hegab and Hufer, 1983).

For events at a given impact parameter b, let $p(m,\Delta y,b)$ be the probability distribution of finding m charged particles in a fixed rapidity window Δy. Then the observed total probability distribution of particles is just the summation of the elementary distribution at each b, weighted by the interaction probability:

$$P(m,\Delta y) = \int d^2b\ (1-e^{-\sigma t})\ p(m,\Delta y,b)/\sigma_i^{pA}\ . \qquad (3.9)$$

Indeed the distribution in m as described by $p(m,\Delta y,b)$ arises from two sources: (i) the fluctuation of n around $\bar{n}(b)$, and (ii) the fluctuation in the spatial distribution of the n particle, so that the fraction m/n that falls within Δy may vary from event to event.

3.2.1 Fluctuation around $\bar{n}(b)$

For the full rapidity window, only the first kind of fluctuation contributes. In an earlier paper (Kiang *et al.*, 1985) hadron-nucleon scattering is regarded as the elementary process and universal KNO scaling at each impact parameter is assumed. The elementary distribution is chosen to be that of hadron-hadron scattering, which is parameterized by Slattery (1972) as

$$\begin{aligned}\psi_o(\xi) &= \bar{n}\cdot p(n) \\ &= \frac{1}{2}\,(3.79\xi + 33.7\xi^3 - 6.64\xi^5 + 0.332\xi^7)\exp(-3.04\xi)\ ,\end{aligned} \tag{3.10}$$

where $\xi = n/\bar{n}$. Although the assumption is over-simplified (e.g there is evidence that the fluctuation of n around $\bar{n}(b)$ varies as $\nu(b)^{-1/2}$ (De Marzo *et al.*, 1982)), the result of the simple model still fits the experimental data very well. This reflects the fact that the total probability distribution is quite insensitive to the width of the elementary distribution $p(n,b)$.

However, the previous assumption implies a slight violation of the conservation law of charges, which becomes important if we wish to discuss negative charge. Let us consider

an incident proton colliding with a target of thickness t(b) and effective cross section area $f\sigma$, where σ is the elastic p-p cross section and $f \sim 1$ is a parameter to be specified. In the target, there should have $f\sigma t(b)Z/A$ positive charges. Then the net charge of the colliding system q_+, including the incident proton, should be equal to $1 + f\sigma t(b)Z/A$. Hence the net charge of the emitted particles should also be equal to q_+, and it is impossible for the number of produced particles, n, to be less than q_+. But the Slattery distribution implies that any $n > 0$, no matter how small, is possible. To avoid this conflict with the conservation law, we modify the Slattery distribution as follows. We describe the system as q_+ positive charges plus τ neutral pairs, $\tau = (n-q_+)/2$, where n is the total number of charged particles emitted. We assume that the distribution of τ around $\bar{\tau}$ is given by the Slattery distribution, with $\tau \geq 0$. Thus the probability that the number of produced particles, n, being less than q_+ is zero. Hence the elementary distribution at b is given by

$$p(n,b) = \begin{cases} 0 & n \leq q_+ , \\ (\bar{n}(b) - q_+)\psi_o(\xi) & n > q_+ . \end{cases} \tag{3.11}$$

where now

$$\xi = \tau/\bar{\tau} = \frac{n - q_+}{\bar{n}(b) - q_+}. \tag{3.12}$$

This guarantees the conservation law of charge is retained. Furthermore in $\bar{p}$-p scattering where q_+ is equal to zero, our model

gives the old result that the distribution in n is Slattery. With this correction, the width of the new elementary multiplicity distribution varies with $\nu(b)$ and is sharper than the Slattery distribution. Hence compared with our old result, the new over-all charged multiplicity distribution in the full rapidity window is shaper. However the difference between the two models is not significant (Fig. 3.1).

It should be noticed that according to the model stated above, the multiplicity distribution of the negative particles at each impact parameter b is just given by the Slattery distribution. Similar calculation as that of all charge multiplicity distribution for full rapidity window can be carried out for the negative particle distribution and our result is shown in Fig 3.2, which shows good agreement with the experimental data of De Marzo *et al.*, (1982). Furthermore we will make use of this idea later to discuss the distribution of negative particles in different rapidity windows.

3.2.2 Fluctuation in spatial distribution

For the particle distribution in a limited rapidity window Δy, we need to confront the problem of the spatial fluctuation of the particle distribution.

Let $\bar{m}(b,\Delta y)$ be the average number of particles emitted in a rapidity window Δy for collision at a given b. Hence the average probability that a particle is emitted into Δy is

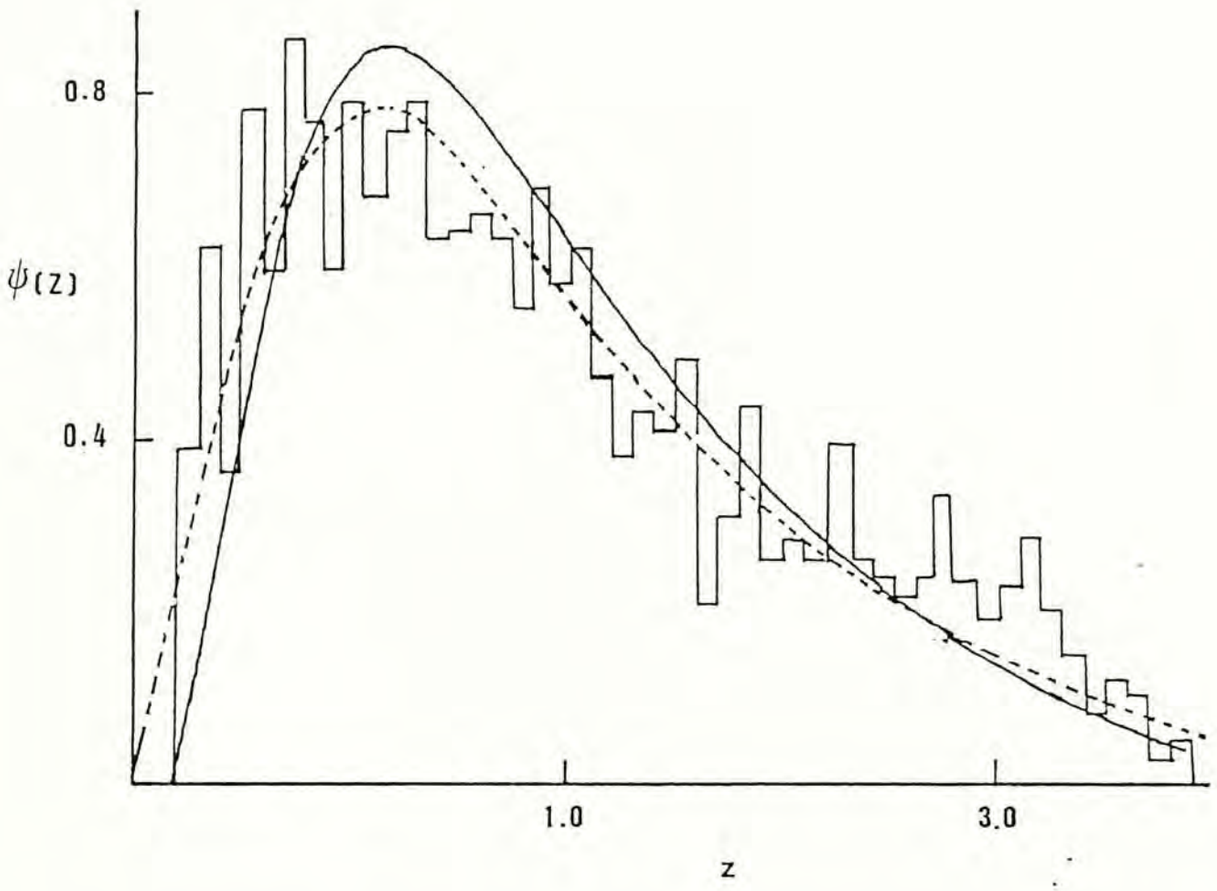

Fig. 3.1 Calculated multiplicity distribution for all charged particles, compared with the experimental data (C. De Marzo *et al.*, 1982) for p + Xe at 200 GeV. The solid curve and the dashed curve represent the calculated results for our new model and that proposed earlier respectively.

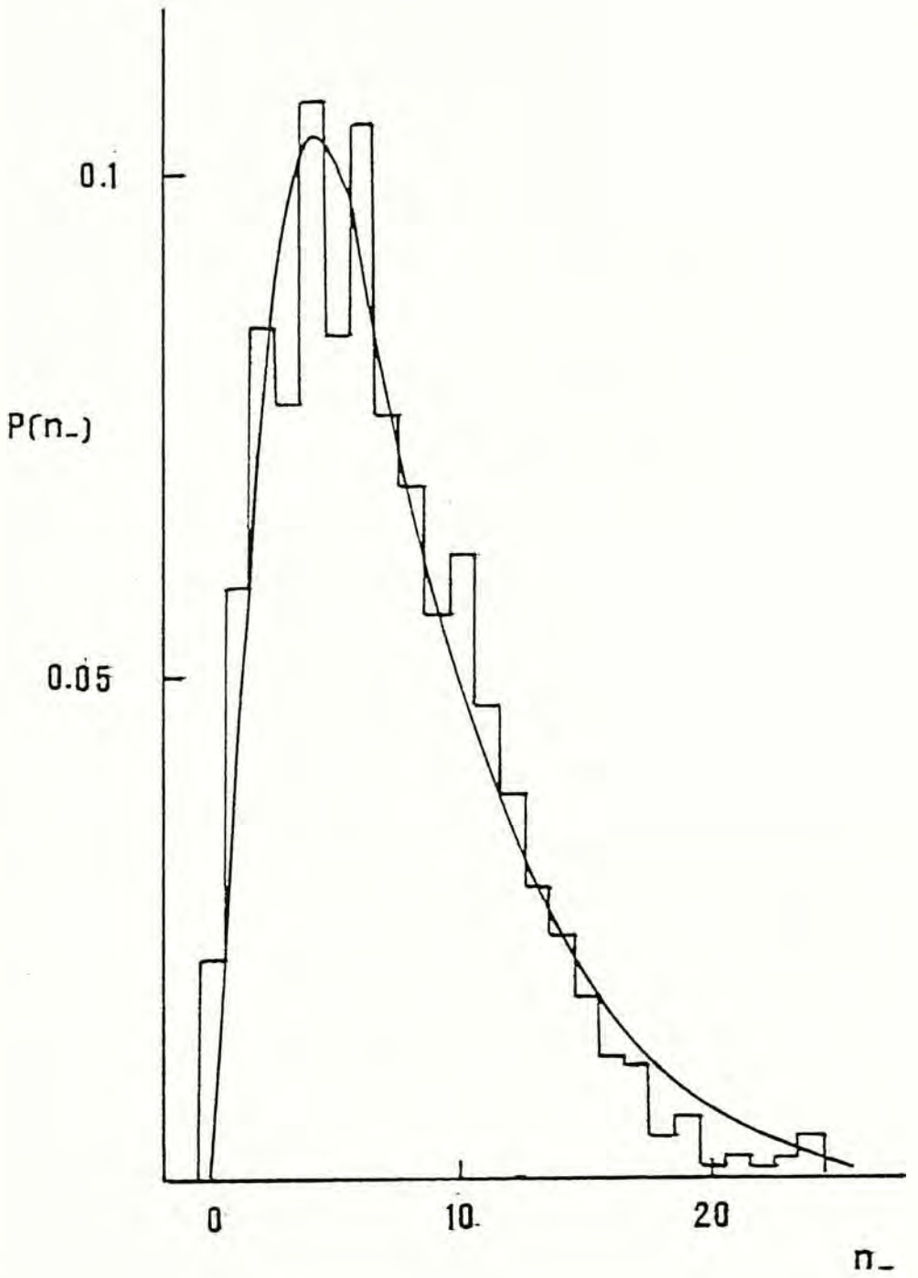

Fig. 3.2 Calculated multiplicity distribution for negative charged only (solid curve), compared with the experimental data (C. De Marzo *et al.*, 1982) for p + Xe scattering at 200 GeV.

$$q(b,\Delta y) = \bar{m}(b,\Delta y)/\bar{n}(b) \quad . \tag{3.13}$$

Then, making the assumption of independent emission, of the n particles produced in an event, the probability that any m will be observed in Δy is

$$Q(m,n,\Delta y,b) = C_m^n \, q(b)^m \, (1-q(b))^{n-m} \quad , \tag{3.14}$$

where C_m^n is the binomial coefficient. Since there is experimental evidence that the produced particles are probably emitted in clusters of s particles (probably s = 2) (UA5, 1983), the above probability distribution should be modified to be

$$Q(m,n,\Delta y,b) = \frac{1}{s} C_{m/s}^{n/s} \, q(b)^{m/s} \, (1-q(b))^{(n-m)/s} \quad . \tag{3.15}$$

We shall adopt Eq.(3.15) in the rest of this report.

3.2.3 Partition-temperature model

Hence the only task left is to determine $\bar{m}(b,\Delta y)$. Once $\bar{m}(b,\Delta y)$ is determined, the problem can be solved. In this paper, the partition-temperature model, which was introduced by Chou, Yang and Yen in 1985, is used. The essential physics of the partition temperature model is that the collision is assumed to be so violent and the number of the produced particle is so large that the colliding system can be treated as a canonical ensemble with temperature T. This thermodynamic model was generalized to

hadron-nucleus scattering a few years ago (Li and Young, 1986), with satisfactory agreement with the experimental data.

By the partition temperature model, the charged-one-particle distribution is obtained by maximizing the entropy S, $= \int F \ln(F)\, d^3p/E$, under the two constraints: (i) Conservation of energy; (ii) Conservation of momentum. The charged-one-particle distribution in laboratory frame as result is given by

$$dn = B\, g(p_\perp) \exp(\lambda p_z - E/T) \frac{d^3p}{E} \qquad (3.16)$$

where $g(p_\perp) = \exp(-\alpha p_\perp)$ is the transverse-momentum cutoff factor. Fitted with the experimental value of $\langle p_\perp \rangle$ (De Marzo *et al.*, 1984), α is chosen to 4.2 GeV^{-1}. While the two parameters 1/T and λ are the Langrange multipliers for the two constraints, i.e. conservation of energy and momentum. Alternatively the exponential factor $\exp(\lambda p_z - E/T)$ can also be understood as the result of the Lorentz transform of the Boltzmann factor $\exp(-E^*/T^*)$ in the center-of-mass frame to the laboratory frame with a velocity β

$$E^* = \gamma(E - \beta p_z) , \qquad \gamma = (1 - \beta^2)^{-1/2} \qquad (3.17)$$

with the identification

$$\frac{1}{T} = \gamma/T^* , \qquad \lambda = \gamma\beta/T^* . \qquad (3.18)$$

To evaluate the distribution of rapidity y, we assume that all the produced particles are pions (chapter 2, section

2.1.3A). In addition, owing to the limitation of experimental setup, only particles with momenta greater than a certain value, which depends on experimental setup, are detected. Hence a cutoff should be imposed in the integral of Eq.(3.16). Since Eq.(3.16) is normalized to $\bar{n}(b)$ as in Eq.(3.5b), the normalization constant B can be determined. Hence there are in total two free parameters λ and T in our model. Instead of using λ and T as our fitting parameters, the effective mass of the target M and the inelasticity h, both with clear physical meaning, would be used.

By Eq.(3.16) the total energy carried by the produced particles is

$$hE_o = \frac{3}{2} \int E \, dn \tag{3.19}$$

where the factor 3/2 accounts for the neutrals. T is chosen so that the equation is satisfied.

The total energy of the colliding system is $E_t = hE_o + M$ and the total momentum of the colliding system is $p_t = hE_o$. Hence

$$\beta = hE_o/(hE_o+M) \tag{3.20}$$

and

$$M \sim hE_o/(2\gamma^2) \tag{3.21}$$

It is seen that the target mass M will determine γ (assuming h is known). Let us think of the target as a tube of length t(b) and area $f\sigma$, where $f \sim 1$ as mentioned above. Thus

$$M = f\sigma t(b) m_p \, . \tag{3.22}$$

We shall use the parameter f instead of M, because f has a clearer physical meaning: it is the ratio of the effective target cross-section to the normal collision cross-section σ, and thus we expect $f \sim 1$. Since in reality, interaction exists between the tube-like target and the rest of the nucleus, f should be slightly greater than 1.

Given the thermodynamic model, the one particle distribution is known, and hence the probability $q(b,\Delta y)$ for any particle to be observed in the window Δy is given by Eq.(3.13) with

$$\bar{n}(b,\Delta y) = \int_{\Delta y} dn \quad ,$$

$$\bar{n}(b) = \int_{-\infty}^{\infty} dn$$

where dn refers to the expression (3.16) with the parameters chosen as described above for the given b. Hence the probability distribution in Δy at b is

$$P(m,\Delta y,b) = \sum_{n=m}^{n=\infty} \frac{1}{s} C_{m/s}^{n/s} \, q(b)^{m/s} \, (1-q(b))^{(n-m)/s} \, p(n,b) \; . \qquad (3.23)$$

Finally superimposing over b, the multiplicity distribution in Δy is

$$P(m,\Delta y) = \int d^2b \, \frac{(1-e^{-\sigma t})}{\sigma_i^{pA}} \sum_{n=m}^{n=\infty} \frac{1}{s} C_{m/s}^{n/s} \, q(b)^{m/s} \, (1-q(b))^{(n-m)/s} \, p(n,b). \qquad (3.24)$$

Notice that if we were to assume that q(b)=q is independent of impact parameter b, then the spatial fluctuation factor $\frac{1}{s} C^{n/s}_{m/s}$ $q(b)^{m/s}$ $(1-q(b))^{(n-m)/s}$ can be pull out of the integral and Eq.(3.24) would be reduced to the simple form with trivial meaning:

$$P(m,\Delta y) = \sum_{n=m}^{n=\infty} \frac{1}{s} C^{n/s}_{m/s} q^{m/s} (1-q)^{(n-m)/s} p(n) \qquad (3.25)$$

where p(n) is just the charged multiplicity distribution of hadron-nucleus scattering in the full rapidity window. As a primitive test, Eq.(3.25) can be evaluated by substituting the experimental data for p(n), and q is determined by $q = \bar{m}/\bar{n}$, where $\bar{m}$, $\bar{n}$ are experimental data for the whole nucleus. This approximate formalism was used by Cai, Chao and Meng (1987). In Fig. 3.3, we show $q(b,\Delta y)$ against b for different rapidity window Δy for p+Au collision at 360 GeV. As Fig. 3.3 showns, except at large value of b_I, $q(b,\Delta y)$ only varies slightly. As the interaction probability $1 - e^{-\sigma t}$ drops to zero at the periphery, $q(b,\Delta y)$ at large b_I does not affect the result at all. Hence the assumption that $q(b,\Delta y)$ is constant does not deviate much from the fact.

3.2.4 Negative charged particles

To evaluate the negative charged particle distribution, several replacement in Eq.(3.24) should be made. The elementary

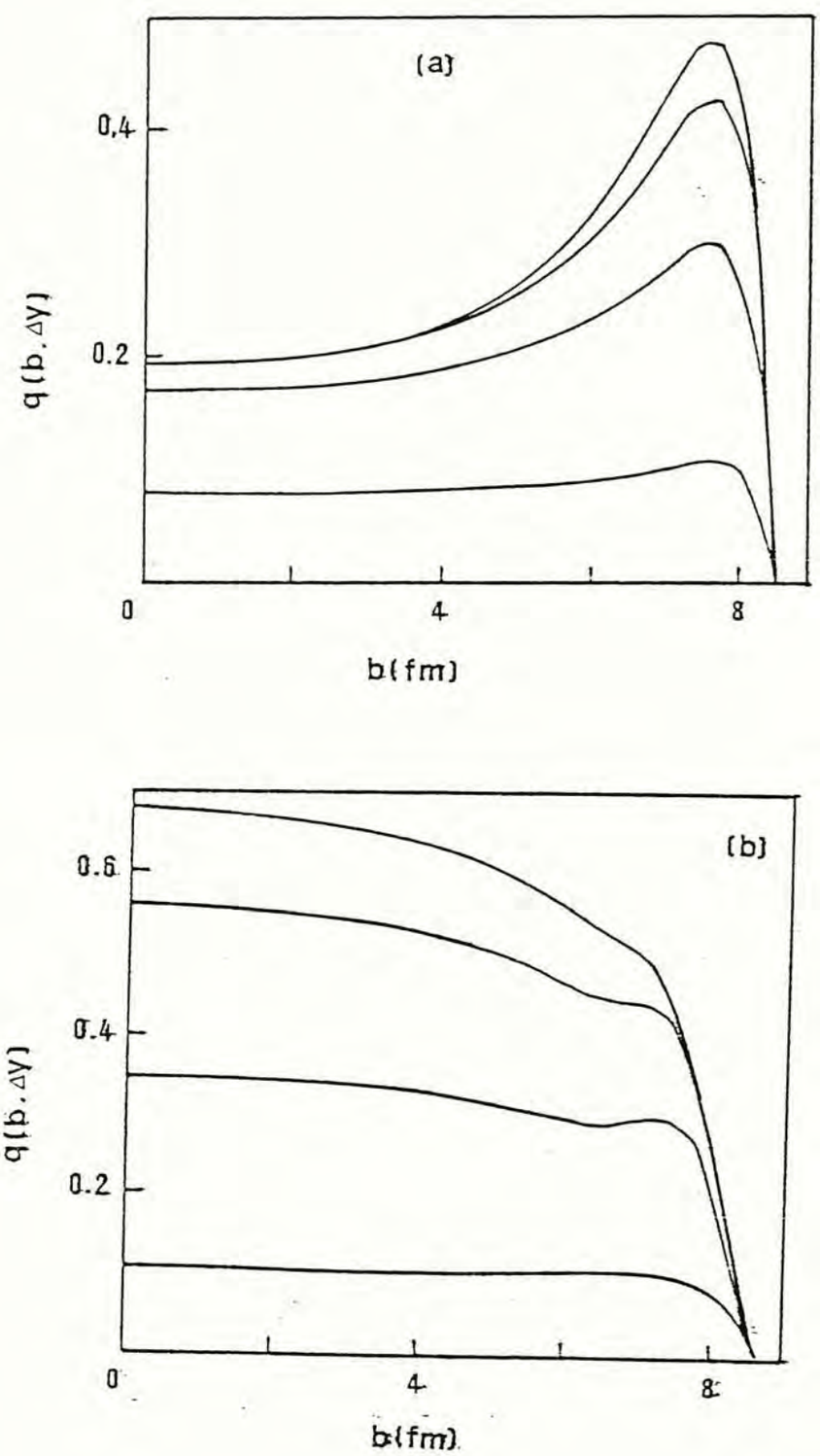

Fig. 3.3 a-b q(b,Δy) Vs b for different rapidity window Δy for p + Au scattering at 360 GeV for (a) forward and (b) backward hemisphere. The intervals from the top to bottom are Δy = 3.5, 2.5, 1.5, 0.5.

multiplicity distribution of all charged particle should be replaced by that of the negative charged particle, which is simply Slattery as we have pointed out before. By conservation of charge, the average multiplicity of negative particles at each impact parameter b is given by

$$\bar{n}_-(b) = (\bar{n}(b) - q_+(b))/2. \qquad (3.26)$$

Furthermore s should be set to 1 in Eq.(3.24) instead, since particles of a given charge are emitted singly. With all these changes the multiplicity distribution of negative charged particle can be evaluated as that of all charged particle.

3.3 Discussion

Fig. 3.5-8 show our results for p+Xe scattering compared with the experimental data by Dengler *et al.* (1986). The free parameters h, f and k are chosen to be 0.7, 1.3 and 0.544 respectively, such that the total average multiplicity $\bar{n}$ and the dn/dy distribution are fitted with the experimental data by De Marzo *et al.* (1982) (Fig. 3.4). For simplicity, h and f would be assumed to be independent of b. It should be pointed out that in the experimental data of Dengler *et al.*, the slow charged particles which are believed to be knocked out from the spectators by the incident proton during the collision have not been excluded. And such particles are not considered in our model. Therefore the average multiplicity given by Dengler *et al.* is

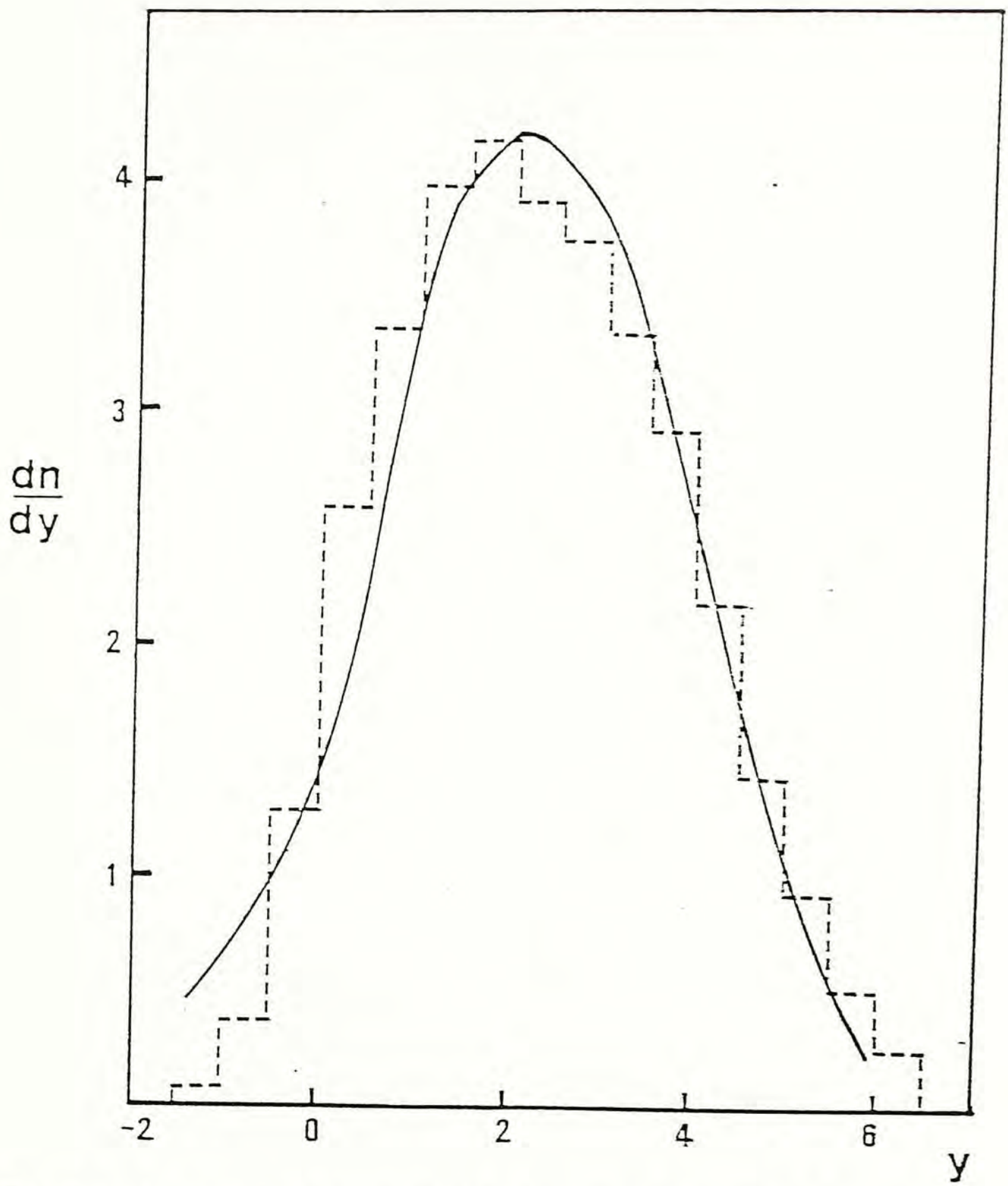

Fig. 3.4 Rapidity distribution dn/dy for p + Xe scattering at 200 GeV. The histogram is the experimental data (C. De Marzo *et al.*, 1982) and the solid line is the fitted result of the present model with f = 1.3, h = 0.7 and k = 0.544.

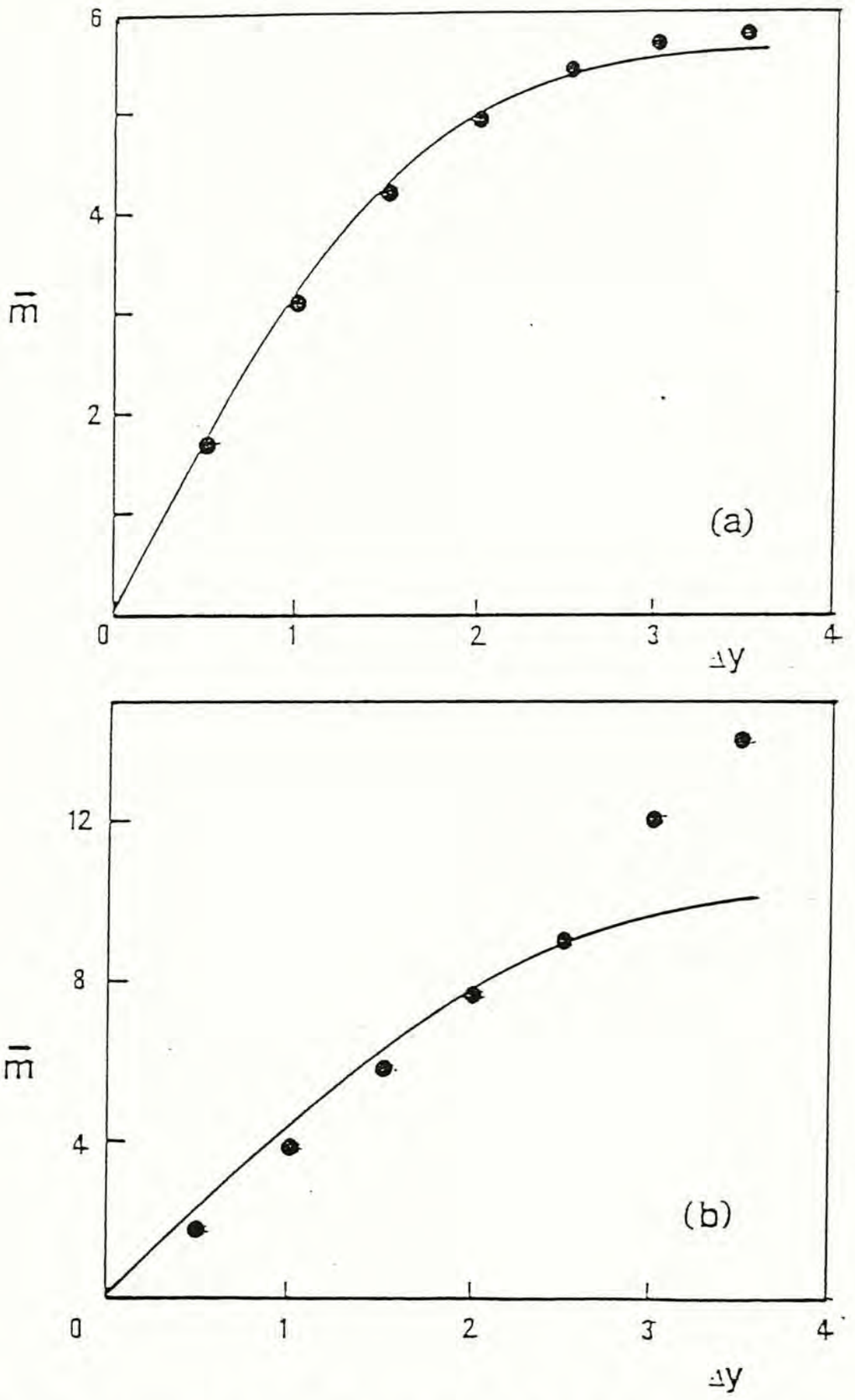

Fig. 3.5 a-b Average charged multiplicity $\bar{m}$ as a function of rapidity intervals Δy for p + Xe collision at 200 GeV: (a) for the forward hemisphere, and (b) for the backward hemisphere. The experimental data are taken from F. Dengler *et al.* (1986) and the solid line is the result of our model.

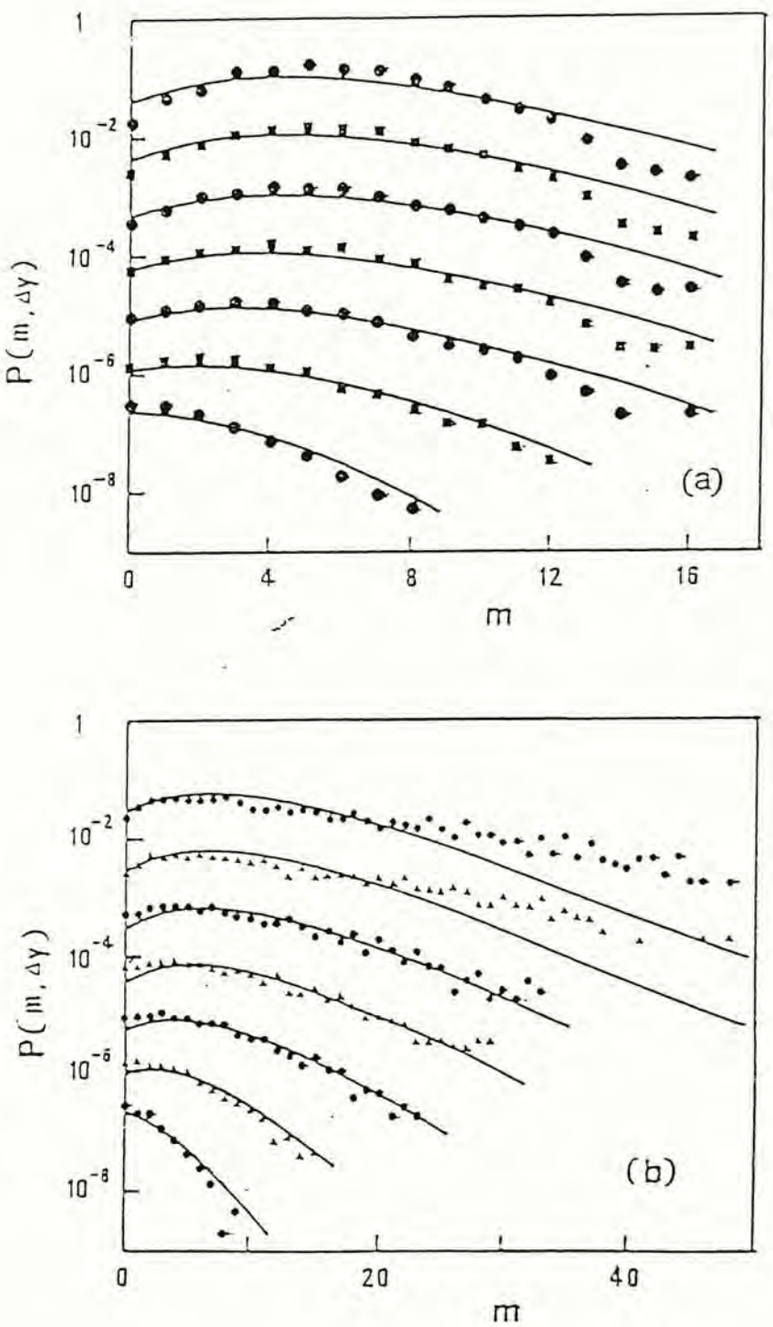

Fig. 3.6 a-b The multiplicity distribution $P(m,\Delta y)$ for all charged particles in various rapidity intervals Δy for p + Xe collision at 200 GeV. The data (F. Dengler *et al.*, 1986) for the largest rapidity interval are referred to the vertical scale shown, and each consecutive one is scaled down by an additional factor of 10: (a) for the forward hemisphere and (b) for the backward hemisphere. The intervals from the top to bottom are Δy = 3.5, 3.0, 2.5, 2.0, 1.5, 1.0, 0.5. Our results are shown by the solid lines.

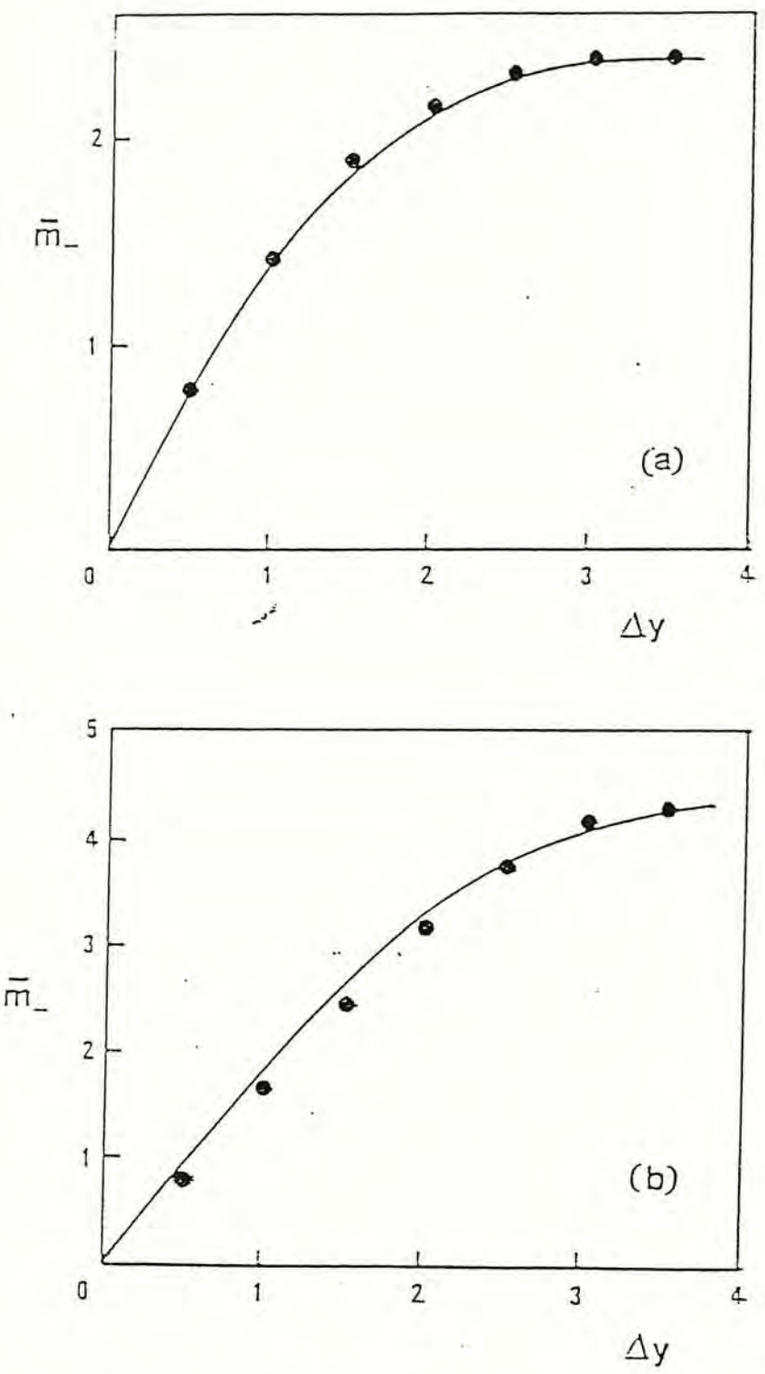

Fig. 3.7 a-b Same as Fig. 3.5, but for negative multiplicity $\bar{m}_-$ in p + Xe collision.

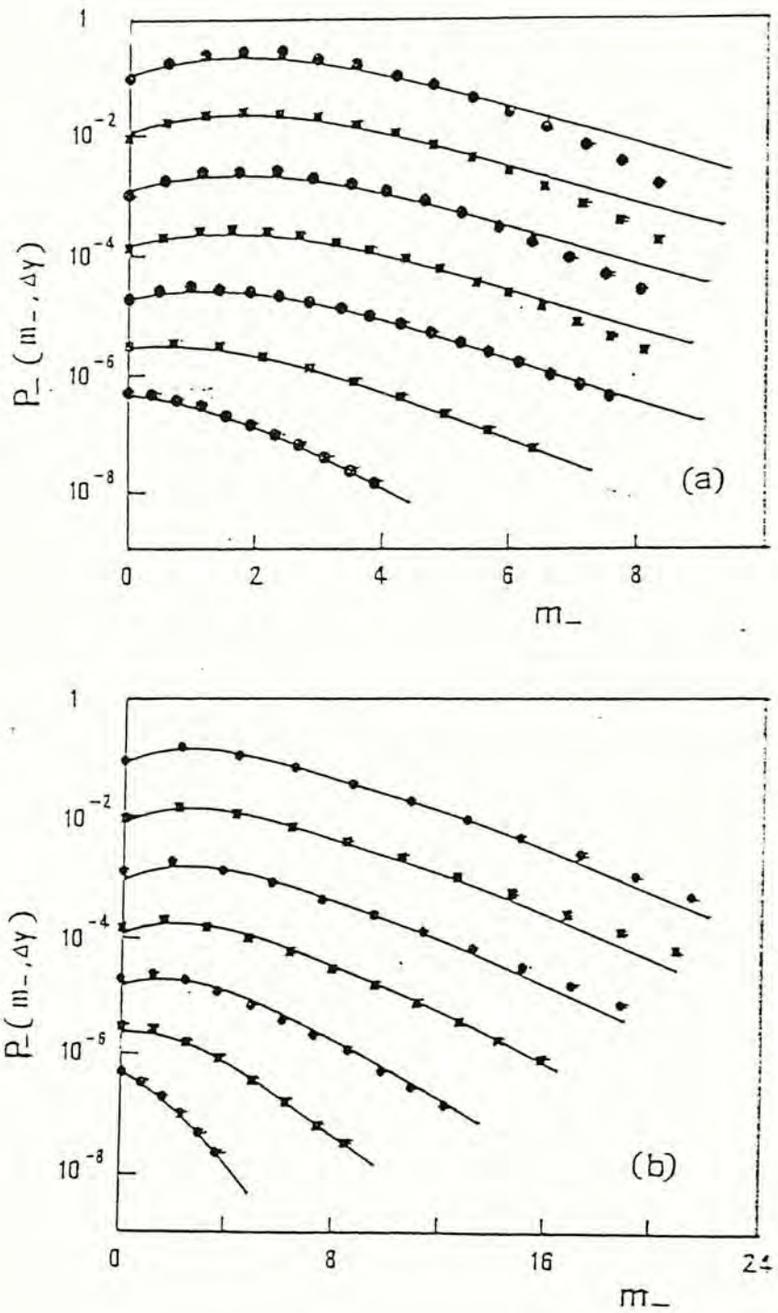

Fig. 3.8 a-b Same as Fig. 3.6, but for negative multiplicity distribution $P_-(m_-,\Delta y)$.

greater than that of the produced particles by De Marzo *et al.*. In spite of this reason, our model still gives satisfactory results which do not deviate very much from the experiment data of all charged particle distribution Fig. 3.5 and 3.6.

For negative charged particles, where the problem of contamination does not exist, our result fits the experimental data extremely well (Fig. 3.7-8).

Fig. 3.9 and 3.10 show our results on p+Au scattering at 360 GeV and compared with the experimental data by Bailly *et al.* (1987). The free parameters h, f and k are determined by fitting to the average multiplicity in different rapidity windows directly, Fig. 3.9, so the slow charged particle is also included. h, f, and k are chosen to 0.65, 2.0 and 0.69 respectively. Comparing with that of p+Xe scattering, f is much greater in p+Au scattering. This is due to the fact that this time we fit the data directly, which include the slow charged particle. Hence the target seems to be much heavier.

3.4 Conclusion

In this paper we combine the geometric picture and the partition temperature model to evaluate the multiplicity distribution of charged particle in different rapidity windows in hadron-nucleus scattering. Our idea has not been completely tested in the result of all charged particle distribution, because the experimental data of charged particle is contaminated by other charged particles originated from other processes beyond our

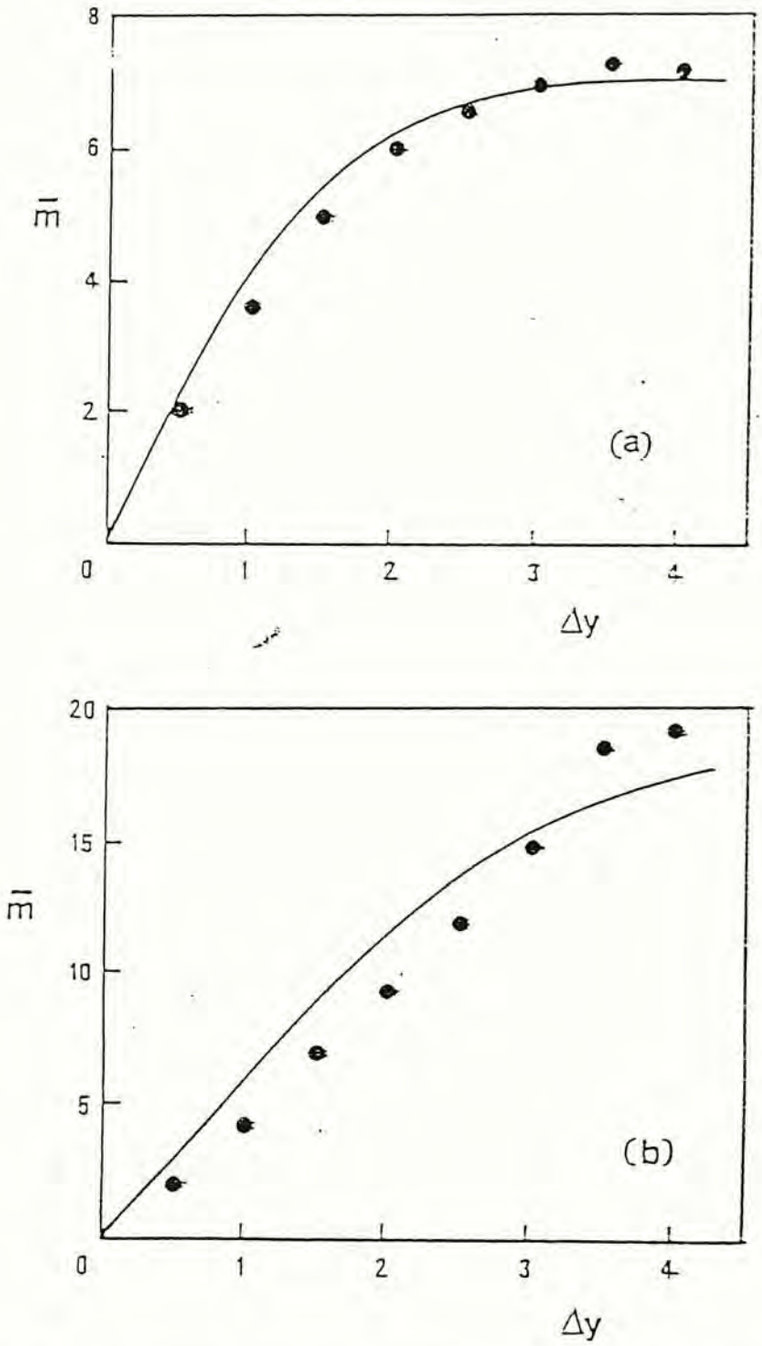

Fig. 3.9 a-b Average charged multiplicity $\bar{m}$ as a function of rapidity intervals Δy for p + Au collision at 360 GeV: (a) for the forward hemisphere, and (b) for the backward hemisphere. The solid line is our fitted result with f = 2.0, h = 0.65 and k = 0.69, compared with the experimental data (J. L. Bailly *et al.*, 1988).

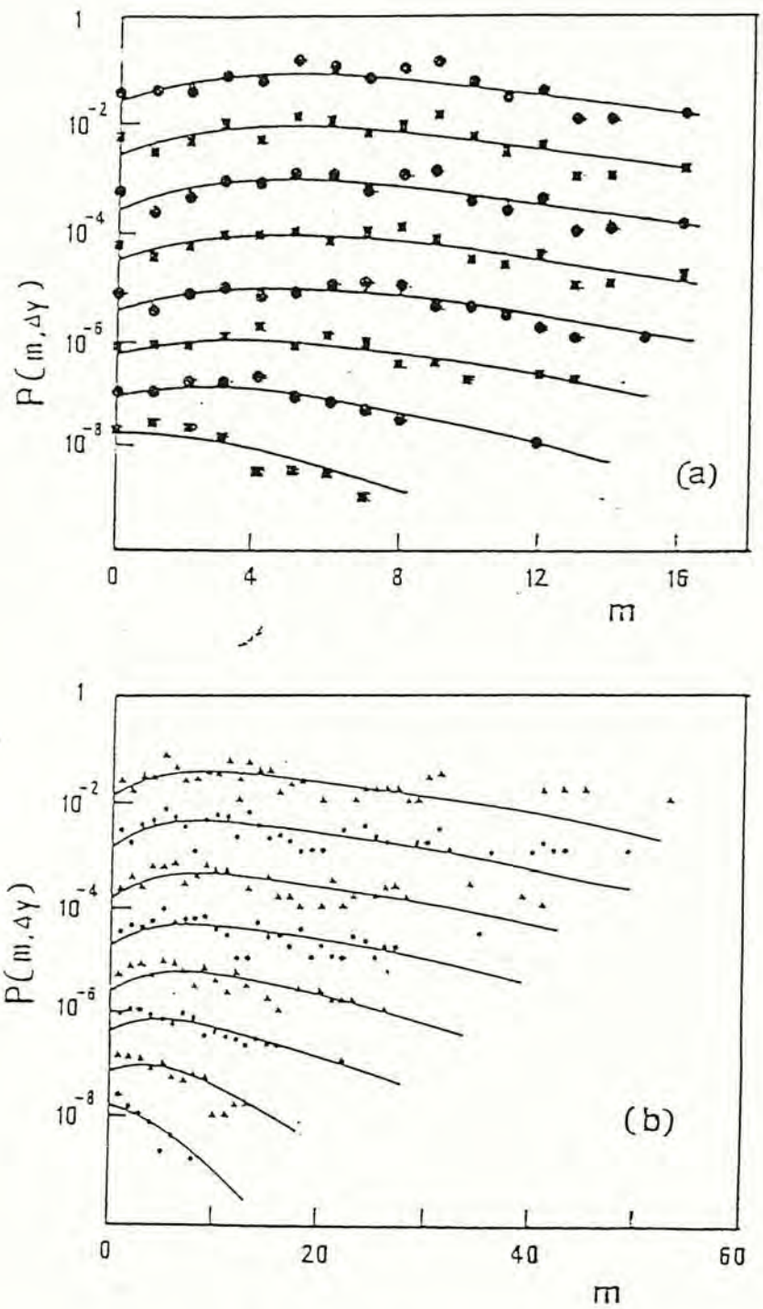

Fig. 3.10 a-b Same as Fig. 3.6, but for p + Au collision at 360 GeV, data from J. L. Bailly *et al.* (1988). The intervals from the top to bottom are Δy = 4.0, 3.5, 3.0, 2.5, 2.0, 1.5, 1.0, 0.5.

consideration. However in the multiplicity distribution of negative charged particle, our idea is being tested with satisfactory result. It should be noticed that in our calculation of negative charged particle distribution no further assumption and free parameter are used. All the free parameters are determined in the calculation of all charged particle distribution. Furthermore to retain the conservation law of charge in our model, we have slightly modified the elementary multiplicity distribution and relaxed the hypothesis of universal KNO scaling at each impact parameter which we proposed before.

Chapter 4

Geometric Model for Multiplicity Distribution in Nucleus-Nucleus Scattering

4.1 Introduction

In the past few years much more attention has been attracted to inelastic nucleus-nucleus scattering and recently experimental data for nucleus-nucleus scattering have been available. These experimental data include the multiplicity distribution for ^{16}O+Cu and ^{16}O+Au scattering at 200 and 60 GeV/nucleon for the full window (NA35, 1988) (Fig. 4.1). Besides, the WA80 and E802 collaboration (1988) have also published the result for the multiplicity distribution of nucleus-nucleus scattering in limited rapidity windows (Fig. 4.2). All these experimental data show the following similar features:

a. For small z ($0.1 \lesssim z \lesssim 1$), the distribution decreases with increasing z;

b. For the region $1 \lesssim z \lesssim 2.5$, the distribution is nearly constant;

c. An abrupt break is observed at large z ($z \simeq 2.5$).

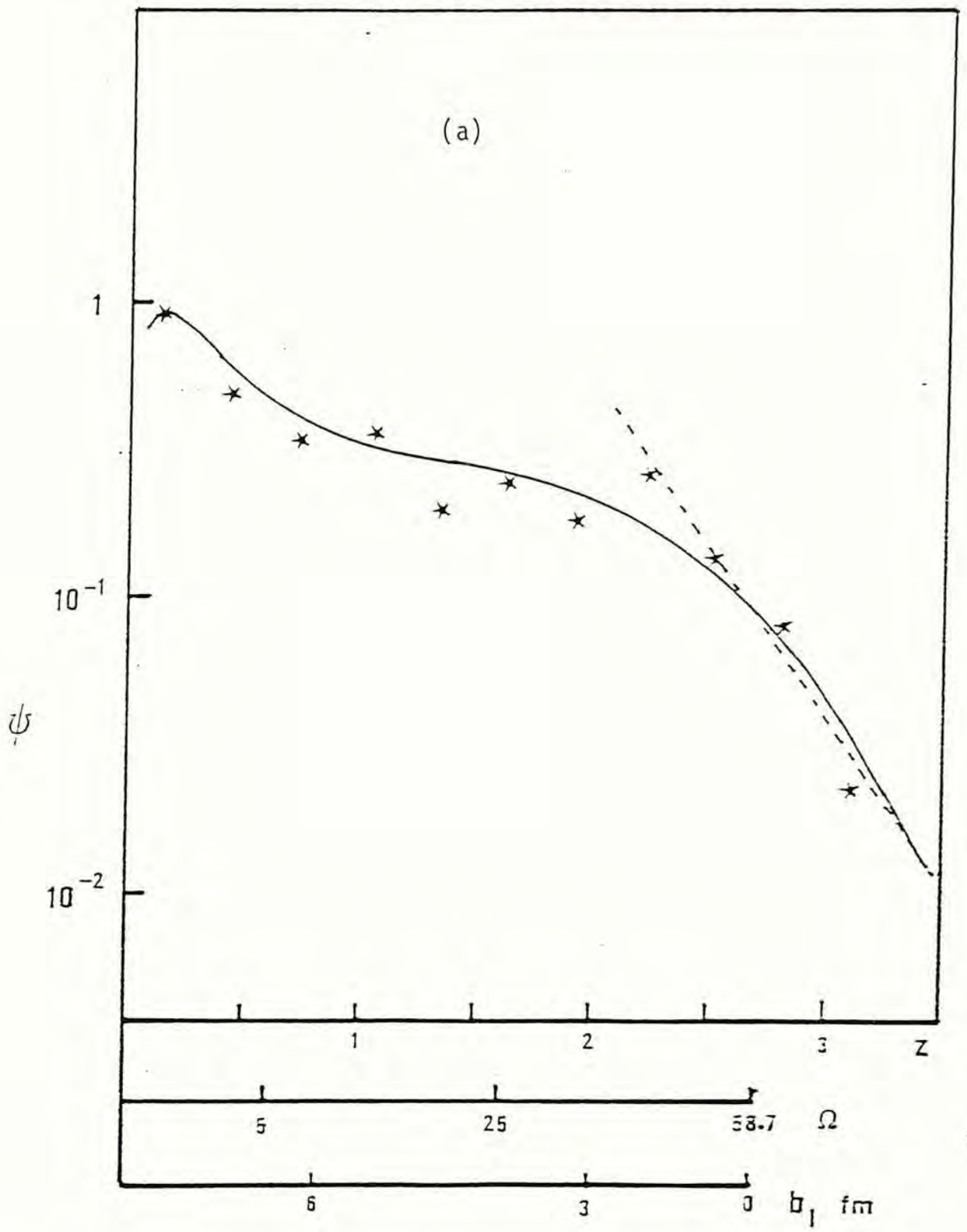

Fig. 4.1 a-b The normalized multiplicity distribution $\psi(z)$ versus $z = n/\langle n \rangle$. The additional horizontal axes are explained in Section 4.2.3. Stars: negative charge only; circles: all charges. The solid lines are the predictions of our Model 3 in Section 3. The broken lines are fits to $\exp(-\alpha z)$ in the region beyond the break. (a) O + Cu at 200 GeV/nucleon; $\alpha = 2.8$, (b) O + Au at 200 GeV/nucleon; $\alpha = 4.2$.

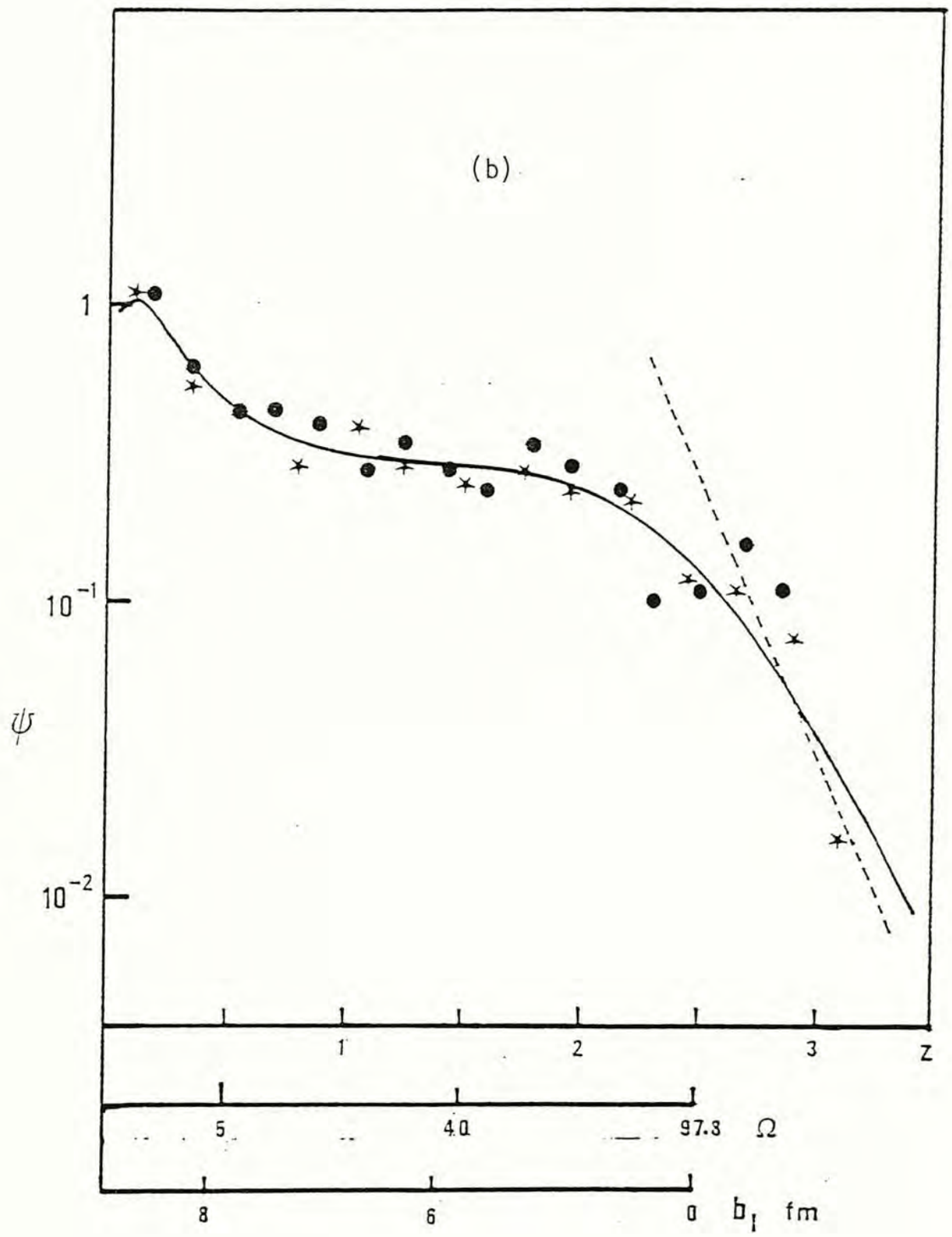
(b)
1
10^{-1}
10^{-2}
ψ
1
2
3
z
5
4.0
97.3
Ω
8
6
0
b_1 fm

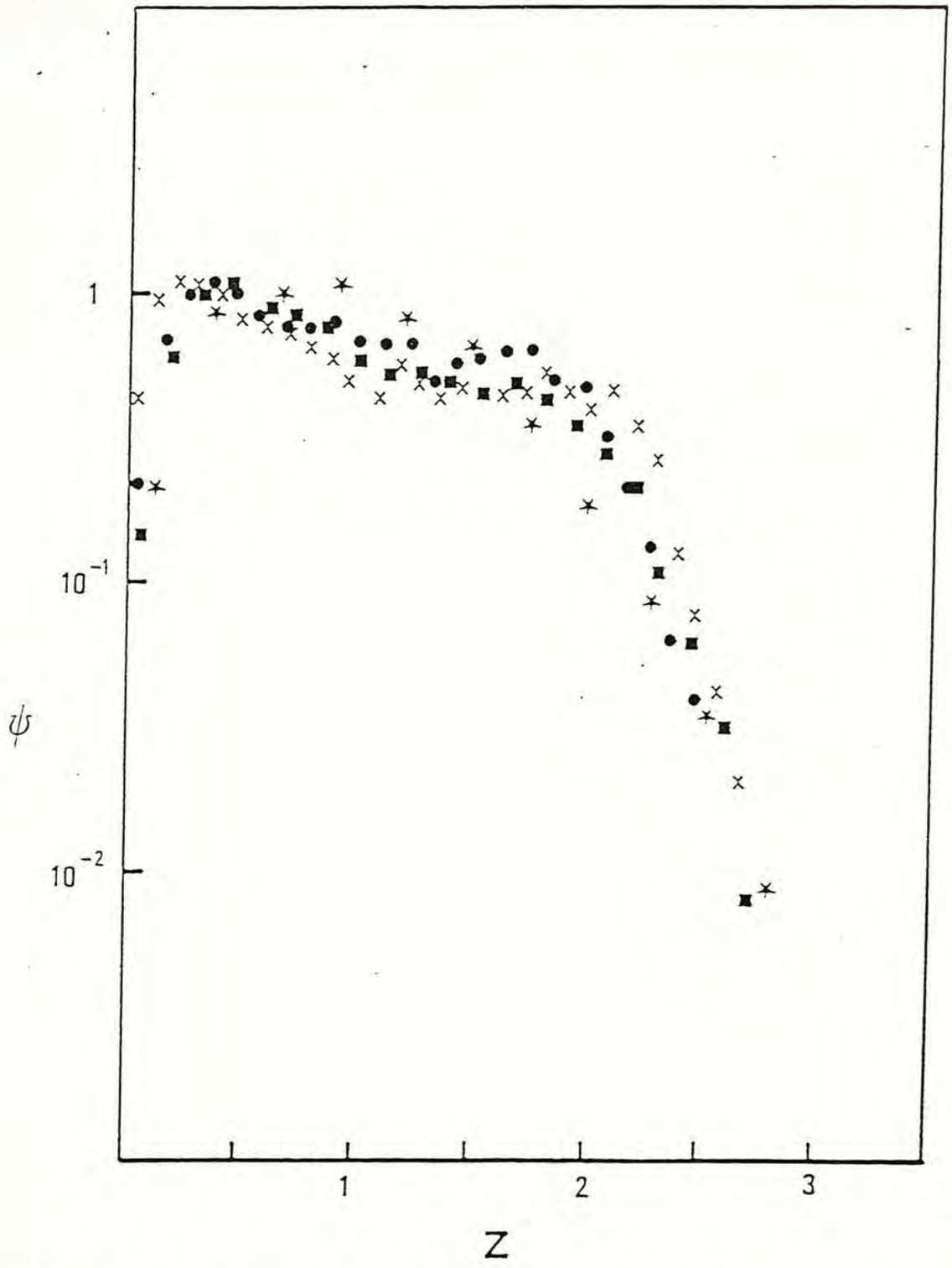

Fig. 4.2 The data on charged particles multiplicity in the pseudorapidity range $-1.7 < \eta < 4.2$ from WA80 (1988) plotted in the variable z. Stars: O+C, square: O+Cu, circles: O+Ag, crosses: O+Au.

All these prominent features are quite different from that of the hadron-hadron and hadron-nucleus scattering at similar incident energy. Until now not many models can give a successful account of these features even though they describe the experimental data of the hadron-hadron and hadron-nucleus scattering very well. For example the FRITOF version of the Lund String model (EMU-07, 1986), the Dual Parton Model of Cappella *et al.* (1987), and the model of Daté *et al.* (1987), based on the hypothesis of universal KNO scaling at each impact parameter, were found not so successful. For the transverse-energy distribution for the nucleus-nucleus scattering, the multisource model (Liu et al., 1988) and the Mutistring Model VENUS (Werner, 1988) give very good description. However for the multiplicity distribution, so far as we konw only the geometrical picture by Chao and Liu (1989), which is basically the same as our model presented here, gives successful description.

Our previous model (Kiang *et al.*, 1985), which was based on the geometrical picture and the hypothesis of the universal KNO scaling at each impact parameter, gives magnificent agreement with the experimental data for the hadron-nucleus scattering, although the universal KNO scaling was later found to be inconsistent with the experimental data (De Marzo *et al.*, 1982). Based on this idea, Daté *et al.* (1987) calculated the result for the nucleus-nucleus scattering, which disagreed with the experimental data. In our work, different from that of Daté *et al.*, we abandon the universal KNO scaling at each impact parameter and replace the elementary distribution with some narrow distributions varied with impact parameter. Indeed, it is one of our themes here to study

the nature of the elementary distribution $\psi_0(z;b_I)$, in particular to see whether it is KNO-like or stochastic. (As we have mentioned before, Chou and Yang have emphasized that the intrinsic distribution in h-h scattering is stochastic.) In the following discussion, we will show how the experimental data for nucleus-nucleus scattering, especially for large n, provide useful testing ground for investigating the nature of $\psi_0(z;b_I)$. Also it should be emphasized that the main attempt in our work is not to get a perfect fitting of the experimental result. We just want to point out the fact that the prominent features of the multiplicity distribution of the nucleus-nucleus scattering is the consequence of the geometrical basis of the scattering. One important feature of the geometrical picture is that the overall result is insensitive to the dynamics. Indeed this idea has been applied to the high energy scattering of the hadron-hadron scattering before (Ling and Young, 1985). And this idea has been verified by the experimental data of $p\bar{p}$ scattering at 900 GeV published recently. This is why the geometrical picture with the over-simplified universal KNO scaling can still describe the hadron-nucleus scattering so well. In the following discussion, it will be seen that even in certain extreme cases, our result does not deviate much from the experimental data.

4.2 Simple Model

4.2.1 Opacity

As usual, the matter density distribution $\rho_A(r)$ of a nucleus with nucleus mass A is parameterized by the Woods-Saxon form as the following:

$$\rho_A(r) = \rho_0\left[1 + \exp(\frac{r - R_A}{s})\right]^{-1} \qquad (4.1)$$

where $R_A = R_0 A^{1/3}$, $R_0 = 1.12$ fm, $s = 0.545$ fm and ρ_0 is fixed by normalization, $\int d^3r\ \rho(r) = A$. Also the thickness function t(b) is defined as

$$t_A(b) = \int dz\ \rho_A(\sqrt{b^2 + z^2}). \qquad (4.2)$$

The same as that in hadron-hadron scattering, the opacity $\Omega(b_I)$, which is just the overlapping matter function in the collision, is equal to the convolution of the thickness function:

$$\begin{aligned}\Omega(b_I) &= \sigma\ t_A \otimes t_B \\ &= \sigma \int d^2b\ t_A(\vec{b})\ t_B(\vec{b}_I - \vec{b})\end{aligned} \qquad (4.3)$$

where σ is the nucleon-nucleon cross section which is well described by Eq.(3.2) in chapter 3.

For a impact parameter b_I, the relative interacting probability $P(b_I)$ is given by the extended Glauber theory (Białas, Bleszyński and Czyż, 1976),

$$P(b_I) = 1 - [1 - \Omega(b_I)]^{AB}. \qquad (4.4)$$

The total cross-section, σ_{AB}, is defined as

$$\sigma_{AB} = \int d^2b_I \; P(b_I) \; . \qquad (4.5)$$

Because for our interest the nuclear masses A and B are quite large, Eq.(4.4) can be simplified as

$$P(b_I) = 1 - \exp(-\Omega(b_I)) \; . \qquad (4.6)$$

Throughout the discussion, Eq.(4.6) will be used instead. Fig. 4.3 shown the opacity $\Omega(b_I)$ versus b_I for O+Au at 200 GeV and the curve fitted by gaussian distribution:

$$\Omega(b_I) = \Omega_m \exp(-b_I^2/b_0^2) \qquad (4.7)$$

where Ω_m and b_0 are fitting parameter, in the following table values of Ω_m and b_0 for different colliding pairs are shown:

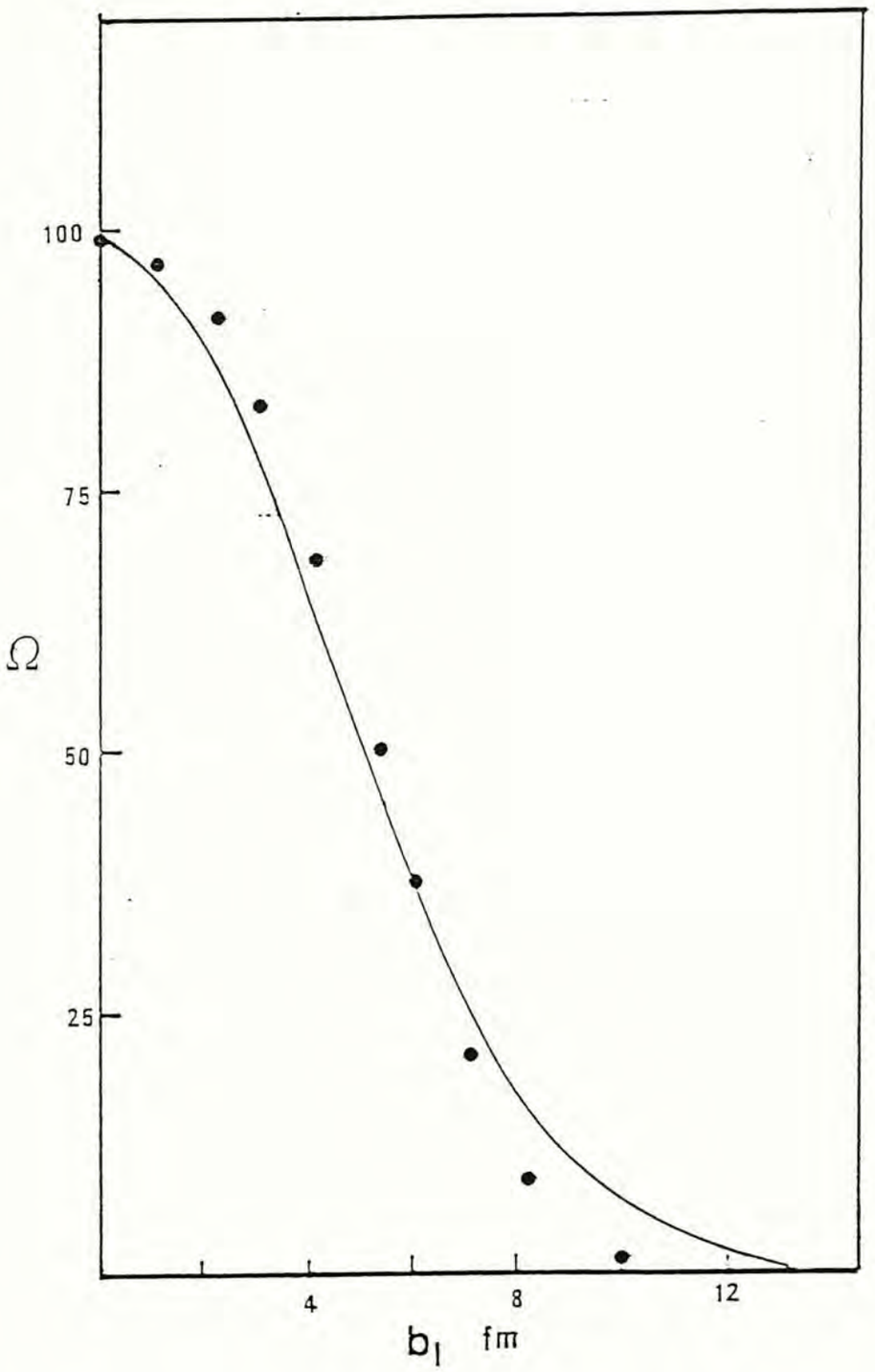

Fig. 4.3 The opacity $\Omega(b_I)$ versus b_I for O + Au at 200 GeV. The points are computed from (4.3) while the line is a gaussian as in (2.7), with $\Omega_m = 97.8$, $b_0 = 6.02$ fm.

A	B	Ω_m	b_0 (fm)
Au	O	97.8	6.02
Cu	O	58.7	4.3
S	S	63.6	4.1
Pb	Pb	980.5	7.0
O	O	21.5	3.5

Table 1: The maximum opacity Ω_m and the width b_0 for the collision of nuclei A + B, defined by Eq.(4.7).

And later in this section we will show that an apparent break will be observed when $\Omega_m \gg 1$.

4.2.2 Average Multiplicity $\bar{n}(b_I)$

Instead of making use of some developed models such as the multichain model (MCM) (Capella and Krzywicki, 1978) or the wounded nucleon model (WNM) (Bialas, Bleszynski and Czyz, 1976), we simply parameterize the average multiplicity $\bar{n}(b_I)$ at different impact parameters as the following:

$$\bar{n}(b_I) = n_0 \, \Omega(b_I)^{\beta} \qquad (4.8)$$

where n_0 and β are free parameters fixed by the experimental data. The total average multiplicity $\langle n \rangle$ is given by

$$\langle n \rangle = \frac{\int d^2b_I \, P(b_I) \, \bar{n}(b_I)}{\int d^2b_I \, P(b_I)} \qquad (4.9)$$

The experimental data of $\langle n \rangle$ for O+Au and O+Cu given by NA35 (1988) are 111 and 81.5 respectively. To give the correct experimental data, β is found to be ~ 0.5. For the case $\beta \sim 0.8$ our simple parameterization is found to agree very well with the MCM and WNM models (Fig. 4.4). Hence β can simply be regard as a phenomenological parameter with value in the range $0.5 \lesssim \beta \lesssim 0.8$. We will show later that the qualitative result is not sensitive to β and in order to get the best fit to the data, we will set $\beta = 0.6$ in the later discussion. Furthermore, the factor n_0 is eliminated in the scaling variable $z = \bar{n}(b_I)/\langle n \rangle$. Hence the multiplicity distribution in scaling form will be independent on the choice of n_0.

4.2.3 The Intrinsic Distribution

The last ingredient we need to specific is the intrinsic distribution $\psi_0(\xi = n/\bar{n}(b_I))$ at each impact parameter b_I. At each impact parameter the number of particles n emitted fluctuates around the average multiplicity $\bar{n}(b_I)$ and the probability of emitting n charged particles is

$$\psi_0(n/\bar{n};\, b_I) \, \frac{dn}{\bar{n}} \, . \qquad (4.10)$$

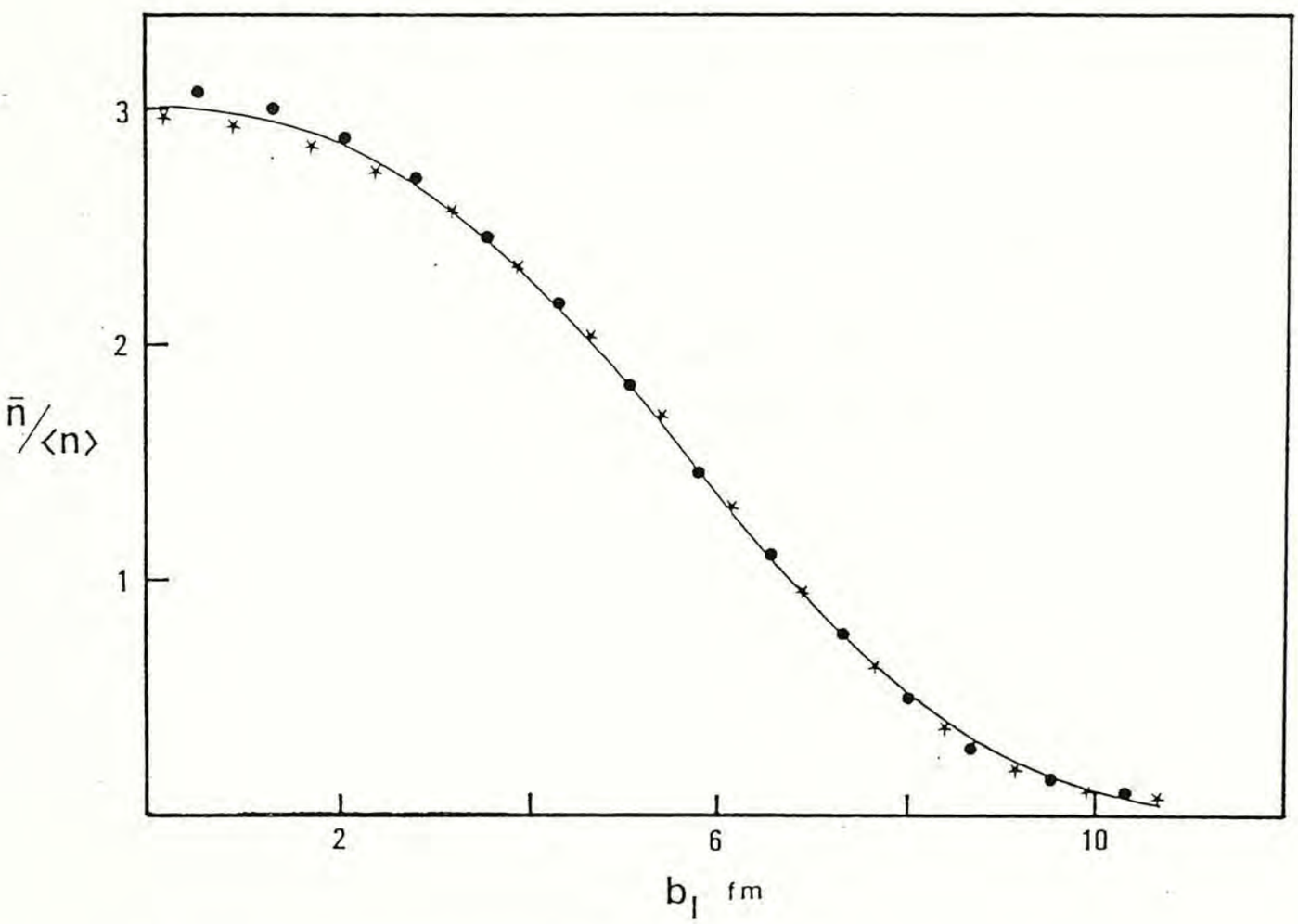

Fig. 4.4 n(b)/<n> versus b for O + Au at 200 GeV. Stars: MCM model; circles: WNM model; they agree almost exactly with each other. The line is calculated from (4.8) with $\beta = 0.8$.

With all these ingredients, the observed n-prong cross -section is just the averaging of the intrinsic distribution at each impact parameter, i.e.

$$\sigma_n = \int d^2b_I \; P(b_I) \; \psi_0(\frac{n}{\bar{n}};\; b_I) \; \frac{dn}{\bar{n}} \tag{4.15}$$

and the total cross section $\sigma_{AB} = \sum \sigma_n$. Since the elementary distribution is rather narrow and with peak at $z \sim 1$, the number of particles emitted

$$n \sim \bar{n}(b_I) = n_0 \; \Omega(b_I)^{\beta} \tag{4.16}$$

By the Gaussian approximation of $\Omega(b_I)$ pointed out before, Ω and b_I can be expressed in terms of n as the following

$$\Omega = (n/n_0)^{1/\beta} \tag{4.17a}$$

and

$$b_I = b_0\{\ln [\Omega_m/\Omega(n)]\}^{1/2} \tag{4.17b}$$

In Fig. 4.1 the horizontal axes labelled by Ω and b_I are also shown. Since there is a maximum Ω_m at $b_I = 0$, there exists a maximum n_b

$$n_b = \bar{n}(b_I = 0) = n_0 \Omega_m^{\beta} \; . \tag{4.18}$$

For the extreme case that $\psi_0 = \delta(n/\bar{n}-1)$, i.e there is no fluctuation around $\bar{n}(b_I)$ and the number of particles emitted at b_I is just equal to $\bar{n}(b_I)$, no event is possible for $n > n_b$. Hence there is an abrupt break at n_b. Indeed this reflects the fact

that the distribution in region $n > n_b$ and $n < n_b$ are attributed to different physics. For the region $n > n_b$, the observed distribution is the result of superposition of the elementary distribution. After the superposition process, the property of the elementary distribution is covered and only the geometrical structure of the nucleus scattering is revealed. Actually for the case $\psi_0 = \delta(n/\bar{n}-1)$, the observed distribution is just the interaction probability with the variable b_I replaced with n by Eq.(4.17b) and with a cut-off at n_b. In reality, of course the intrinsic distribution will not be so sharp as a δ-function. For region $n > n_b$ the observed distribution will mainly attribute to the intrinsic distribution at $b_I = 0$. Hence a break is expected. By the shape of the distribution after the break n_b, much information of the intrinsic distribution can be displayed.

The location of the break is given by

$$z_b = n_b/\langle n \rangle = \frac{\Omega_m^{\beta} \int d^2 b_I \; P(b_I)}{\int d^2 b_I \; P(b_I) \; \Omega^{\beta}} \qquad (4.19)$$

With approximation of gaussian profile, Eq.(4.19) is cast into

$$z_b = \frac{\int_0^1 \frac{dy}{y} \left[1 - \exp(-\Omega_m y)\right]}{\int_0^1 dy \; y^{\beta-1} \left[1 - \exp(-\Omega_m y)\right]} \qquad (4.20)$$

which can be explicitly calculable for any Ω_m and β. Fig. 4.5a shows z_b versus β for various Ω_m while in Fig. 4.5b, z_b is plotted for different values of Ω_m with $\beta = 0.6$. For $\beta = 0.6$, z_b is found

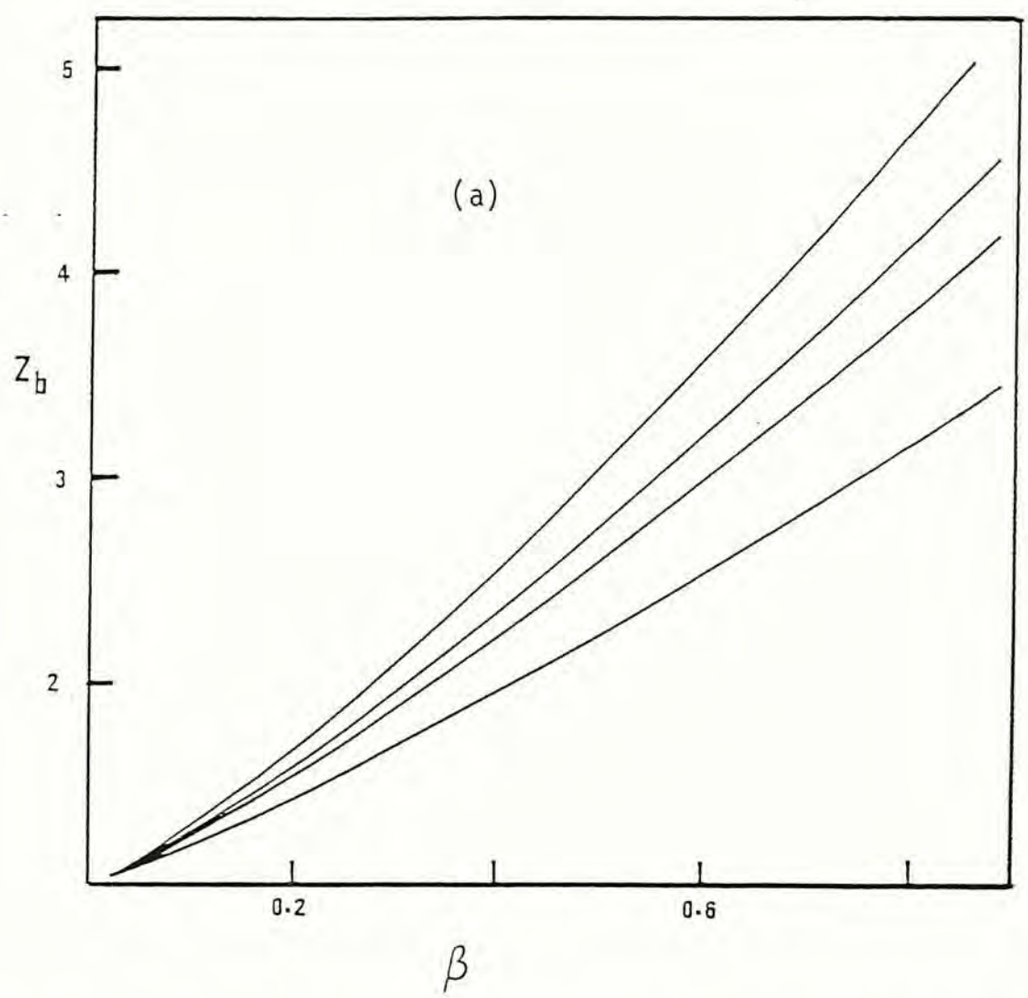

Fig. 4.5 a-b The position of the break z and of the peak z_a in the analytic approximation of Section 2. (a) Z_b versus β. The curves refer to, from top to bottom, Ω_m = 981 (Pb+Pb), Ω_m = 97.8 (O+Au), Ω_m = 58.7 (O+Cu), Ω_m = 21.5 (O+O). (b) Upper curve: z_b versus Ω_m for β = 0.6. Lower curve: z_a versus Ω_m for β = 0.6.

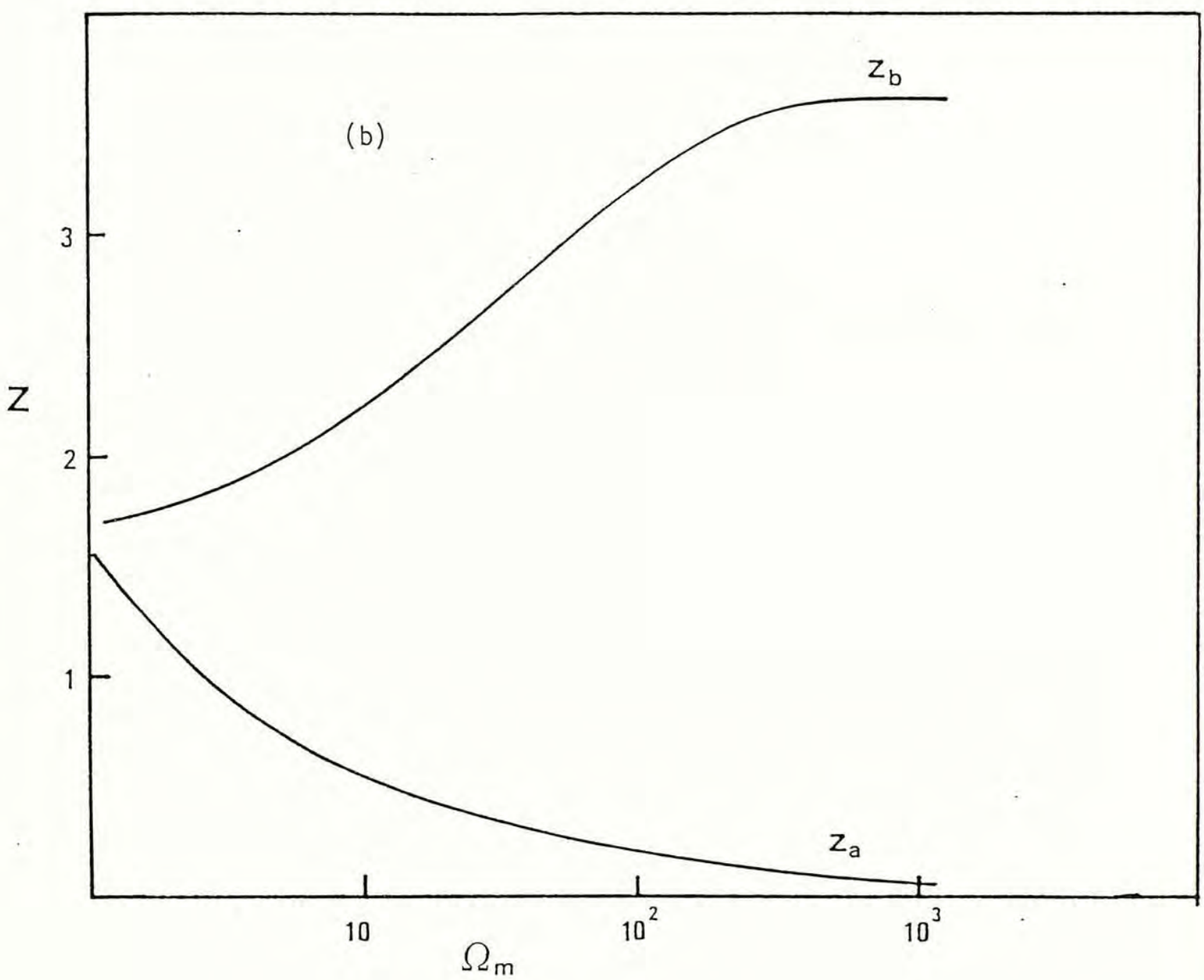
(b)
z_b
z_a
Z
3
2
1
10
10^2
10^3
Ω_m

to be 3.2 for O+Au at 200 GeV/nucleon which is qualitatively correct. Notice that z_b increases monotonously with Ω_m, which increases with the mass number of the colliding nuclei. Hence for heavy colliding nuclei, the break z_b should shift to larger value of z.

4.3 Analytic Form for $\psi(z)$

For the extreme case that $\psi_0(z;b_I) \sim \delta(z-1)$, σ_n can be calculated analytically (of course with the assumption of the gaussian profile). By Eq.(4.15),

$$\sigma_n \propto \int db_I\, b_I\, (1 - e^{-\Omega})\, \delta(n/\bar{n} - 1)\, (1/\bar{n})\, \theta(n_b - n)$$

$$\propto \left(\frac{n_0}{n}\right) \left\{1 - \exp[-(n/n_0)^{1/\beta}]\right\} \theta(n_b - n) \qquad (4.21)$$

With the Eq.(4.18) and the relation $z/z_b = n/n_b$, Eq.(4.21) becomes

$$\psi(z) = a/z \left\{1 - \exp[-\Omega_m (z/z_b)^{1/\beta}]\right\} \theta(z_b - z) \qquad (4.22)$$

where a is the normalization constant. Fig. 4.6a and 4.6b show the calculated distribution for O+Au and O+Cu respectively with different values of β. In the figure we also show the experimental data of NA35 (1988). And Fig. 4.7 show the distribution for different Ω_m values with $\beta = 0.6$.

It can be seen that all the prominent features of the experimental data, which we have pointed out in section 1, is

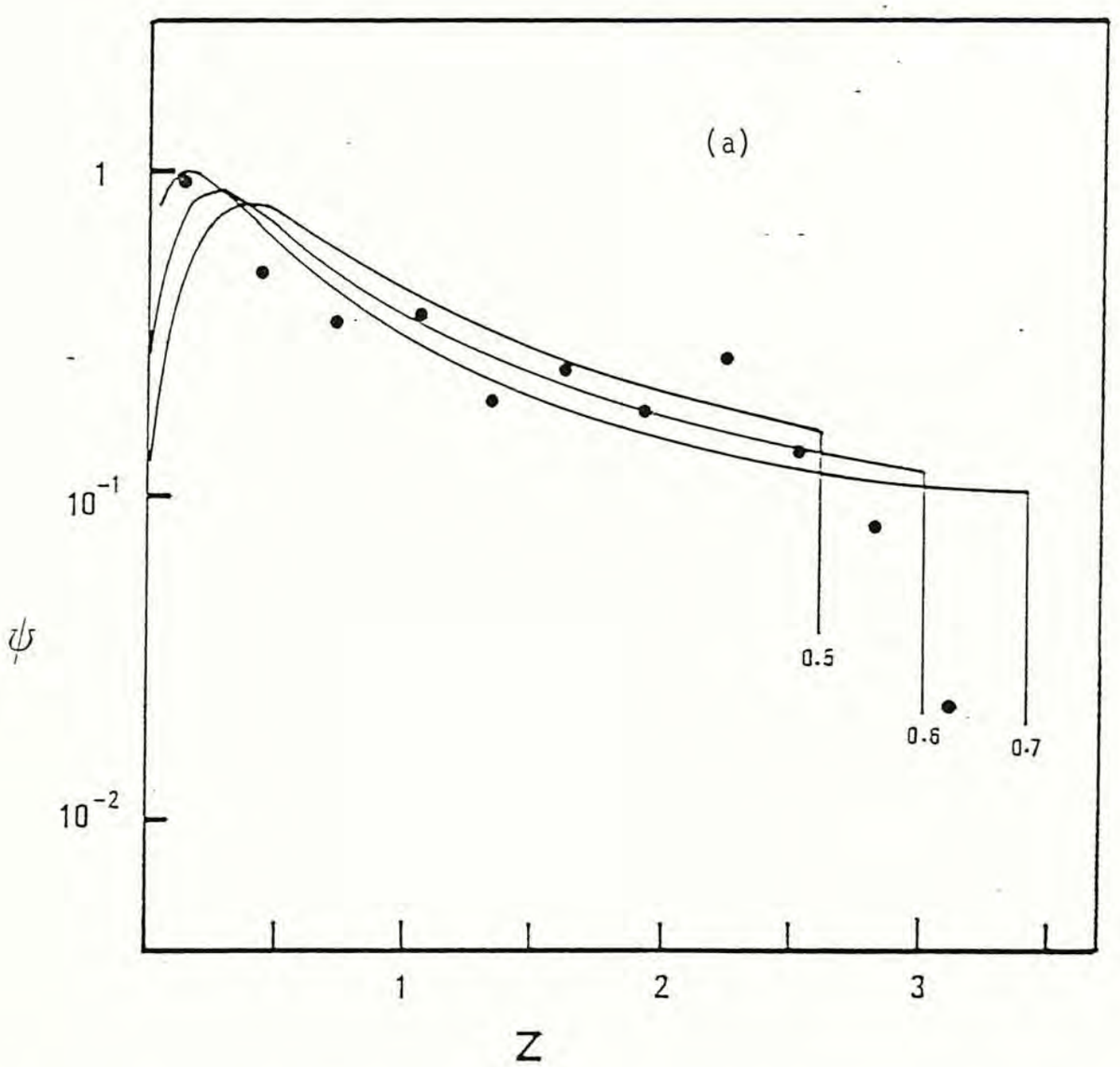

Fig. 4.6 a-b The predicted $\psi(z)$ in the analytic approximation of Section 4.3, for different β values as labelled, (a) O + Cu (Ω_m = 58.7), (b) O + Au (Ω_m = 97.8). Points are data for negative charges only.

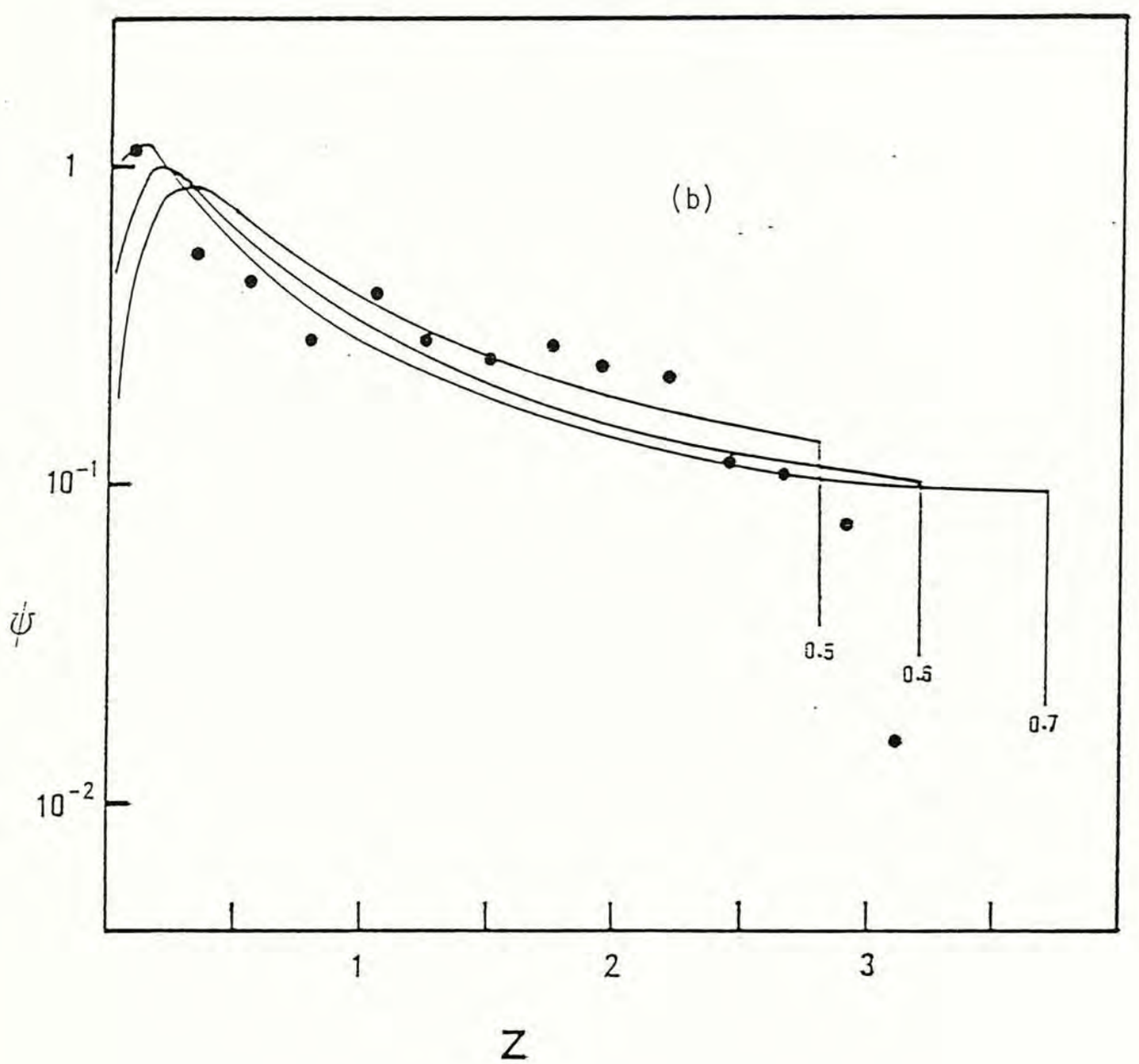
(b)
1
10^{-1}
10^{-2}
ψ
0.5
0.6
0.7
1
2
3
Z

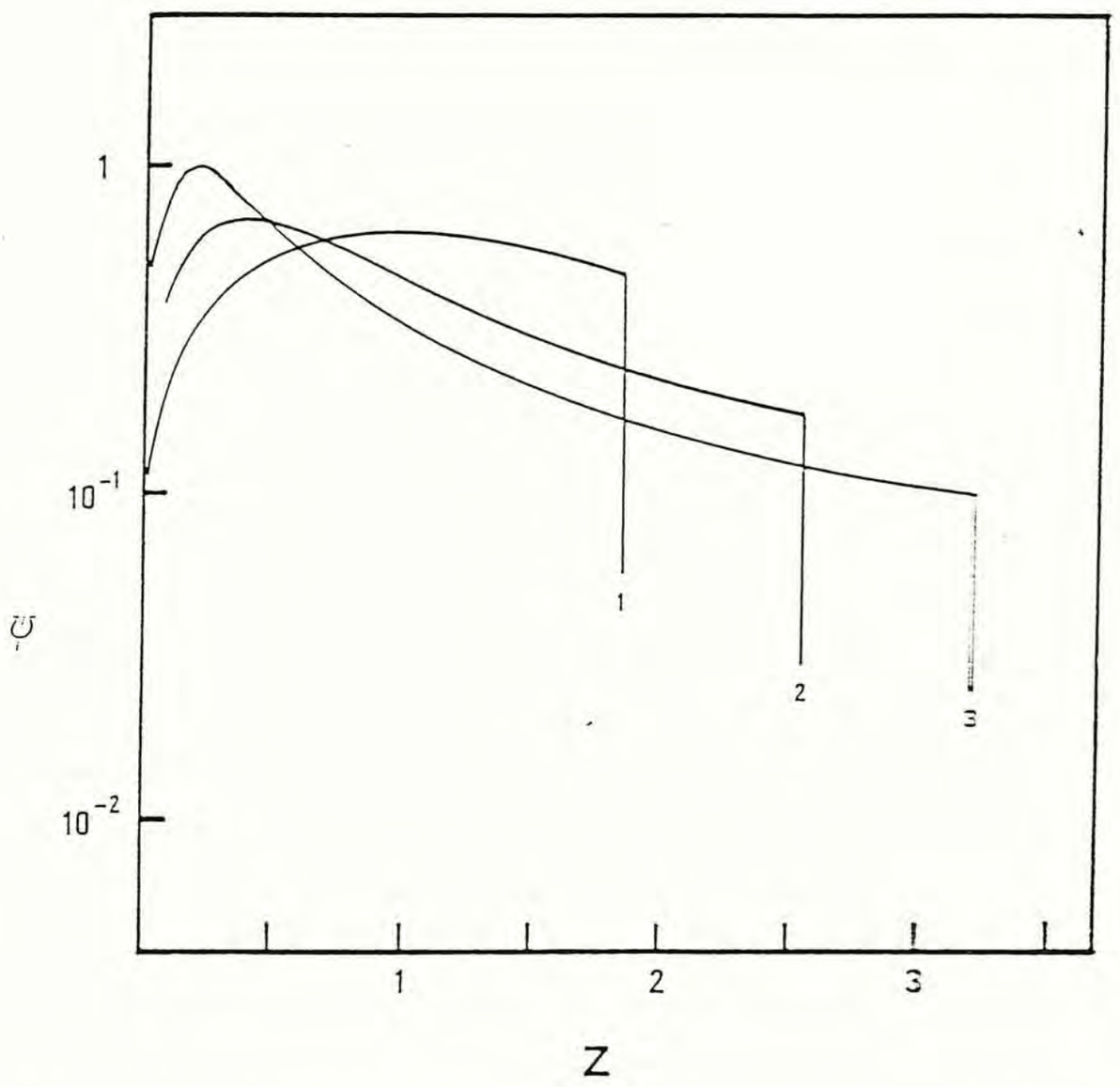

Fig. 4.7 The predicted $\psi(z)$ in the analytic approximation of Section 4.3, for different Ω_m values and $\beta = 0.6$.
Curve 1: $\Omega_m = 3.0$ (p+p); Curve 2: $\Omega_m = 21.5$ (C+O);
Curve 3: $\Omega_m = 97.8$ (O+Au).

observed in our result. In our calculated results, one apparent feature which is not observed in the experimental data is the appearance of a peak at small value of z (z_a). In Fig. 4.5b we plot also z_a against Ω_m for $\beta = 0.6$. Let us divide our calculated distribution into three region, i.e. (i) the rapid increasing region, $z < z_a$; (ii) decreasing region, which become nearly flat later, $z_a < z < z_b$; and (iii) the rapid decreasing region, $z_b > z$. From Fig. 4.5b, it can be seen that as Ω_m increases, the peak z_a shifts to smaller value of z. For O+Au or O+Cu scattering with $\beta = 0.6$, z_a shifts approximately to 0.2. Due to the limitation of the accuracy of the experimental apparatus, the rapidly increasing region can hardly be resolved for such small value of z. However in the experimental data of multiplicity distribution in limited rapidity interval for heavy ions collision (Fig. 4.2) this feature is indeed observed. Besides, as Ω_m increases, the difference of $z_b - z_a$ increases. It is evident that in order to observe a plateau region and a clear break, it is necessary to have a wide region (ii). Hence large value of Ω_m favors a plateau region and a clear break. For the case of small Ω_m, for example $\bar{p}p$ scattering for which $\Omega_m \sim 3$, the break is not clear enough to be observed. Moreover, the curves in Fig. 4.5 show that in a large part of the $z_a < z < z_b$ region, $\psi(z)$ is roughly independent of Ω_m except for normalization, which agrees with the fact that the O+Cu and O+Au data appear to show no substantial difference from each other.

Fig. 4.8 shows $\Omega(b_I)/\Omega_m$ versus b_I/b_{rms}, where

$$b_{rms}^2 = \frac{\int d^2b_I \; \Omega(b_I) \; b_I^2}{\int d^2b_I \; \Omega(b_I)} \tag{4.23}$$

for different nuclear pairs. For equal nuclei, there is only one length scale $R_A = R_0 A^{1/3}$, so that once b_{rms} is scaled out, Ω is universal. For unequal nuclei Ω is flattened near $b_I = 0$, so that a larger range of b_I all contribute to $n \lesssim n_b$, and $\psi(z)$ for $z \lesssim z_b$ is relatively large. Hence in order to obtain a clear break, (i) $\Omega(m)$ should be large; (ii) the colliding nuclei should be unequal.

4.4 Intrinsic Distribution

The existence of the break also depends on the the width of the elementary distribution $\psi_0(z)$. As we have pointed out before, the two region $z \lesssim z_b$ and $z \gtrsim z_b$ are attributed to different physics. The region $z \gtrsim z_b$ will reveal the natural of the elementary distribution $\psi_0(z; b_I = 0)$. We fit the experimental data for O+Au in the region $z \gtrsim z_b$ with $\exp(-\alpha z)$ (the fitted curve is shown by the broken line in Fig. 4.1). α is found to be approximately equal to 4.2.

The distribution in this region is dominated by $\Omega \sim \Omega_m$ or $b_I \sim 0$,

$$\sigma \propto \psi_0(n/n_b;\; b_I = 0) = \psi_0(z/z_b;\; b_I = 0) \tag{4.24}$$

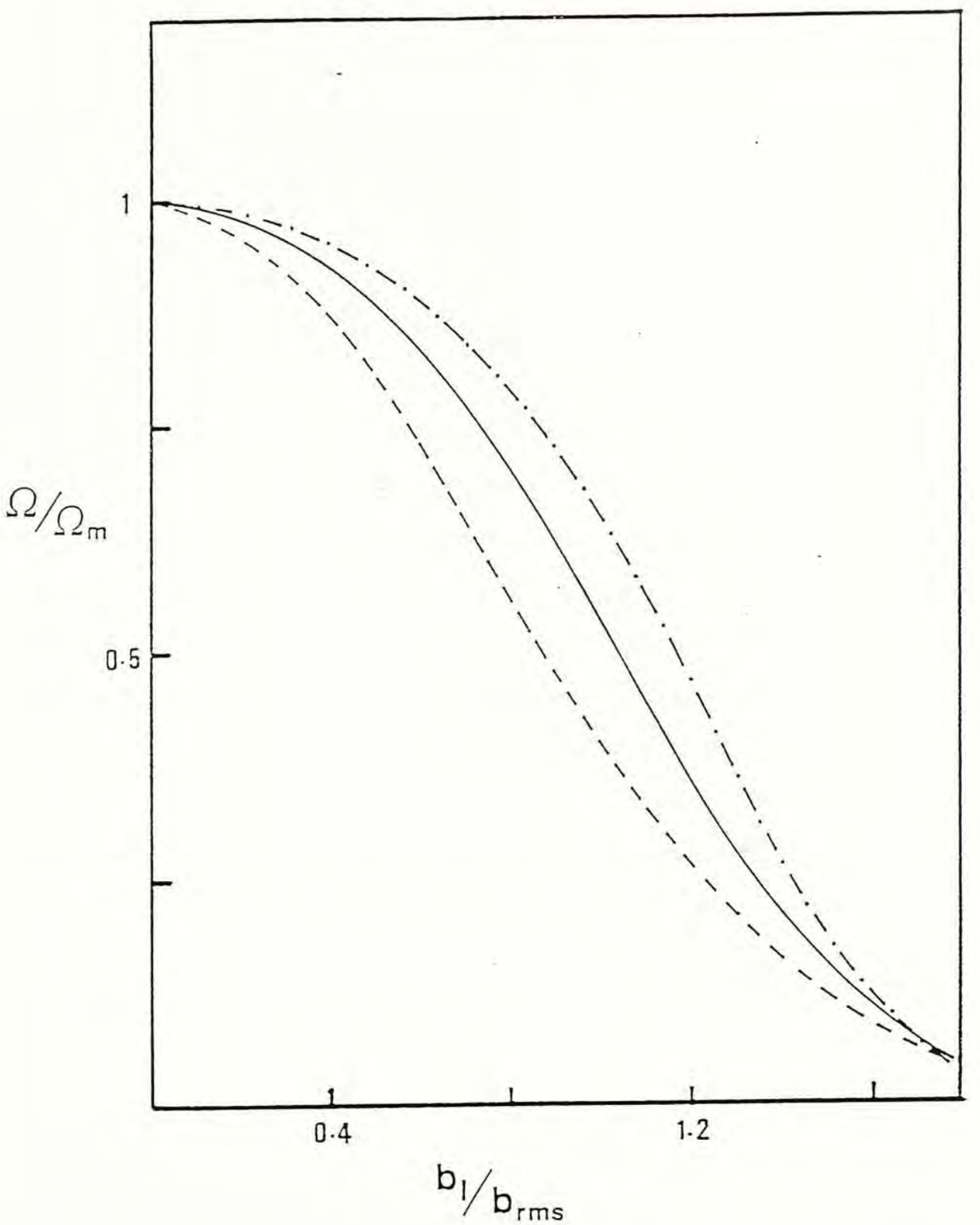

Fig. 4.8 $\Omega(b_I)/\Omega_m$ versus b_I/b_{rms}. The curves, from bottom to top, refer to (1) an equal mass case (O+O); (2) an unequal mass case (O+Au); (3) a very unequal mass case (p+Au).

Hence, $\psi_0 \propto \exp(-\alpha_0 z)$, when

$$\alpha_0 = \alpha z_b \tag{4.25}$$

with a value ~ 12 for O+Au.

For the KNO function of $p\bar{p}$ scattering, $\alpha \sim 3\text{-}4$. Hence the universal KNO scaling, which gives magnificent agreement with the experimental data for hadron-nucleus scattering, should not be applied here. And the intrinsic distribution for nucleus-nucleus scattering should be much narrower than the KNO function. In the following discussion, models with three different kinds of intrinsic distribution will be given and their result will be compared with the experimental data. All models are based on Eq.(4.21) for σ_n, with $\Omega(b_I)$ computed form Eq.(4.3); the gaussian approximation is <u>not</u> used. And the average multiplicity distribution $\bar{n}(b_I)$ is given by Eq.(4.8) with $\beta = 0.6$.

4.4.1 <u>Model 1</u>

In this model KNO scaling at each impact parameter b is still assumed. However instead of the Slattery parameterization, we parameterize the KNO distribution $\phi(z)$ by a gamma distribution

$$\psi_0(z;b_I) = \phi(z) = \frac{k^k}{(k-1)!} z^{k-1} e^{-kz} \tag{4.26}$$

with k = 4, which agrees with the Slattery parameterization very well. Furthermore, the gamma distribution can be regarded as the

limiting form of the negative binomial distribution in n, as pointed out in chapter 2. The use of the gamma distribution is just for convenience of convolutions in the later discussion. Except for the average multiplicity $\bar{n}(b_I)$, model 1 is just the same as the model of Daté *et al.* (1987) (in which $\bar{n}(b_I)$ is given by the MCM and WNM models). The result of model 1 is shown in Fig. 4.9. As expected, owing to the fact that the non-stochastic KNO function is too broad, no break is observed.

4.4.2 Model 2

Chou and Yang (1984) have emphasized that the intrinsic distribution in h-h scattering is stochastic and they argued that in e^+e^- —> hadrons, since there is no superposition of impact parameter, the intrinsic stochastic distribution should be observed. In model 2, the non-stochastic distribution in model 1 is replaced with the stochastic distribution, Poisson distribution,

$$P_\infty(n) = \frac{\bar{n}^n}{n!} e^{-\bar{n}}$$

$$\psi_0(z;b_I) = \bar{n}\, P_\infty(\bar{n}z) = \frac{\bar{n}^{\bar{n}z+1}}{(\bar{n}z)!} e^{-\bar{n}} \qquad (4.27)$$

In Fig. 4.9, the result of model 2 is shown by curve 2. A sharp break is now observed. However, the break occurs at too small a value of z and the fall-off beyond the break is too rapid. By the results of models 1 and 2, it seems that in order to get a good

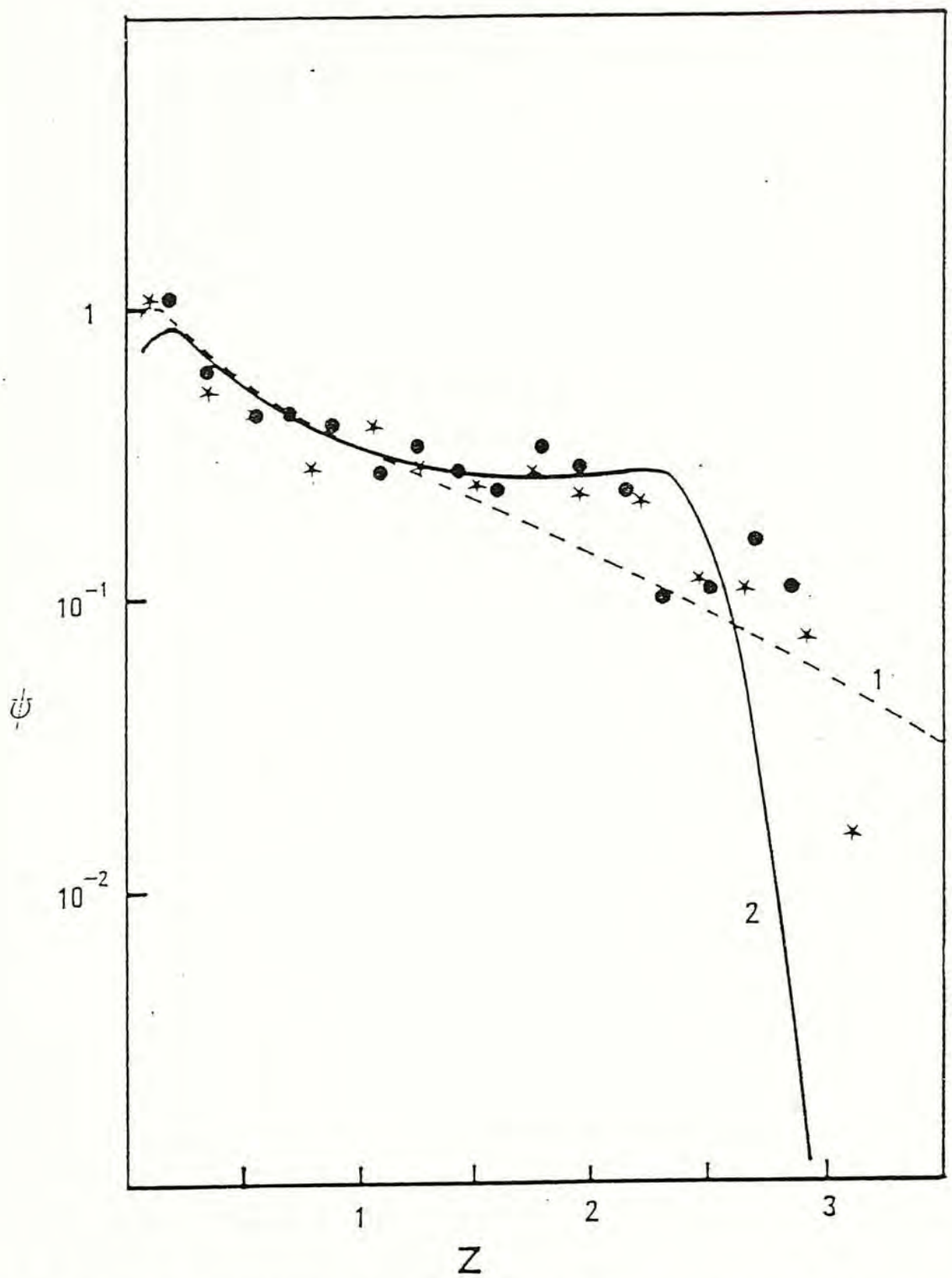

Fig. 4.9 The multiplicity distribution for O+Au. Data are as in Figure 1. Line 1 is the prediction of Model 1; line 2 is the prediction of Model 2.

fit result, the intrinsic distribution should lie between a fully KNO-like distribution and a fully stochastic distribution.

4.4.3 Model 3

In this model, the intrinsic distribution lying between a stochastic distribution and a KNO distribution will be used. The idea is the following: At impact parameter b_I, let the shaded overlapping area S (Fig. 4.10) be written as

$$S = R_0^2 \, f(b_I/R_0). \tag{4.28}$$

It is natural to assume that the collision is described by p independent tube, each with cross-section area πR_0^2, so

$$p = S/(\pi R_0^2) = \frac{1}{\pi} f(b_I/R_0) \tag{4.29}$$

with the proviso that $p \geq 1$. In Fig. 4.11 we show p versus b_I for O+Au collision with p varying from 1 to $p_{max} \sim 6.5$ ($p_{max} = B^{2/3}$, where B is the mass number of the smaller nucleus).

Assume that the multiplicity distribution for each tube is KNO-like, i.e. $\Delta m/m \sim 1$ and the total number of particles emitted $n = m_1 + m_2 + \cdots + m_p$ where m_p is the number of particles emitted for each tube. Since the tubes are independent,

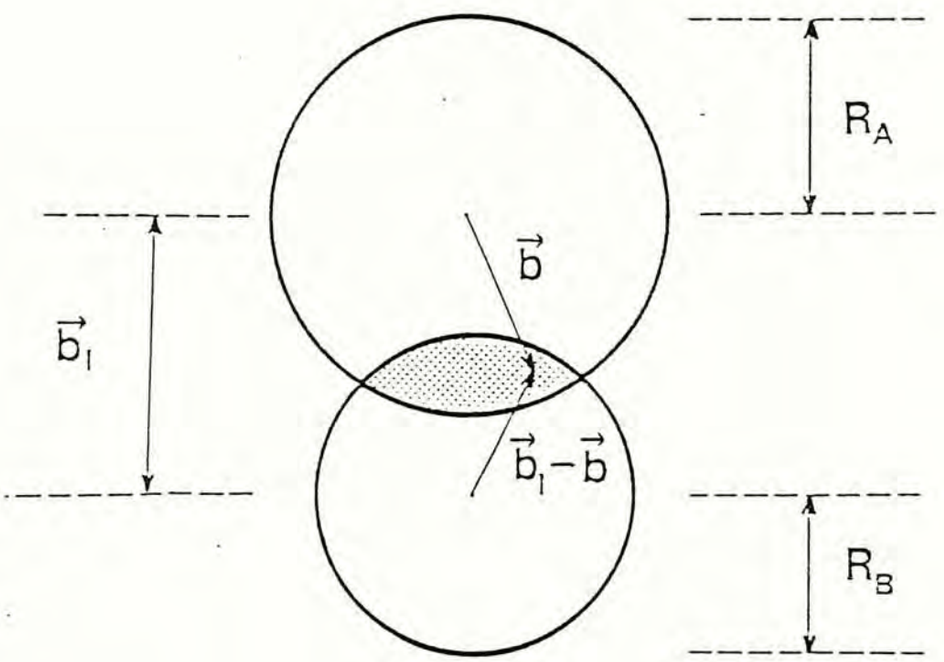

Fig. 4.10 The collision of two nuclei in the impact parameter plane.

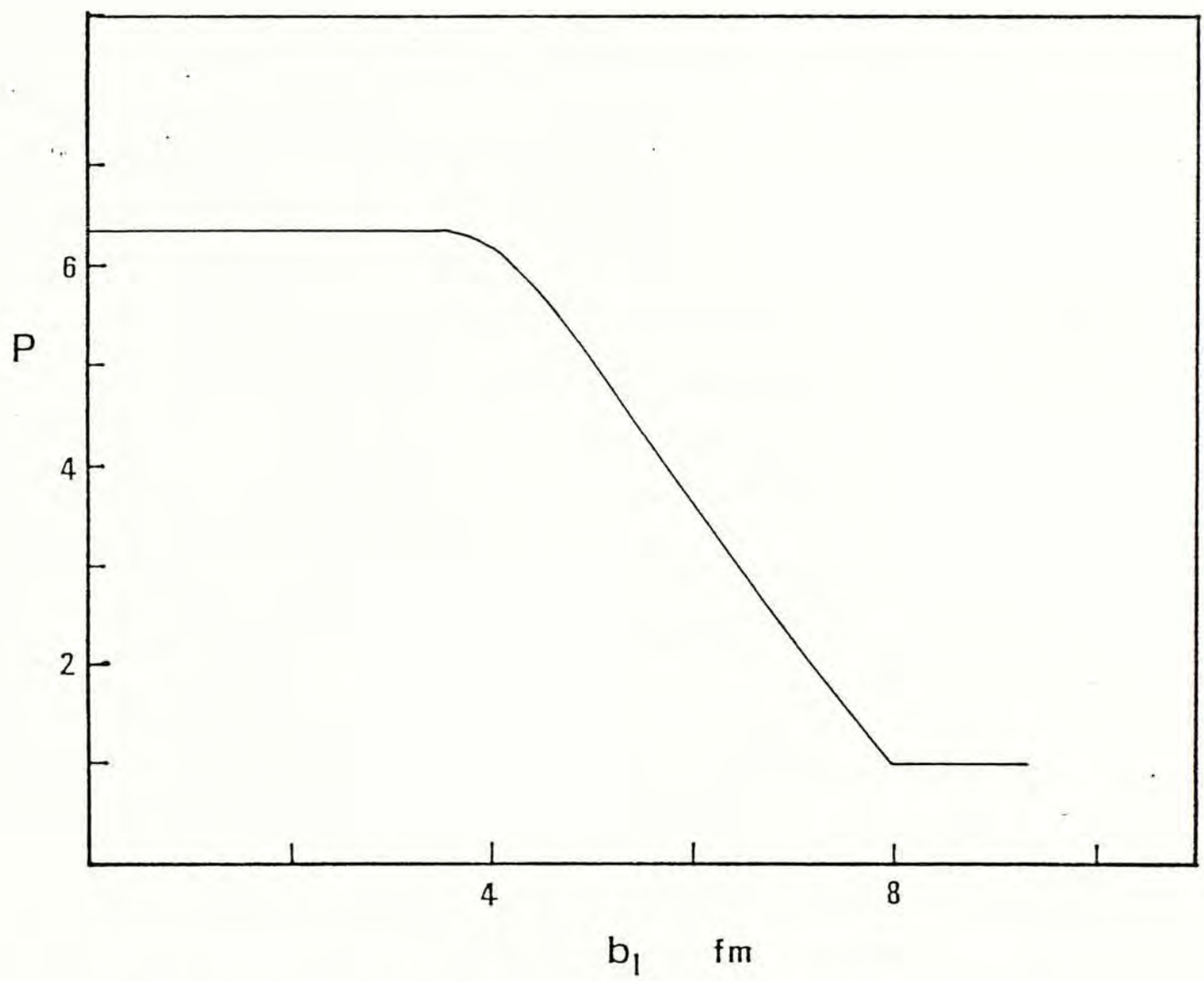

Fig. 4.11 The number of tubes, p, versus b_I, in O + Au scattering.

$$\frac{\Delta n}{n} \sim \frac{1}{\sqrt{p}} \frac{\Delta m}{m} \qquad (4.30a)$$

$$\sim 1/\sqrt{p} \qquad (4.30b)$$

which lies between fully KNO-like ($\Delta n/n \sim 1$) and fully stochastic ($\Delta n/n \sim 1/\sqrt{n}$). If the distribution for each tube is stochastic, i.e. $\Delta m/m \sim 1/\sqrt{m}$, then $\Delta n/n \sim 1/\sqrt{mp} \sim 1/\sqrt{n}$ and we revert to Model 2 which is ruled out by the data.

Furthermore, we assume the p tubes to be identical. Hence the average multiplicity $\bar{m}$ for each tube is equal to $\bar{n}/p$. The distribution at each impact parameter b_I is given by the convolution of the KNO-like distribution for each m,

$$\frac{1}{\bar{n}} \psi_0(n/\bar{n};\ b_I)$$

$$= \int \frac{dm_1}{\bar{m}} \cdots \frac{dm_p}{\bar{m}} \phi(m_1/\bar{m}) \cdots \phi(m_p/\bar{m})\ \delta(m_1 + \cdots + m_p - n) \qquad (4.31)$$

which is again a gamma distribution with k replaced by pk. The result of this model is shown in Fig. 4.1a and b for O+Cu and O+Au respectively. Our model agrees with the experimental data very well. All the prominent features of the experimental data are captured. Owing to the smearing of the elementary distribution ψ_0, instead of a break at $z \sim 3.2$, the break is now moved to smaller values of z.

At asymptotic z,

$$\psi(z) \sim \psi_0(z/z_b; b_I = 0) \sim e^{-\alpha z} \tag{4.32}$$

where

$$\alpha = p_{max}\, k/z_b = B^{2/3}\, k/z_b \tag{4.33}$$

with a value ~ 8 for O + Au. This is larger than that obtained from the crude fit of the experimental data (~ 4). This may be due to one of two reasons. First of all, the largest z in the experimental data is not yet asymptotic. Secondly, p_{max} is overestimated, i.e. for each tube the cross section is greater than πR_0^2.

4.4.4 Second Moment

In the following table (4.2), the reduced second moment C_2, defined as:

$$C_2 = \langle z^2 \rangle = \int dz\, z^2\, \psi(z) \tag{4.34}$$

for different nuclei pairs are shown and is compared with the experimental data. The results are in good agreement with the measured values.

A	B	theory	expt
Au	O	1.68	1.67 ± 0.09
Cu	O	1.68	1.69 ± 0.11
S	S	1.71	1.89 ± 0.2
Pb	Pb	1.83	-
Cu	S	1.77	1.80 ± 0.2

Table 4.2: Our calculated reduced second moment C_2 for different nuclei pairs A + B and the experimental data.

4.5 Discussion

In Fig. 4.12a, theoretical result for Sr+Sr scattering is shown and is compared with that of the O+Au scattering at the same incident energy (200 GeV/nucleon). The maximum opacity Ω_m for Sr+Sr is approximately equal to that of O+Au. As mentioned before, for all things (in particular Ω_m) being equal, unequal nuclei favors the appearance of a prominent break. Besides, the calculated $\psi(z)$ for S+S and Pb+Pb, for which experiments are planned, are shown in Fig. 4.12b. With the maximum number of tubes $p_{max} \sim A^{2/3} \sim 10$, 35 respectively, it is apparent that the break is much more prominent for Pb+Pb. Furthermore the central plateau is broader and the break occurs at larger value of z for large nuclei. Note also that for Pb+Pb the peak z_a shifts to very small z and it is barely visible in the figure, so that experimentally it will probably be indistinguishable from a

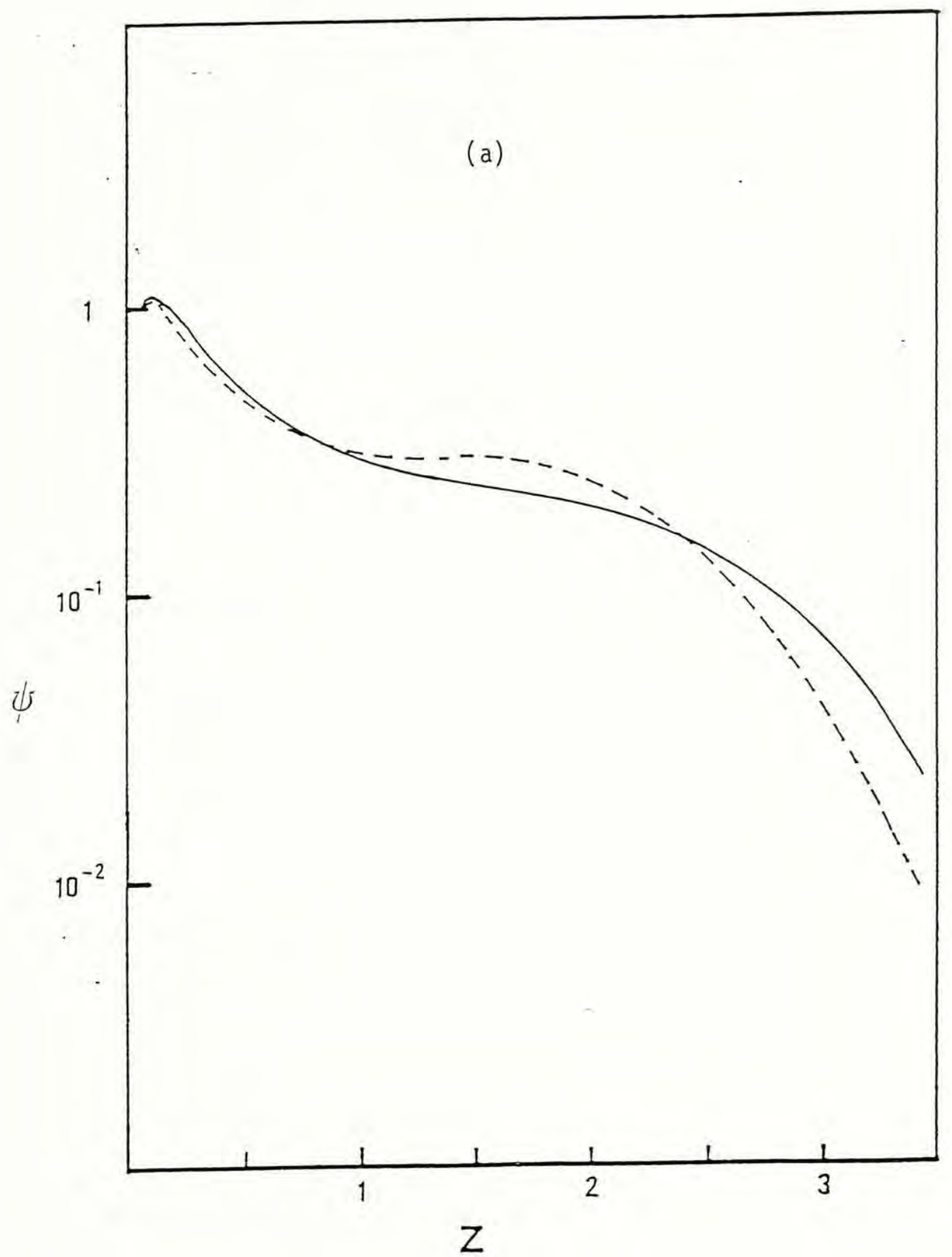

Fig. 4.12 a-b Predicted $\psi(z)$ for various A+B scattering processes at 200 GeV. (a) Comparison of equal versus unequal nuclei at approximately the same Ω_m. Solid line: Sc + Sc. Broken line: O + Au. (b) Solid line: S + S; broken line: Pb + Pb.

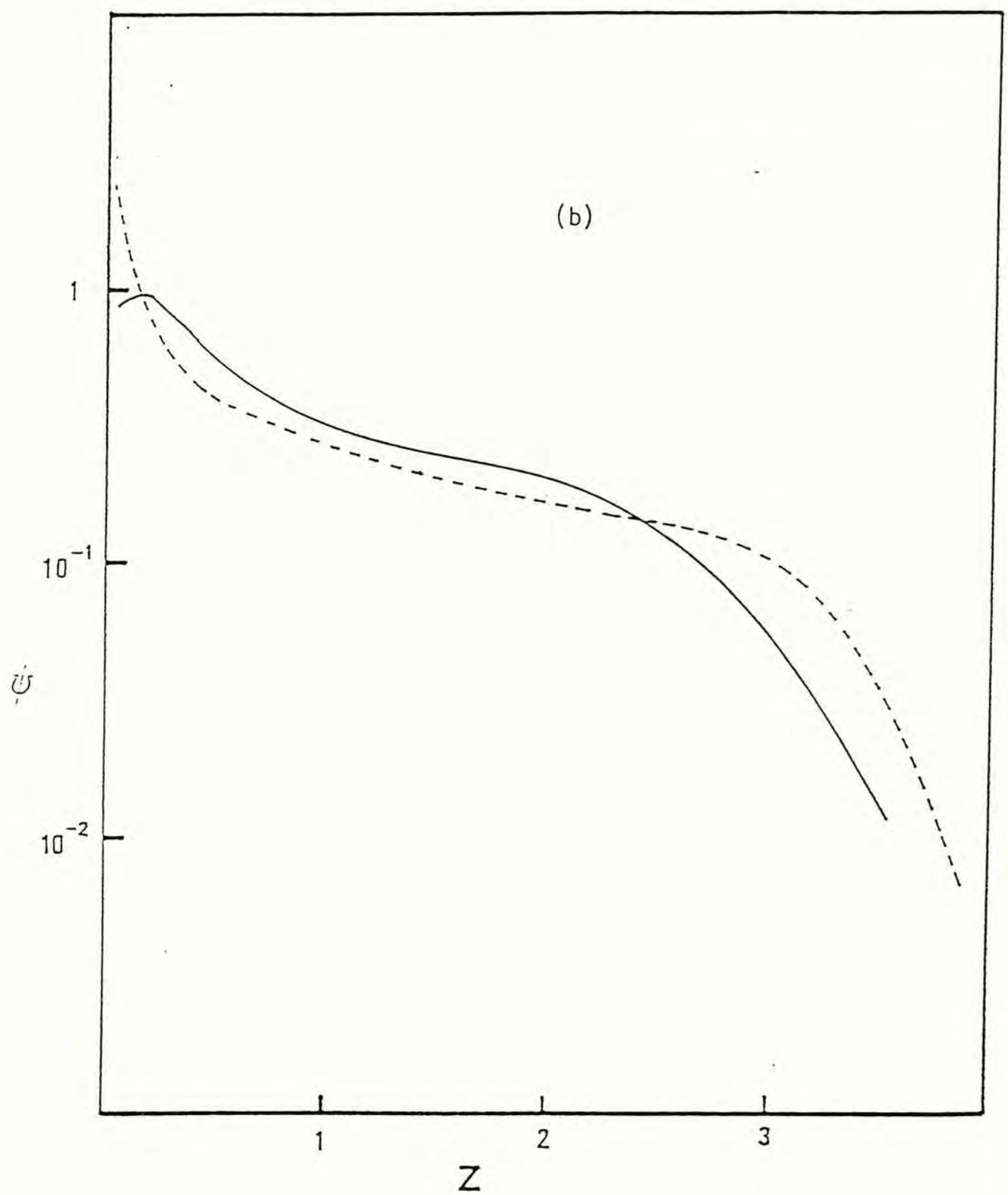
(b)
1
10^{-1}
10^{-2}
$\dot{\psi}$
1
2
3
Z

distribution rising all the way to $z = 0$.

In our model, we have emphasized the narrow intrinsic distribution is the result of the collision of p independent tubes. For each tube the intrinsic distribution is non-stochastic and is given by the KNO-distribution. For $p = 1$, this model converts to the our previous model for hadron-nucleus scattering (Kiang *et al.*, 1985). However there is experimental evidence that the width of the intrinsic distribution is proportional to $1/\sqrt{\nu}$ and the universal KNO scaling is not valid. Hence our assumption that for each tube the distribution is universal may be oversimplified. This point will deserve further investigation.

As I have mentioned in the Introduction, so far as we know only the geometrical model proposed by Chao and Liu (1989) gives successful description to the experimental data. Indeed, it is not surprising that both of the models, i.e. the geometrical model proposed by Chao and Liu and our model presented here, can give good accounts for the experimental data, even though different ingredients were used. For the region $z < z_b$, the distribution is insensitive to the input distribution. And with elementary distribution with appropriate width at $b_I = 0$, the resulting distribution should well fit the experimental data which indeed do not involve much dynamic details.

4.6 Conclusion

Based on the geometrical picture, a quantitative discussion on heavy-ion collision is presented. The prominent features of the experimental data for nucleus-nucleus scattering

are shown to be the general features of the geometrical model. We claim that for small and medium z region, the distribution is the result of the superposition of the intrinsic distribution at different impact parameters b_I and only the geometrical structure of the nucleus is revealed. While for the large z region, the distribution is just the tail of the intrinsic distribution at $b_I = 0$. Since these two regions are due to different physics, also under suitable conditions: (i) large Ω_m; (ii) unequal nuclei pair and (iii) narrow intrinsic distribution, a prominent break will be obtained. By investigating the experimental data at large z, we conclude that the intrinsic distribution for nucleus-nucleus is narrower than the non-stochastic KNO distribution and should be laid between the KNO distribution and the Poisson distribution. Furthermore we have suggested the idea of interaction of $p(b_I)$ independent tubes at each impact parameter with KNO-like distribution for each tube. The convolution of these KNO-like distribution results in a much narrow distribution. Applied to O+Au collision, with only one free parameter β, our model gives excellent agreement with the experimental data. Predictions for S+S and Pb+Pb collisions are also made. These experiments are planned and their experimental result will provide interesting testing ground for our ideas given here.

CHAPTER 5

Conclusion

In this thesis, my work in the past two years has been presented. They include the investigation of (i) the charged (both all charge and negative charged) multiplicity distribution for hadron-nucleus scattering in limited rapidity windows; (ii) the charged multiplicity distribution for nucleus-nucleus scattering. These works are both based on the same idea: the geometrical picture. With the thermodynamic model and the assumption of independent emission of the produced particle, we give a good account for the experimental data in part (i). Moreover all the prominent features of the experimental data of the multiplicity distribution for the heavy ion collision can be beautifully captured by the geometrical picture. All these support further the geometrical basis of the multi-particle production in the hadronic interaction.

Of course for certain aspects our model is rather crude. The form we take for the intrinsic distribution may be an oversimplification as stressed previously. However, the essential

physics revealed by our model will remain with more sophisticated refinement.

The excellent agreement of the model with the experimental data for the hadron-nucleus case reveals that the intrinsic distribution is rather broad or KNO-liked. However, as Chou and Yang claimed, the KNO distribution is the result of superposition of the elementary stochastic processes (h-h scattering). Then for hA scattering, at each impact parameter the intrinsic distribution should be the result of the convolution of these stochastic processes, which should turn out to be stochastic also, and should be much narrower than the KNO distribution. We have indeed tried replacing the KNO distribution with the Poisson distribution in our model for the h-A scattering. This results in a rise of a bump which is inconsistent with the experimental data. Moreover, as we have shown in chapter 4, for heavy ion collision, a fully stochastic intrinsic distribution (i.e. Poisson) would be to narrow to get a good fit result comparing with the experimental data. Hence it is clear that a unified theory for the natural of the intrinsic distributions for different kinds of scattering (hadron-hadron, hadron-nucleus and nucleus-nucleus) is needed and it should be our major task for the future.

Comparing with the experimental data, the situation may be improved if, instead of the usual Poisson distribution, a modified Poisson distribution

$$P(n) = \frac{1}{2} \frac{(\bar{n}/2)^{n/2}}{(n/2)!} \exp(-\bar{n}/2)$$

which is wider, is employed. There is some justification to this modification, since it is now well accepted that the produced charged particles are emitted in neutral cluster form. It is clear that a unified theory for the nature of the intrinsic distributions for different kinds of scattering (hadron-hadron, hadron-nucleus and nucleus-nucleus) is needed and it should be a major task for the future.

References

Amaldi, U., in High Energy Collisions — 1973, Proceedings of the Fifth International Conference, Stony Brook, New York, edited by C. Quigg.

Bailly, J. L., *et al.*, 1988, Z. Phys. C40, 215.

Bialas, A., M. Bleszynski and W. Czyz, 1976, Nucl. Phys. B111, 461.

Biswas, N. N., *et al.*, 1986, Phys. Rev. D33, 3167.

Cai, X., W. Q. Chao and T. C. Meng, 1987, Phys. Rev. D36, 2009.

Capella, A. and A. Krzywicki, 1978, Phys. Rev. D18, 3357.

Capella, A., *et al.*, 1987, Phys. Rev. D35, 2921.

Chao, W. Q., M. K. Hegab and J. Hufner, 1983, Nucl. Phys. A395, 482.

Chao, W. Q. and B. Liu, 1989, Z. Phys. C42, 337.

Chou, T. T. and C. N. Yang, 1984, Phys. Lett. 135B, 175.

Chou, T. T. and C. N. Yang, 1985, Phys. Rev. D32, 1692.

Chou, T. T., C. N. Yang and E. Yen, 1985, Phys. Rev. Lett. 54, 510.

Clarke, D. J. and S. Y. Lo, 1979, Phys. Lett. 87B, 379.

Daté, S., *et al.*, 1987, Phys. Rev. D36, 2744.

De Marzo, C., *et al.*, 1982, Phys. Rev. D26, 1019.

De Marzo, C., *et al.*, 1984, Phys. Rev. D29, 363.

Dengler, F., *et al.*, 1986, Z. Phys. C33, 187.

E802, 1988, Z. Phys. C38, 35.

EMU-07, L. M. Bashier *et al.*, to be published.

Fermi, E., 1950, Prog. Theor. Phys. 5, 570.

Feynman, R. P., 1969, Phys. Rev. Lett. 23, 1415.

Fuglesang, C., 1988, XIXTH International Symposium On Multiparticle Dynamics 1988, P.257.

Glauber, R. J., 1959, in "High-Energy Collision Theory," Lectures in Theoretical Physics, Vol. I, ed. W. E. Brittin *et al.*, (interscience, New York).

Greenwood, M. and G. U. Yule, 1920, J. R. Stat. Soc. 83, 255.

Hwa, R. C., 1987, in Multiparticle Production, edited by R. C. Hwa and Q. B. Xie, P.431.

Hwa, R. C. and X. N. Wang, 1989, Phys. Rev. D39, 2561; 2573.

Jeffreys, H., 1961, Theory of Probability (Oxford).

Kiang, D., *et al.*, 1985, Phys. Rev. D31, 31.

Kiang, D., *et al.*, 1990, Can. J. Phys. 68, 145.

Knox, W. J., 1974, Phys. Rev. D10, 65.

Koba, Z., H. B. Niselen and P. Olesen, 1972, Nucl. Phys. B40, 317.

Lam, C. S., D. Kiang and T. Ochiai, 1989, preprint, to appear in Int. J. Mod. Phys. A.

Laudau, L. D., 1953, Izv, Akad. Nauk SSSR, Ser. fiz. 17, 51.

Li, T. S. and K. Young, 1986, Phys. Rev. D34, 142.

Ling, S. H. and K. Young, 1985, Can. J. Phys. 63, 954.

Liu, L. S., *et al.*, 1988, Phys. Rev. D38, 3405.

NA35, 1988, Phys. Lett. B205, 583.

Perl, M., 1973, High Energy Hadron Physics (John Wiley & Sons).

Slattery, P., 1972, Phys. Rev. Lett. 29, 1624.

TASSO, 1989, Z. Phys. C45, 193.

Thomé, W., *et al.*, 1977, Nucl. Phys. B129, 365.

UA5, 1983, Phys. Lett. 123B, 361.

UA5, 1984, Phys. Lett. 138B, 304.

UA5, 1985a, Phys. Lett. 160B, 193.

UA5, 1985b, Phys. Lett. 160B, 199.

UA5, 1986, Phys. Lett. 167B, 476.

UA5, 1987, Phys. Report 154, 247.

WA80, 1988, Z. Phys. C38. 51.

Werner, K., 1988, Phys. Lett. B208, 520.

Werner, K., 1989, Phys. Rev. D39, 780.

Wu, T. T. and C. N. Yang, 1965, Phys. Rev. B137, 708.